Theoretical Studies On Molecular Quantum Dynamics And Electron Transport

Thesis Submitted for the degree of
Doctor of Philosophy (Sc.)
in
Chemistry (Physical)

by

ANIRBAN KARMAKAR

UNIVERSITY OF CALCUTTA
2018

TO MY GRANDFATHER
LATE APURBA KUMAR DEY

Acknowledgements

With much pleasure I do introduce my thesis which is the outcome of my research work. In this connection, I take the opportunity to acknowledge all the persons who have accompanied and supported me.

At first, I convey my heartiest gratitude to Prof. Gautam Gangopadhyay, S. N. Bose National Centre for Basic Sciences, Kolkata for his kind guidance in preparing and finalizing the thesis. It is due to his inspiration, I have got enough space to think, analyze and solve research problems independently and learnt a lot from him about the basic formalisms of what is presented here.

I would like to thank all the faculty members of the Department of Chemical, Biological and Macromolecular Sciences, SNBNCBS for for their assistance and active co-operation. I also express my gratitude to all academic and non-academic staff members of this centre for providing me vibrant research atmosphere in the centre during my stay.

My family is the source of all my strength and inspiration. My parents, my grandparents, my wife Mrs. Satabdi Karmakar and my little son Achyut always encouraged me to proceed with my studies giving protection from external perturbations. In this regard, I would like to acknowledge the kind contribution from my father Dr. Pranab Kumar Karmakar who have always stood in front of me as the greatest inspiration to understand and learn science, since my birth. It is due to him, my interest in quantum physics grew up and today what I am, is solely due to his nurturing me as a child. I also remember here the contribution of my mother Mrs. Anupama Karmakar who always served as a driving force to complete my thesis.

I have learnt a lot from my beloved and respected teachers during my entire student life. Here I want to particularly mention the blessings that I have received from Dr. Hrishikesh Chatterjee (Ramakrishna Mission Residential College, Narendrapur, Kolkata), Dr. Murari Priya Ray (Dinabandhu Andrews College, Kolkata) and Late Dr. Swaraj Bhushan Maity (Bangabasi College, Kolkata) who motivated me to take up chemistry as a subject amongst others in my career. Last but not the least, I acknowledge the contribution of the respected members of the faculty in the Department of Chemistry, Calcutta University for their active support during my M.Sc tenure in Science College.

I also acknowledge here the Department of Science and Technology, Government of India and S. N. Bose National Centre for Basic Sciences for the financial support to carry out my research and related activities.

Date:

Anirban Karmakar
Satyendra Nath Bose National Centre for Basic Sciences
Block-JD, Sector-III, Salt Lake, Kolkata, India.

Contents

Chapter 1

Introduction

The most celebrated milestone of electronic conduction is the discovery of transistor on the material base of Germanium in 1947 from Bell Labs[1] followed by the introduction of the first silicon transistor by Texas Instruments in 1954. Since then, journey has began in the development and search of suitable material that can act as a transistor to satisfy the pace of modern day engineering and technology[2]. As the next step in developing electronic circuits, it is discovered that for mesoscopic system size of the material, quantum effect becomes important specially when the electronic mean free path is of the order or more than the system size leading to coherent conduction[3, 4, 5, 6] of electrons. On one hand, modern research is knocking at the the door of Chemistry for new materials[7] for electronic circuit component which subsequently created the field of Molecular Electronics[8] and at the same time, complexity of quantum dynamics of a single molecule shows the possibilities of new route of amplification, switching and coherence[5, 6] along with several other kinds of control over the conductance[9]. The major theme in the domain of molecular electronics[8, 9] lies in the construction, measurement, characterization and understanding of the current- voltage response of an electronic circuit in which molecules act as conducting bridge. A metal-molecule-metal junction is traditionally comprised of thin molecular films between macroscopic metal electrodes[9, 10]. Molecular transport junction currents can also be monitored to characterize the electronic and vibrational modes and also their coupling present and hence the study of current-voltage feature can be viewed as a kind of spectroscopy[10, 11, 12, 13, 14, 15, 16]. Although the main challenge is to understand the nature of coupling of individual molecular structures to metal-electrodes under non-equilibrium situation which has its origin from early work of Kuhn[17], the ultimate goal is the incorporation of a single molecule junction[18] in the circuit[19, 20].

The present scenario in the developing theory and methodologies to study the current characteristics in molecular junction[21] involves few knotty issues. In the first place, studying the effect of vibrational contributions and electron-nuclear coupling[22] in molecular transport plays a significant role in the transport signature

through a single molecule junction. The vibrational modes associated in a molecular junction setup may promote[23, 24] or even demote[25] electron transport through it. For a model system consisting of array made of three quantum dots[26, 27], the internal electronic coherence gives rise to interesting features of sequential tunneling for weak interdot coupling. On the contrary, in the coherent strong coupling regime, phenomena of electron transport against bias voltage[28] has been reported. In the regime of arbitrary strong[29] electron-phonon coupling, as the phonon coupling increases, it first plays a constructive role to assist the transport which is followed by its repression. Apart from this, theoretical models are also considered to study electronic transport in the spin-blockade regime[30] and also to study the dynamics of nanomechanical resonator coupled to superconducting single electron transistor[31], which can also drive the resonator leading to its dynamical instabilities[32]. It has been reported recently that in case of carbon nanotube double quantum dot, depending on the relative position of the two dots, the electron-phonon interaction can lead to negative differential conductance[25, 33] along with suppression in the magnitude of current which may also be assisted by cooling of the ground state vibrations[34]. If the two-site molecular junction is coupled to a vibrational environment, say, in case of exciton transport in photosynthetic complexes, the vibrational interactions can significantly enhance the current through specific molecular orbitals[35]. In addition, the electron interactions can significantly affect the thermoelectric transport in a length dependent manner[36]. On the contrary, reports are there which tells us regarding the electron-vibration coupling in quantum dots that can lead to a strong suppression of the average current in the sequential tunneling regime. But if the system is subjected to time-dependent driving in terms of oscillatory gate voltage[37], an exponential growth of the relative change in the average current with the drive strength, is observed. Very recently, an interesting feature is reported[38] which talks about nonequilibrium vibrational states that can be detected in hand by the asymmetric behavior of the inelastic current peaks with respect to the gate voltage. The metal-molecule coupling in the electron transport setup has also been reported to be dependent on nuclear coordinate[39] which is called electronic friction[40, 41]. The study of full counting statistics[42, 43] of the vibrationally assisted electronic conduction shows that at large bias, the conductance and current can identify the structural and energetic properties of the molecular junction even when measured by a quantum point contact[44]. In case of magnetically active molecules[45], the charge transport is also dependent on the magnetic regime in which it takes place. Another issue, which is important in the context of molecular electronic conductance is the control of shot noise in current and its signature present in the system in terms of the operational vibrational modes. Shot noise[5] in an electrical conductor is a consequence of the charge quantization unlike the case for thermal noise. Recognition of shot noise in a molecular junction is based on the study of the non-

equilibrium state associated with the electron transport through the system. For single molecule quantum dots and coupled quantum dots, in the resonant tunneling regime, the shot noise spectrum exhibits different behavior in different regimes[46] of effective phonon numbers. Current-noise spectrum of a double quantum dot can also serve as a probe[47] to detect its nanomechanical oscillations. It is also relevant to mention here that the current noise of the single superconducting electron transistor[48] is strongly influenced by the energy fluctuations in the resonator thus providing a useful indicator of the dynamics of the vibrational mode. In case of a molecular junction which is comprising of a single electronic state and coupled to multiple vibrational modes, a weak to moderate electronic- vibrational coupling may result in high noise levels[49], especially at the onset of resonant transport, which is in close proximity with earlier experimental findings[50].

In the proposed thesis, our main motivation is to study the quantum dynamic aspects of some model of molecular quantum systems engaged in the electron transport processes with the emphasis on coherence of the degrees of freedom of the reservoir, non-adiabatic electron-vibration interaction in the molecules, molecular currents due to electron transport and its associated noise. To deal with such a degree of complications, we resort to the approach involving quantum master equation [51, 52] which offers a general framework to characterize a quantum dynamical system in terms of dissipation and decoherence in the transport domain. But, prior to go in depth of the electron transport studies and to understand the dynamics and coherent property of the fermionic bath, we undertook the studies of the decoherence dynamics of a quantum system coupled to a fermionic reservoir and compared the result with its bosonic counterpart. In addition, the dissipative dynamics is studied in terms of strong-field resonance fluorescence spectra for fermion bath. In the present thesis, we have also introduced the definition of fermionic thermocoherent state and also have discussed its implications in terms of electron transport. Finally, we have studied the electron transport dynamics in steady state and time-dependent regime in terms of Fano factor for two specific systems, a class of interacting resonating dimers and also for molecule having conical intersection exhibiting cis-trans isomerization. The common underlying thread here is a master equation description of electron transport to understand the molecular quantum dynamics in steady state regime by which ultimately the effect of molecular electron-vibration modes can be identified and characterized. In the present thesis entitled, Theoretical studies on molecular quantum dynamics and electron transport, we have discussed the related issues with the emphasis on the following topics.

A. Dissipationless decoherence

In the study of quantum open systems starting from the FeynmannVernon theory[53] and later popularized by Caldiera and Leggett[54] as quantum Brownian motion, the

environment is considered to be consisting of a very large number of non-interacting harmonic oscillators. The bosonic description of environmental modes is a natural realization of most of the open quantum systems that occur with decoherence and dissipation, which is evidenced by a large body of literature[55, 56, 57, 58]. A renewed interest in the manipulation of the quantum state of matter and in quantum information processing has emerged that necessitates understanding and control of environmental decoherence of the system even in the absence of an appreciable loss of energy. This aspect has also been extensively explored by several authors in which the system interacts with its environment via quantum non-demolition (QND) type interaction[59, 60] utilizing the decoherence model[60, 61, 62]. Study of decoherence dynamics from the system-reservoir model perspective where the quantum system is coupled to a fermionic environment instead of a bosonic one should bear an interesting feature. The fermionic environment may serve as a theoretical realization of a bath consisting of two-level systems corresponding to localized modes such as defects, impurities and nuclear and paramagnetic spins[63, 64]. It has also proved useful for the proper understanding[65] of magnetic relaxation of molecular crystals[66] and in quantum coherence measurements[67, 68]. However, dissipation along with decoherence happens to remain an integral part of all these problems. As a result, exact dissipationless decoherence model of a system interacting with a fermion bath has to be proposed and the theory should meet the need of the present scenario.

B. Resonance fluorescence spectra due to fermion bath

The dynamics of dissipation of an open quantum system[56, 58, 69] generally depend on the quantum statistical nature and the energy level structure of the environment degrees of freedom with which the system interacts. The traditional approach is to assign a bosonic description of the environment and to calculate correlated noise observed for bosonic particles, which can be explained within the frame of a classical field description having fluctuating amplitudes and phases. On the contrary, dynamic anticorrelations in the noise for a fermionic bath do not have any classical analogue. Recently static antibunching is observed in a degenerate atomic Fermi gas released from optical lattice made of ^{40}K atoms arranged periodically in one-dimension[70]. Equilibrium temperature dependence of the anticorrelation showed a robust tool to measure antibunching unlike the bosonic case where antibunching is usually understood in terms of the constructive and destructive interference of two possible propagation paths that the two particles follow to reach the detector as in the experiment of Hanbury-Brown-twiss [71, 72, 73]. At the same time, dynamic antibunching observed in the emission of strong field resonance fluorescence is well studied in the context of Mollow spectra[74, 75, 76]. However, if the bath is of fermionic nature which possesses an inherent anticorrelation effect, the emitting

atom can be affected in a nontrivial way specially when the effect of bath is magnified at a higher chemical potential. In this context it is reasonable to study how the Mollow resonance fluorescence and probe absorption of the driven system is modified due to fermionic bath at low non-zero temperature and high chemical potential. A strong modification of the antibunching characteristics of the emitted radiation is expected as the bath here already is already antibunching in nature unlike the bosonic case. Recently focus have been thrown to get fluorescence from semiconductor quantum dots[77, 78, 79, 80] as well as several experimental reports are also available in the context of the photon antibunching from similar systems[71, 72, 73]. Thus it is needed to analyze the experimental results of the temperature dependent antibunching to find the signature of a fermionic bath in the dissipative dynamics and its root in the quantum fluctuation-dissipation relation which is modified due to the interaction and closely follow the physical role played by Grassmann algebra in this case, if any.

C. Fermionic analogue of Glauber-Lachs state and modification of Landauer conductance

Recently the electron transport [81, 82, 83, 84, 6] properties of small systems with a discrete energy level structure have attracted much interest where the quantum dynamics are dominated by coherent effects. For example, quantum tunneling in a system of self assembled quantum dot array reveals antibunching[85, 86] and near life-time limited line-widths[87]. Furthermore, in an effort to achieve coherent control of single electron or electron spin, quantum transport have been used to detect the quantized motion of electrons in nanostructures[88, 12, 5]. A great deal of theoretical[89, 90, 91] and experimental[92] results are already available which involve a coherent transfer of electrons from the source to sink reservoirs maintained at different chemical potentials[84]. The availability of a coherent source of electrons[93] can be utilised to inject coherence[93, 94] into thermal electron source for the suppression of noise [95, 96, 5, 97]. Noise reduction can usually be observed in terms of the interference effects[6, 86, 5] as in the examples of emitted electrons from a carbon nanotube[98] and correlation function of time-dependent amplitude and phase of solid-state single-electron sources[5]. The coherent characteristics are well understood for bosonic systems and the idea of incorporating thermal noise into coherent source, thereby giving a thermocoherent state in case of light was originally conceived long ago by Lachs[99]. Here, the essential need is thus to construct a fermionic thermocoherent state similar to the bosonic thermocoherent state on the same footing. As an immediate application of fermionic thermocoherent state, we examine its effect on electron transport through a single level quantum system if the source reservoir is maintained in a thermocoherent state with the sink reservoir

in thermal state and the consequent modification of Landauer conductance formula due to coherence of the source.

D. Electron transport in resonating dimeric structures

Coupling of a quantum system with two reservoirs serves as a theoretical spectroscopic tool to study electron transport dynamics through a molecular system[95, 100]. Inspite of a great deal of theoretical and experimental investigations in the context of electron transport through systems[101, 102, 103, 104, 105, 106, 107, 108], physical insights about coherent dynamics of entangled electron-vibration motion in molecules are very limited in this context. When a molecule is coupled to two electron reservoirs, the difference in chemical potential of the two reservoirs drives transport of electrons through it. In molecular electronic devices where a molecule is typically coupled to two electron leads, inelastic effect appears in the molecular transport junctions[109] along with vibrational effects[110]. Traditionally, three effects dominate transport of electrons through a quantum system: (1) The tunnel effect, which is a quantum mechanical phenomenon where electrons can cross an electrostatic potential barrier from the emitter lead and reach the collector lead through the intervening system. (2) The charging effect which is due to the discreteness of the electronic charge and is commonly known as the Coulomb blockade effect, and (3) size quantization effect which is due to the smallness of the system, leading to discrete energies. Out of these three, the Coulomb blockade effect plays the most important role and is sufficient enough to explain the simplest cases observed in the earlier experiments[111] on quantum dots in terms of simple charging diagrams. From a theoretical point of view, this corresponds to a description of sequential tunneling through the system in terms of simple rate equations[112]. In this thesis, our motto is to utilize master equation formalism to study the electron transport process through a molecule coupled to two fermionic reservoirs and include the effect of the vibrational modes characterizing the system on the transport properties under steady state conditions. For the purpose of calculating the current noise and fano factor, formalism of quantum regression in correlation function[55] is to be utilized.

E. Conical-intersection and electron transport

The importance of going beyond the Born-Oppenheimer approximation[113, 114] forms the doorway to several unexpected phenomena like radiationless relaxation of excited electronic states, photoinduced unimolecular decay and isomerization processes of polyatomic molecules. Vibronic coupling which is an an essential ingredient of *conical intersection*(CI) between electronic states, is a unique theoretical concept commonly used to describe the mechanistic pathway and its underlying features in

molecular system in non-adiabatic regime[115, 116, 117, 118]. Understanding the effect of quantum entanglement among various degrees of freedom in a molecule on its observables is not easy in comparison to the entanglement between two spatially separated objects due to the added complexity of the non-adiabatic dynamics. As a consequence, quantification of electron-vibration entanglement in a molecular species exhibiting conical intersection[116, 118] opens up as a robust tool for superior understanding of the molecular quantum dynamics in the non-adiabatic regime. In this thesis, we have shown a possible quantification by measuring the electron current when it is put into a transport setup.

1.1 Scope of the thesis

The scope of theoretically studying the effects of molecular quantum dynamics in the electron transport for molecules of various complexity is vast. Therefore, in the present thesis, we have worked on some issues involving specific aspects of this broad topic theoretically with model systems using relevant experimental parameters for realistic applications. The electron transport phenomena is well researched[9] in the context of conduction spectra[10, 12, 16], coherent states[119] and also involving the Born-Oppenheimer approximation[113, 114] which can account for a large number of experimentally observed phenomena as mentioned earlier. The study of the electron transport dynamics covers two principal aspects: (1) The transport of electrons through simple systems with few electronic states and (2) the role of electron-vibration entanglement and conical intersection involving non-adiabatic molecular electronic states. Along with these, there are several other complexities which affect the molecular electronic transport. In the first place, the statistical nature of the leads to which the molecules are coupled dominantly affects the quantum dynamics in the transport setup. Traditionally, the reservoir is considered to be bosonic in nature. The bosonic description of environment is useful to explain a large variety of physical situations[120, 121, 122, 123, 124, 125, 126, 127, 128, 129, 130, 131, 132] such as, spontaneous emission, polaron formation, exciton motion, macroscopic quantum tunneling etc., in atomic physics, condensed matter physics[13] and quantum optics[56]. The study of dynamical aspects of the quantum to classical transition[133, 134, 135] has put a major thrust to study the effect of fermionic reservoirs instead of a bosonic one on the quantum dynamics of a system, which is integrally coupled to it. The dissipationless decoherence model[59, 60] has also been utilized to study the phase diffusion phenomena for physically relevant systems under various initial conditions[136, 137, 138]. The fermionic nature of the environment serves as a theoretical model for a bath composed of spin-$\frac{1}{2}$ particles which provides a scope to study the new dynamical aspects of the system which emerge when it is coupled to such environment. Fermionic bath has also recently been studied in

several contexts to understand the phenomenon of phase diffusion[139], spin-boson models[140], dynamical localization[141] and optical conductivity and direct current resistivity[142]. However, the dissipation along with decoherence happens to remain as an integral part of all these problems. This stimulates us to propose an exact analytical solution for a model to describe the coherent dynamics of a quantum system interacting with a fermionic reservoir via QND type interaction where no dissipation of energy is taking place. In addition, the dissipative dynamics of a system coupled to a fermionic reservoir can be studied in terms of the strong-field resonance fluorescence mollow spectra[76] and also the absorption spectra. The next issue, which becomes important in this respect is to study the coherent characteristics of the reservoir to which the system is coupled. The idea of bosonic thermocoherent state was originally proposed by Lachs[99] which arose out of natural consequence of the superposition of the thermal and coherent fields in terms of the quasiprobability P-distribution function. Although fermionic coherent states were studied in several contexts[143, 144], as spin coherent state[145], quantum many particle[146] systems of electrons, however, Cahil and Glauber[147] in 1999 first systematically introduced fermionic coherent state and the corresponding quasiprobability distribution functions similar to the bosonic coherent state[119]. Thus, in this thesis we have utilized the scope to introduce the fermionic thermocoherent state using the definition of fermionic coherent state of Cahil and Glauber[147] in terms of the quasiprobability distribution functions. We have also investigated on the possibility of physical realization of this newly introduced fermionic thermocoherent state by showing its relation with the displaced thermal state and explore its relation with the displaced number state(DNS). As an immediate application, we have examined its effect on electron transport through a single level quantum system if the source reservoir is maintained in a thermocoherent state with the sink reservoir in thermal state. The motivation is to study the modification of the current noise[56, 55, 148] by introducing some coherent character in the source reservoir. The steady state behavior of current is monitored in terms of current noise spectrum[149, 150] and the possible modification of conductance[96, 3, 4] in this context is shown. We have also shown its relevance through the effect of reduction of noise which are usually done through a coherent driving mechanism[94] of the system[95, 96] when the two reservoirs are in thermal states. Within the scope of this thesis, we now choose to explore the electron transport characteristics for model molecular systems. For the sake of our study, we have adopted a quantum system[151, 152] which is consisting of two equivalent resonating structures in terms of a dimer, each of them being described in terms of an electronic basis which is coupled through a vibrational mode. This type of system has also been examined in the context of electron-vibration entanglement in model molecular systems[153, 154] which can provide a physical insight of the quantum dynamics from electron transport through molecules. Although the conductance

of trapped single monomer is seen to be much prominent than its dimer, but the choice of preparing dimer-based metal-molecule-metal contacts have been seen to be highly advantageous due to high-ended fabrication of single molecule device[155] and a very accurate reproducibility of the temperature dependence of conductance measurement[155] can be checked. As vibrational mode is plays the key role in dimeric interaction, a sensitive dependence of temperature in current is expected which is exemplified in the present thesis for a class of five molecular systems with detailed numerical exploration. In this thesis, we have calculated the current through the molecular dimer as a function of internal as well as the external bias voltage and considered the effect of electron-vibration entanglement on both the current-voltage profile as well as on the current versus internal bias profile. We have also examined the current noise spectrum for electrons flowing through the single molecule junction. For this purpose, we have adopted the formalism of quantum regression in correlation function[55] and calculated the steady state noise fluctuation. The next agenda which we encounter in the thesis is to probe and characterize electron-vibration entanglement and conical intersection through electron transport measurement. Several non-adiabatic reactions and processes can be cited as an example of the conical intersection among which the cis-trans isomerization is a prominent example. Investigation and the control of photoinduced cis-trans isomerization[156] about C=C bonds using specially designed femtosecond laser pulses has been a subject of long-standing research interest [157, 158, 159, 160, 161, 162]. This isomerization forms the leading step in many photobiochemical processes namely vision[163, 164], light-induced ion pumping and plays vital role in producing photomemories and light triggered switches[165]. Generally the theoretical characterization of the CI point in such systems involve study of phase space quasiprobability distribution functions namely the Wigner distribution function[166, 57], Among other measures von-Neumann entropy[167] and ATAS technique[168] are also utilized popularly from the joint density matrix. Experimental features of CI are performed by several techniques[169, 170, 171, 172, 173, 174, 175] including ultrafast electron diffraction studies[176], extensive studies on the measurement of electron-vibration entanglement of trapped atoms and ions[177, 178]. With this background in mind we have made the following theoretical studies as our own contribution in the flow of the related research and development.

At first, on the basis of the formalism of the fermionic coherent state of Cahil and Glauber[147], we have provided an exact solution to a model of a harmonic oscillator coupled to a fermionic environment via a quantum non-demolition type interaction. Unlike the quantum Brownian case, the decoherence dynamics does not depend on the structure of the system Hamiltonian. We have observed that our result converges to the Born-Markov limit under suitable conditions, which is drastically different

from the bosonic bath case. In this context, we have also studied the quantum phase diffusion and the linear entropy dynamics which shows their signature felt by the suppression of decoherence with temperature in comparison to the bosonic bath case. This is worth investigating for their application in the coherent dynamics domain at finite temperature. We have also shown that an unconventional motional narrowing of the quantum Kubo oscillator, which is realized from this dissipationless decoherence model due to the antibunching character of fermionic quantum noise. It thus becomes possible to bring out the results explicitly by the consideration of the non-commutative property of interaction coefficients obeying the Grassmann algebra.

Next, we have derived the modied Bloch equation from the generalized master equation due to the fermionic bath where one needs to consider Grassmann algebra to obtain the similar mathematical structure of the reduced system dynamics, as in the case of a bosonic bath. We have shown that there is an enhancement of antibunching in the photon emission with an increase in effective temperature. This is in principle a manifestation of the antisymmetric two-particle dynamic anticorrelation in the fermionic bath with a definite value of chemical potential characterized by the forbidden overlapping. This is evident from the modifed fluctuationdissipation relation. We have compared it thoroughly with an experimental result in the temperature dependent emission characteristics within an environment of quantum dots in a Hanburry-BrownTwiss set-up. For the fermionic bath, an effective temperature assisted coherence phenomenon is induced in the system dynamics, which is reflected in the resonance fluorescence spectrum with the variation of chemical potential. In the Mollows absorption spectra, when the Rabi frequency is sufciently low, the side peaks appear as chemical potential induced coherence phenomenon rather than the traditional field induced one. The subsequent gain in the probe wave is evidently of thermal origin, where the energy is fully supplied by the fermionic bath at non-zero temperatures. This is not possible for a bosonic bath. Thus we have provided an example of the extraction of coherence from the fermionic bath.

Then we have systematically introduced the fermionic thermocoherent state on the basis of Cahill and Glauber[147] in terms of the quasiprobability distribution which shows the appropriate thermal and coherent limits as in the bosonic case or the Glauber-Lachs state. We have shown that the fermionic thermocoherent state can be realized as a displaced thermal state of fermions. Its relation with the fermionic displaced number state and the fermion-added coherent states are explored in the spirit of the bosonic case. We have investigated the nature of the average current and the suppression of noise due to the thermocoherent character of the source. The theory is thus applied to the problem of electronic conduction. A modification of the Landauer conductance formula is suggested which reflects the role of nonzero

coherence of the source in electron transport.

As a next problem, we have studied the electron transport problem through molecular dimer. Electron transport happens through molecules depending primarily on the superposition of molecular electronic orbitals and their coupling strength to the metallic leads. Thus vibrationally coupled resonating structures of dimer of various conjugated electron rich molecules is the basic testing ground in electron transport spectroscopy. However, dynamical coherence and fermionic correlation in molecule-molecule and molecule-lead coupling necessitates a delicate approach to treat the current and its noise level theoretically to validate the experimental result and going beyond to predict more complicated situation which can be envisaged, for example, in presence of variable external bias and temperature dependence of conduction and its level of fluctuation. Based on the formulation of master equation for fermionic bath, we have estimated electron transport through a molecular dimer which is coupled to two electron leads with a vibrational manifold. The molecular current is studied both for internal and external bias for a class of molecules as well as the current noise. Numerical results for resonating structures of a diverse chemical class of molecules show that electron-vibration coupling can serve as a good indicator of current noise and coherent electron transport. An additional electron transport channel through coupling to the vibrational mode gives rise to a vibrational Coulomb blockade structure which can be used as a marker for the functioning vibrational mode in the system.

Finally, we have ended up with the study of probing electron-vibration entanglement and conical intersection through electron transport setup when they are coupled to two fermionic reservoirs at infinite difference in the chemical potential. Due to the presence of a high degree of non-adiabaticity near the *conical intersection*(CI) point, the electron-vibration entanglement plays a key role in the quantum dynamics of a molecule which supports indulgence in the measurement of entanglement for its proper characterization. To find the effect of CI, we have studied cis-trans isomerization in a molecule in an electron transport setup with electronic source and sink composed of fermions. Vibronic coupling introduces quantum entanglement and non-classicality which is typically enhanced in the CI point. Wigner function and other measures of entanglement and non-classicality can be correlated with the electron transport through the molecule. As the torsion angle gradually reaches the value corresponding to the CI point, the current shows a sharp enhancement which can also be used as a quantification of the persistent and some sensitive kind of entanglement present in the system.

1.2 Plan of the thesis

We have presented the contents of the thesis in the following chapters. In Chapter-2 we have given a brief overview regarding the theoretical aspects of molecular quantum dynamics and electron transport.

In Chapter-3 the dissipationless decoherence model for a fermionic reservoir is studied where an exact solution in density operator elements have been provided for a harmonic oscillator coupled to fermion bath. We have also studied the dynamics of phase distribution pattern and linear entropy and shown its connection to a stochastically modulated oscillator.

In Chapter-4 we have constructed the master equation for a two-level system coupled to a fermion bath under strong external driving and analyzed the photon antibunching, absorption spectra and Mollow spectra of the system.

Chapter-5 is devoted to introduce fermionic thermocoherent state which can be realized physically as a displaced thermal state of fermions and also investigated its relation with the displaced number state of fermions. We have also investigated the nature of the average current through a quantum system and its suppression of noise level to explore the efficiency of electron transport due to thermocoherent character of the source with a thermal sink.

In Chapter-6, we have estimated electron transport through a molecular dimer which is coupled to two electron leads with a vibrational manifold. The molecular current is studied both for internal and external bias for a class of molecules as well as the current noise.

Chapter-7 is devoted to study the effect of electron-vibration entanglement and conical intersection in a molecule in the context of cis-trans isomerization in an electron transport setup with electronic source and sink. Here, we have shown that the vibronic coupling introduces quantum entanglement and non-classicality which is typically enhanced in the CI point.

Chapter 2

Overview on the quantum dynamics and electron transport through molecules

Quantum dynamics of a system is historically described in terms of time evolution of the wave packet. To clarify, if we consider the existence of a system Hamiltonian H, the time-dependent state vector $|\psi(q,t)\rangle$ is in accordance with the Schrodinger equation $i\hbar\frac{\partial}{\partial t}|\psi(q,t)\rangle = H|\psi(q,t)\rangle$. Here, two cases, may particularly arise: Case-(i) When the Hamiltonian H is explicitly time independent, the system is said to be conservative and the time dependent solution of the wave function[56, 57, 58] assumes the form

$$|\psi(q,t)\rangle = \exp\left[-\frac{i}{\hbar}H(t-t_0)\right]|\psi(q,t_0)\rangle, \tag{2.1}$$

where, $|\psi(q,t_0)\rangle$ is the wave function describing the system at some initial time t_0 and q is the position coordinate. This is popularly recognized as *Schrodinger picture*(SP), where the operators are considered time-independent whereas, the state function evolves with time. The other extremity is encountered in terms of the *Heisenberg picture*(HP), where the operators evolve while the state remains time-independent. In the case-(ii) when H explicitly contains time in it, no such straightforward solution will emerge. In this case, the problem is usually tackled in terms of the *Interaction picture*(IP), which serves as a bridge between SP and HP and which is much more general than these two. In IP, the part of the dynamics which is associated with free uncoupled evolution is contained within the operators while that arising from coupling appears in the state or vice-versa. In IP, the state vector can be expressed as

$$i\hbar\frac{\partial}{\partial t}|\psi_I(t)\rangle = e^{\frac{i}{\hbar}H_0^S(t-t')}V_S e^{-\frac{i}{\hbar}H_0^S(t-t')}|\psi_I(t)\rangle, \tag{2.2}$$

where, the total system Hamiltonian is expressed as $H^S = H_0^S + V_S$, with H_0^S being the time independent part and V_S may or may not have explicit time dependence.

The unitary transformation between the SP and IP can be performed using the relation[56, 58] $|\psi_S(t)\rangle = \exp\left[-\frac{i}{\hbar}H_0^S(t-t')\right]|\psi_I(t)\rangle$. Upto this, we have assumed that sufficient measurements are made so that the system state $|\psi_S(t)\rangle$ can be clearly known at any given time in SP. But this situation is not always true in practice. In most of the cases, we do not have enough information to specify completely the state of a system and hence cannot form its wave function. In that case, the system is described in terms of a mixed state represented by a density matrix ρ[56, 57, 58]. They arise frequently in problems[56, 57, 58] involving coupling of an open quantum system to its environment. In general terms, an open system is a quantum system S which is coupled to another quantum system B called the environment. It thus represents a subsystem of combined total system $S + B$, which is considered closed following Hamiltonian dynamics[179]. The state of the subsystem S will change as a consequence of its internal dynamics and its interaction with the environment, so that in general it becomes important to follow the reduced dynamics of the system S, also called reduced system. Traditionally, the environment is considered to be comprised to large collection of harmonic oscillators[56] with the frequency modes considered as continuum. The dynamics of the subsystem S, which is treated most commonly in the framework of the quantum master equation both in IP ans SP follows dissipation as well as decoherence. Dissipation or damping refers to a mechanism, where the subsystem loses energy to the reservoir. This is commonly monitored by the dynamics of several relevant physical properties[57] in the system subspace. On the other hand, decoherence refers to time evolution of the off-diagonal elements of the density matrix ρ_{mn} in the system subspace.

In the present thesis, our main purpose is to theoretically do a model study of the quantum dynamics of an open system and use its formalism in relation to study electron transport through molecules. The use of the formalism of the physics of open quantum system in the domain of electron transport has been done by several authors [180, 181, 182, 183, 184, 185, 186] in the perspective of electron counting statistics[187, 188, 189], non-equilibrium quantum fluctuation theorems[190, 191] and also in thermal transport. The uniqueness of such model is to couple a quantum system simultaneously to two electron reservoirs considered as environment at different chemical potential, so that in the steady state domain, a continuous flow of electrons can be encountered through the molecule[6]. Thus, as a general overview for the present thesis, one must present a proper understanding of the quantum theory of damping[56] in terms of the quantum master equation when it is coupled to a single bosonic bath. This is addressed in the Section.(2.1) The next issue which is important in this regard is to address is the decoherence dynamics which is integrally associated with dissipation for a system-reservoir model. The understanding of decoherence model which is presented in Section.(2.2) provides a background for the Chapter-(3) of the thesis, where we have provided a similar dis-

sipationless decoherence model for a general quantum system coupled to a fermionic bath. As an application of the quantum master equation, we have provided a very basic overview of the strong-field resonance fluorescence spectra, popularly called Mollow spectra[76] in the Section-(2.3). This also provides a general background for Chapter-(4) of the present thesis which considers the resonance fluorescence spectra and fermionic antibunching feature of a quantum system coupled to a fermionic bath under strong external driving. The next interesting feature, is to study the dynamical change that would happen if the reservoir character would have been fermionic(as electron leads are fermion reservoirs)[69, 6] in the electron transport setup instead of being bosonic[56, 57, 58]. Thus we have discussed the basic qualities of a fermion reservoir and its underlying feature using Grassmann numbers in the Section-(2.4). In the chapter-(5) of present thesis, we have discussed some interesting features of fermionic thermocoherent state along with its implication on current noise[5, 95] in the context of quantum transport when the reservoir is prepared in such states. This needs a basic discussion of bosonic and fermionic coherent states along with the associated quasiprobability distribution functions used in quantum optics as a formalism to construct such states which is done in Sections-(2.5) and (2.6). It is important here to note that the bosonic version of thermocoherence was formulated much earlier[99] which is presented as an overview in the Section-(2.7). In the Section-(2.6), we have also provided a thorough discussion of Wigner function[192] and Wigner function matrix[178] to understand the effect of non-classicality of the vibrational states and the electron-vibration entanglement present in a molecular system involved in transport. In the Section-(2.8), we have provided a very basic idea of electron transport from the point of view of Landauer-Buttiker[96, 5] formalism and also the Coulomb Blockade effect in transport. The overview that we have provided will serve as a background to understand electron transport through molecules from phenomenological view-point. Finally, in the Section-2.9, we have given a brief discussion of the non-adiabatic molecular processes in regard to the molecular dimer that is studied in the electron transport setup.

2.1 Quantum theory of damping

The quantum physics of open systems has been traditionally developed in the context of dissipative dynamics, with the focus primarily only on reduced density operators[56, 69] of the system. Dissipation in an open quantum system is always present which originates from coupling to the environment comprising a much larger system or ensemble of states. This coupling is typically weak compared with the couplings within the system of interest but as we will see, it profoundly affects the dynamics of the system of interest. Quantum theories of dissipation cover topics ranging from various second-order quantum master equations[57, 181, 193, 194, 195,

196, 197] to the FeynmanVernon inuence functional path integral formalism[53]. In this section, we will mainly focus on the reduced dynamics of a quantum system, commonly considered as a harmonic oscillator coupled to a reservoir comprising of a large collection of harmonic oscillators[56] in terms of a quantum master equation.

To start with, we consider the total Hamiltonian

$$H_{tot} = \hbar\omega a^\dagger a + \sum_j \hbar\omega_j b_j^\dagger b_j + \sum_j g_j(a^\dagger b_j + a b_j^\dagger), \tag{2.3}$$

where, $a(a^\dagger)$ is the annihilation(creation) operator for the system oscillator and $b_j(b_j^\dagger)$ is the same for the $j-$th mode of the reservoir oscillator and g_j are the real system-bath coupling constants. We may assume a very general type of system-reservoir coupling of the type XX_j , which contains terms such as $ab_j^\dagger$, $a^\dagger b_j$, $a^\dagger b_j^\dagger$, ab_j, but using the rotating-wave approximation arguments[56], which amounts to ignore the terms like ab_j and $a^\dagger b_j^\dagger$ corresponding to simultaneous creation and annihilation of phonon, we only keep the counter-rotating terms for weak system-reservoir coupling. Now, we define the density operator for the total system ρ, so that the Liouville equation for the complete system comes out as

$$i\hbar\frac{d\rho}{dt} = [H_{tot}, \rho]. \tag{2.4}$$

The interaction picture is defined in terms of the free Hamiltonian $H_0 = \hbar\omega a^\dagger a + \sum_j \hbar\omega_j b_j^\dagger b_j$ and the corresponding density operator appears as $\bar{\rho} = e^{\frac{iH_0 t}{\hbar}}\rho e^{-\frac{iH_0 t}{\hbar}}$. Differentiating $\bar{\rho}$ with respect to time, with the notation $\bar{H}_1 = e^{\frac{iH_0 t}{\hbar}}(\sum_j g_j(a^\dagger b_j + ab_j^\dagger))e^{-\frac{iH_0 t}{\hbar}}$, we get

$$\frac{d\bar{\rho}}{dt} = -\frac{i}{\hbar}[\bar{H}_1, \bar{\rho}]. \tag{2.5}$$

Now, formally integrating the Liouville equation and substituting back in Eq.(2.5)twice, one obtains

$$\frac{d\bar{\rho}}{dt} = -\frac{i}{\hbar}[\bar{H}_1, \bar{\rho}] - \frac{1}{\hbar^2}\int_0^t dt'[\bar{H}_1(t), [\bar{H}_1(t'), \bar{\rho}]]. \tag{2.6}$$

The final step to find the master equation for the damped harmonic oscillator is to evaluate the double commutator appearing in Eq.(2.6) and also a fundamental step to assume that $\bar{\rho}(t) = \bar{\rho}_{sys}(t) \otimes \bar{\rho}_{res}(0)$, which is the **Markovian approximation**, one can get the equation of motion of the density operator for the system ρ_{sys} after transforming in the Schrodinger picture as

$$\dot{\rho}_{sys} = -i\omega_0\left[a^\dagger a, \rho_{sys}\right] + \frac{\gamma}{2}(\bar{n}+1)(2a\rho_{sys}a^\dagger - a^\dagger a\rho_{sys} - \rho_{sys}a^\dagger a)$$
$$+\frac{\gamma}{2}\bar{n}(2a^\dagger\rho_{sys}a - aa^\dagger\rho_{sys} - \rho_{sys}aa^\dagger), \tag{2.7}$$

with,

$$\omega_0 = \omega + P\int_0^\infty d\omega' \frac{|g(\omega')|^2\kappa(\omega')}{\omega - \omega'}, \tag{2.8}$$

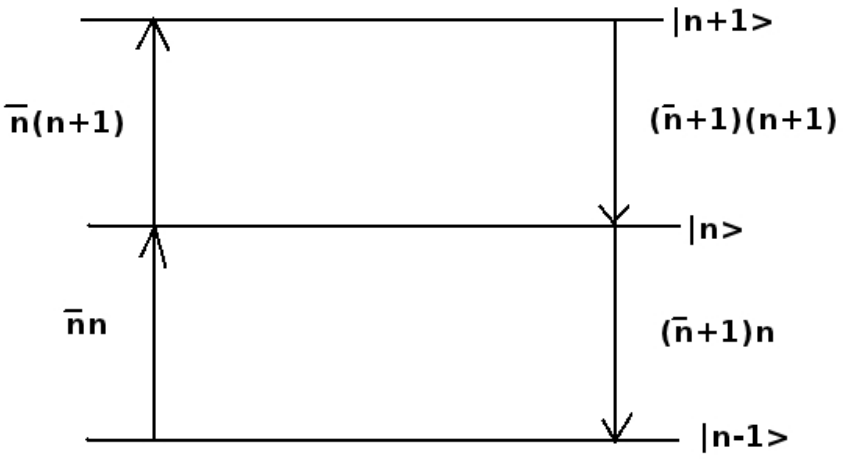

Figure 2.1: Schematic representation of transition between the quantum states $|n-1\rangle, |n\rangle$ and $|n+1\rangle$ for the harmonic oscillator. p_{n-1}, p_n, p_{n+1} represents the occupation probability of the $n-1$-th, n-th and $n+1$-th state. The coefficients in the master equation[see Eq. (2.9)] represent the rate of transition between the states.

where, P denotes the Cauchy-principal value, $\kappa(\omega')$ is the reservoir density function and $\bar{n} = (e^{\frac{\hbar\omega}{k_B T}} - 1)^{-1}$. The damping rate constant is defined in Eq.(2.7) as $\gamma = 2\pi|g(\omega)|^2\kappa(\omega)$. This is the master equation for the damped harmonic oscillator coupled to a thermal bosonic reservoir. It has the following properties: (1) The Hermitian conjugate of the master equation gives back the same equation. (2) The density operator ρ_{sys} is always normalized so that at all times $Tr_{sys}\rho_{sys} = 0$. The physical interpretation follows from the rate equations satisfied by the probabilities $p_n = \langle n|\rho_{sys}|n\rangle$ for the oscillator to be found in its $n-$th energy eigenstate:

$$\dot{p}_n = \gamma(\bar{n}+1)(n+1)p_{n+1} - \gamma\bar{n}n(p_n - p_{n-1}) - \gamma\bar{n}(n+1)p_n. \tag{2.9}$$

The terms on the right-hand side of the Eq.(2.9) describe transition rates into and out of the $n-$th energy level (see Fig.(2.1)).

2.2 Dissipationless decoherence

In true sense, when a system is coupled to practically infinite number of degrees of freedom, in addition to the energy dissipation which is described by the master equation(see Eq.(2.7)), an integral part of the problem, which is associated is the decoherence which is described by the dynamics of the off-diagonal terms of the density matrix. Due to the intricate interplay between decoherence and dissipation present in the reduced system subspace, the dynamics is widely influenced which largely affects and modifies the system-reservoir interaction.

In this section, we are interested here in a process wherein the system undergoes decoherence but with no dissipation of energy. Such dissipationless decoher-

ence models are studied by many authors[60] in the Markovian limit or the high-temperature limit and also for the case where the reservoir is acting as a source of classical noise[198]. A similar model is also studied by Shao et.al[62]. They have focused their attention towards an exact solution of the problem, which can be given also by a similar operator disentanglement method[61]. After that they solved the problem when the bath is composed of two-level systems instead of harmonic oscillators which is also studied in detail in Ref.[199].

To provide a brief overview of the topic, we consider an interaction between a system with its surroundings, For that purpose, we have considered a total Hamiltonian H_T as

$$H_T = H_s + H_R + H_{int}. \tag{2.10}$$

The reservoir Hamiltonian, H_R, is composed of an infinite number of harmonic oscillators such that,

$$H_R = \sum_j \hbar\omega_j b_j^\dagger b_j, \tag{2.11}$$

with $\left[b_j, b_j^\dagger\right] = 1$, which is a well known result in quantum mechanics that stems from uncertainty relation. We have assumed that the interaction is of quantum non-demolition type, satisfying

$$[H_s, H_{int}] = 0. \tag{2.12}$$

This kind of system-reservoir interaction is also considered by others to obtain the pure decoherence dynamics of the reduced system[60]. Equation(2.12) implies that H_{int} is a constant of motion which is generated by H_s. For the simplest possible variant of such interaction, we assume[61],

$$H_{int} = H_s \sum_j g_j \left(b_j + b_j^\dagger\right), \tag{2.13}$$

where g_j is a coupling constant, which is in general complex. In order to understand the decoherence dynamics of various quantum systems, Tameshtit and Sipe[60] have derived a master equation for involving the total density operator involving the system and reservoir using BornMarkov (BM) approximations as

$$\dot{\rho} = -\frac{i}{\hbar}\left[H_s, \rho\right] - \frac{\gamma_0 KT}{\hbar}\left(H_s H_s \rho + \rho H_s H_s + 2H_s \rho H_s\right), \tag{2.14}$$

with,

$$\gamma_0 = \lim_{\omega\to 0} 2\pi \frac{|g(\omega)|^2 I(\omega)}{\omega}. \tag{2.15}$$

Here $I(\omega)$ is the spectral density of the bath and a high-temperature approximation is introduced in concurrence with the Markov approximation. The exact solution of this problem in the context of fermionic reservoir has been furnished in

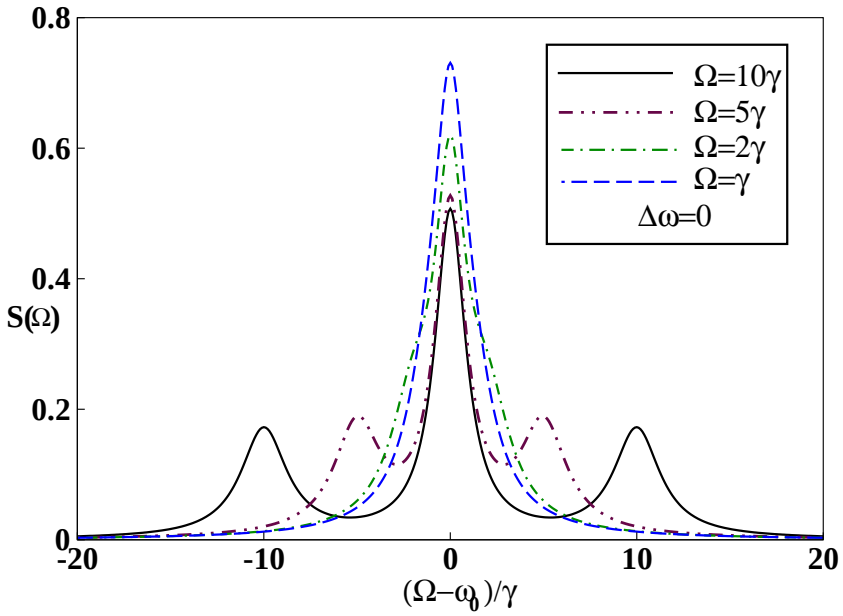

Figure 2.2: Plot of fluorescence spectrum for $\Omega = 10\gamma$, $\Omega = 5\gamma$, $\Omega = 2\gamma$ and $\Omega = \gamma$. In all cases we took $\Delta\omega = 0$. It is evident that the sidebands appear as we increase the laser intensity at the positions $\omega \pm \Omega$, with their heights in a ratio $3:1$, with respect to the central peak.

Ref.[199]. The exact solution of the Eq.(2.14) has been provided in the Ref.[61] in terms of the matrix elements of the reduced system density operator ρ^s as

$$\rho^s_{nm}(t) = e^{-i(E_n - E_m)t/\hbar} e^{i\eta(t)(E_n^2 - E_m^2)} e^{-(E_n - E_m)^2\gamma(t)} \rho^s_{nm}(0), \tag{2.16}$$

where, $\eta(t) = -\sum_j \frac{g_j^2}{\hbar^2\omega_j^2} \sin(\omega_j t)$ and $\gamma(t) = 2\sum_j \frac{g_j^2}{\hbar^2\omega_j^2} \sin^2(\omega_j t/2) \coth\left[\frac{\hbar\omega_j}{2KT}\right]$. Here, E_n defines the energy corresponding to the $n-th$ state of the system. But, interestingly one can note here, that the result is independent of the structure of the system Hamiltonian.

2.3 Mollow spectrum and Resonance fluorescence

When an tom is excited exactly on resonance, the conditions needed to apply perturbation theory are not met as the resonant light dynamically alters the eigenfunctions and eigenenergies of the atom. The original work was done by Mollow[76] and it shows that strong field resonance fluorescence from a two-level system consists of three lines. Theory of Mollow spectrum and resonance fluorescence therefore provides a very good illustration of the quantum master equation which we have discussed in Section (2.1). We are thus concerned here with a two-level atom irradiated by a strong monochromatic laser field. The experimental realization relies on the accessibility of a viable two-level quantum system by carefully restricting the optical transitions beyond the energy window of interest.

To begin with, let us choose a two-level system with characteristic frequency ω_0 driven by a classical monochromatic light field of frequency ω and coupled to an infinite number of degrees of freedom at thermal equilibrium. The system is characterized by operators σ_+, σ_- and σ_z and on the other hand, the reservoir is considered to be composed of infinite number of harmonic oscillators with characteristic frequencies ω_k and reservoir operators b_k and $b_k^\dagger$ follows the usual commutation relation $[b_k, b_j^\dagger] = \delta_{kj}$. Within this framework, the system Hamiltonian H_S and the reservoir Hamiltonian H_B assumes the form

$$H_S = \frac{1}{2}\hbar\omega_0\sigma_z, \tag{2.17}$$

$$H_B = \sum_k \hbar\omega_k b_k^\dagger b_k. \tag{2.18}$$

The system-bath interaction is given by

$$V = \sum_k \hbar(g_k^*\sigma_+ b_k + g_k\sigma_- b_k^\dagger), \tag{2.19}$$

where g_k and g_k^* are dimensionless interaction coefficients. The classical driving term in 'Rotating Wave Approximation' can be expressed as

$$V_{ext}(t) = \hbar E_0(\sigma_+ \exp(-i\omega t) + \sigma_- \exp(i\omega t)). \tag{2.20}$$

Therefore, the reduced density operator equation of motion in the Schrodinger picture becomes (see Eq.2.7)

$$\begin{aligned}\dot{\rho} = -\frac{i}{\hbar}[H_S + V_{ext}, \rho] - \int_0^t dt'\{&[\sigma_+\sigma_-'\rho'(t') - \sigma_-'\rho'(t')\sigma_+]\langle\sum_k |g_k|^2 b_k b_k^\dagger e^{-i\omega_k(t-t')}\rangle_B \\ &-[\sigma_+\rho'(t')\sigma_-' - \rho'(t')\sigma_-'\sigma_+]\langle\sum_k |g_k|^2 b_k^\dagger b_k e^{-i\omega_k(t-t')}\rangle_B\} \\ - \int_0^t dt'\{&[\sigma_-\sigma_+'\rho'(t') - \sigma_+'\rho'(t')\sigma_-]\langle\sum_k |g_k|^2 b_k^\dagger b_k e^{i\omega_k(t-t')}\rangle_B \\ &-[\sigma_-\rho'(t')\sigma_+' - \rho'(t')\sigma_+'\sigma_-]\langle\sum_k |g_k|^2 b_k b_k^\dagger e^{i\omega_k(t-t')}\rangle_B\},\end{aligned} \tag{2.21}$$

where, $(\sigma_\pm\rho(t'))' = e^{-\frac{i}{\hbar}H_s(t-t')}\sigma_\pm\rho(t')e^{\frac{i}{\hbar}H_s(t-t')}$ and, $\langle ...\rangle_B$ implies quantum statistical average of any operator X over the bath coordinates and is defined as $\langle X\rangle_B = \frac{Tr_B X e^{-H_B/KT}}{Tr_B e^{-H_B/KT}}$. In the next step we introduce the slowly varying operators as ξ_+, ξ_- and ξ_z such that $\xi_+ = \langle\sigma_+\rangle\exp(-i\omega t)$, $\xi_- = \langle\sigma_-\rangle\exp(i\omega t)$ and $\xi_z = \langle\sigma_z\rangle$. The Equations of motion for the Bloch components taking into consideration of Markov approximation are now given as:

$$\dot{\xi}_+(t) = i\Delta\omega\xi_+(t) + \frac{i}{2}E_0\xi_z(t) - \frac{\gamma}{2}(1 + 2\bar{n}(\omega_0))\xi_+(t), \tag{2.22}$$

$$\dot{\xi}_-(t) = -i\Delta\omega\xi_-(t) - \frac{i}{2}E_0\xi_z(t) - \frac{\gamma}{2}(1+2\bar{n}(\omega_0))\xi_-(t), \tag{2.23}$$

$$\dot{\xi}_z(t) = iE_0[\xi_+(t) - \xi_-(t)] - \gamma - \gamma(1+2\bar{n}(\omega_0))\xi_z(t), \tag{2.24}$$

where, $\gamma = 2\pi|g(\omega_0)|^2P(\omega_0)$, with, $P(\omega_0)$ being the frequency dependent spectral density function at the system frequency $\omega = \omega_0$ along with the detuning parameter $\Delta\omega = \omega_0 - \omega$ and $\bar{n}$ is the Bose-Einstein distribution function. This physically corresponds to the possibility of preparation of a thermal bath composed of harmonic oscillators each with two levels having a characteristic size(energy) distribution of a large width ensuring a constancy in the value of the dissipation constant γ. The actual distribution of the energy level structure of the reservoir in fact depends on the practical situation at hand. However, here we note that the set of equations (Eqs.2.22, 2.23, 2.24) are only valid under a low temperature as a high temperature condition has to be treated in a Non-Markovian way.

We arrive at the asymptotic solution of the Bloch equations as follows:

$$\xi_+(t\to\infty) = \frac{\frac{i}{2}E_0}{\gamma_0 + i\beta}\xi_z(t\to\infty), \tag{2.25}$$

$$\xi_-(t\to\infty) = \frac{-\frac{i}{2}E_0}{\gamma_0 - i\beta}\xi_z(t\to\infty), \tag{2.26}$$

$$\xi_z(t\to\infty) = -\frac{\gamma_0^2+\beta^2}{(1+2\bar{n}(\omega_0))[\frac{E_0^2}{2}+\gamma_0^2+\beta^2]}. \tag{2.27}$$

where $\beta = \Delta\omega$ and $\gamma_0 = \frac{\gamma}{2}(1+2\bar{n}(\omega_0))$.

Resonance fluorescence spectra is defined as an incoherent part of the spontaneous emission of a two-level atom irradiated by a continuous, monochromatic field[76]. It is typically characterized by one central peak, along with two side bands appearing at the strong field-induced Rabi frequency, It is formally defined as[75]

$$S(\Omega) = 2Re\left[\lim_{t\to\infty}\int_0^\infty dt' e^{-i(\Omega-\omega)t'}\langle\sigma_+(t+t')\sigma_-(t)\rangle\right]. \tag{2.28}$$

In Fig.(2.2), we show the resonance uorescence spectrum for $\Omega = 10\gamma$, $\Omega = 5\gamma$, $\Omega = 2\gamma$ and $\Omega = \gamma$. In all cases we took $\Delta\omega = 0$. It is quite striking that the sidebands appear as we increase the laser intensity at the positions $\omega \pm \Omega$, with their heights in a ratio $3:1$, with respect to the central peak.

2.4 Fermionic reservoir and Grassmann variables

A system coupled to a collection of many degrees of freedom gives a platform to study of dynamics associated quantum dissipation and decoherence over many decades[54, 200, 201]. In general, the reservoir is treated as a collection of oscillators with a predefined characteristic distribution of frequencies. But the dissipative dynamics will give drastically changed outcome if the reservoir characteristic

would have been fermionic instead of bosonic. The importance of the fermionic bath can be realized in the view of experimental evidences involving the electromagnetic trapping of fermions[202] and evaporative cooling of trapped fermions below micro-Kelvin temperature[203, 204].

This have opened up new possibilities of realizing the conditions conducive to a high-density fermionic bath. The dynamics of the fermions in a bath is guided principally by the anti-commutation rule $\{\sigma_k, \sigma_k^\dagger\} = 1$ and the following algebra:

$$\sigma_k^2 = \sigma_k^{\dagger 2} = 0, \tag{2.29}$$

$$\left[\sigma_k^\dagger, \sigma_k^\dagger \sigma_k\right] = -\sigma_k^\dagger, \tag{2.30}$$

$$\left[\sigma_k, \sigma_k^\dagger \sigma_k\right] = \sigma_k, \tag{2.31}$$

$$\left[\sigma_k^\dagger, \sigma_k\right] = 2\sigma_k^\dagger \sigma_k - 1, \tag{2.32}$$

where, $\sigma_k^\dagger(\sigma_k)$ is the creation(annihilation) operator for the $k-$th fermion. This is in sharp contrast to the bosonic case where the anti-commutator is substantiated by the commutator. The speciality of this fermionic field lies in the fact that the eigenvalues which are anti-commuting numbers obey rules of Grassmann algebra[205] which in the corresponding bosonic case are in general complex. It is due to the beauty of such algebra that one can find a close correspondence in the quasiprobability distribution and moments of various order in both cases. For the sake of clarity, we have outlined the basics of the Grassmann algebra and Grassmann calculus which are well-studied in mathematics[206] and field theory[205, 207].

Let $z = \{z_i\}, i = 1, 2, ..., n$ define a set of generators of a fermion field which satisfy anti-commutation properties $\{z_i, z_i\} = 0$, which in particular implies that the numbers are nilpotent i.e., $z_i^2 = 0$, which is an important property for fermions. The anticommuting numbers z_i and their complex conjugates z_i^* behave independently so that they satisfy $\{z_i, z_i^*\} = 0$. The Grassmann numbers also anticommute with their fermionic operators σ_i and $\sigma_i^\dagger$ such that $\{z_i, \sigma_i\} = 0$ and $\{z_i, \sigma_i^\dagger\} = 0$.

2.4.1 Grassmann Calculus

An analytic function of a Grassmann z variable gets its expression as

$$f(z) = f_0 + f_1 z. \tag{2.33}$$

As a square of any Grassmann number vanishes, any analytic function must be linear in the Grassmann variable. Now, if we have two generators z and z^*, then any two-variable function will have the general form

$$A(z, z^*) = a_0 + a_1 z + \bar{a}_1 z^* + a_{12} z^* z. \tag{2.34}$$

Even and Odd functions

A function $\phi(z)$ is said as even when it commute with Grassmann varibales and odd when it anticommutes. So, for a function having even parity

$$\phi(-z) = \phi(z), \tag{2.35}$$

whereas, that for a function having odd parity,

$$\phi(-z) = -\phi(z). \tag{2.36}$$

Differentiation and Integration with Grassmann variables

The variable z(or z^*) has to be on the right next to the operator $\frac{\partial}{\partial z}$(or $\frac{\partial}{\partial z^*}$) while performing differentiation with Grassmann variables. If it is not the case, then it has to be anticommuted through the relation $zz^* + z^*z = 0$.Thus

$$\frac{\partial}{\partial z}(z^*z) = \frac{\partial}{\partial z^*}(-zz^*) = -z^*. \tag{2.37}$$

Therefore, for the double derivative of a function of Grassmann variables, we should have[see Eq.(2.34)]

$$\frac{\partial^2}{\partial z^* \partial z} A(z, z^*) = -\frac{\partial^2}{\partial z \partial y^*} A(z, z^*), \tag{2.38}$$

so that $\{\frac{\partial}{\partial z^*}, \frac{\partial}{\partial z}\} = 0$.

Again, in case of integration[205], the fundamental rules involving the complex Grassmann variables are as follows:

$$\int dz = 0, \tag{2.39}$$

$$\int dz^* = 0, \tag{2.40}$$

$$\int dzz = 1, \tag{2.41}$$

$$\int dz^*z^* = 1. \tag{2.42}$$

We are typically concerned with pairs of anticommuting variables z and z^*, and for such pairs we have $\int d^2z = \int dz^*dz$.

2.5 Coherent states

The idea of coherent states was first conceived by Schrodinger[208] and later retold and popularized by Glauber[119] as a very close approximation of a classical state in the quantum domain. It is a purely quantum mechanical state that allows us to have a "classical" flavour in a host of quantum situations. In this section, we will briefly outline the basic features of the bosonic and fermionic coherent states.

2.5.1 Bosonic coherent state

The bosonic coherent states were formally introduced by Glauber and Sudarshan[119] which is defined as the eigenstate $|\alpha\rangle$ of the harmonic oscillator annihilation operator a. For a single mode, we have

$$a|\alpha\rangle = \alpha|\alpha\rangle, \tag{2.43}$$

where, α is a complex number. Now, if we expand $|\alpha\rangle$ in the Fock-state basis as $|\alpha\rangle = \sum_{n=0}^{\infty} c_n|n\rangle$, where $c_n = \langle n|\alpha\rangle$ is the transformation between the number and the coherent state representation, and operate a on $|\alpha\rangle$, then keeping in mind that $a|n\rangle = \sqrt{n-1}|n-1\rangle$, we have

$$a|\alpha\rangle = \sum_{n=1}^{\infty} c_n\sqrt{n}|n-1\rangle = \sum_{n=0}^{\infty} \alpha c_n|n\rangle. \tag{2.44}$$

After doing a straight forward algebra[56, 55], one can express the coherent state as an expansion of the number basis as

$$|\alpha\rangle = e^{-\frac{1}{2}|\alpha|^2} \sum_{n=0}^{\infty} \frac{\alpha^n}{\sqrt{n!}}|n\rangle. \tag{2.45}$$

Here, one should note that the squared modulus of the quantity c_n which is $|\langle n|\alpha\rangle|^2$ defines the probability distribution of the system over the number states, which happens to be Poissonian[56]. Here, we digress a little on some properties of the bosonic coherent state.

Bosonic coherent states are not orthogonal

To show, the orthogonality of the bosonic coherent states, we consider the quantity[see Eq.(2.45)] $\langle\beta|\alpha\rangle$ which gets its expression as

$$\langle\beta|\alpha\rangle = \exp\left[-\frac{1}{2}(|\alpha|^2 + |\beta|^2) + \alpha\beta^*\right]. \tag{2.46}$$

Evidently, the states are not orthogonal as $\langle\beta|\alpha\rangle \neq 0$ and the quantity $|\langle\beta|\alpha\rangle|^2$ would be non-zero for $\alpha \neq \beta$. Interstingly, it is to be noted that, as $|\alpha - \beta|^2$ increases, the two states become approximately orthogonal.

Bosonic coherent states are overcomplete

To show the overcompleteness of the bosonic coherent state space, we evaluate the integral $\int |\alpha\rangle\langle\alpha|\frac{d^2\alpha}{\pi}$ and for that purpose, we change to polar co-ordinates with $\alpha = x+iy = re^{i\theta}$ so that $d^2\alpha = dxdy = rdrd\theta$. Thus the integral in polar coordinate becomes

$$\int |\alpha\rangle\langle\alpha|\frac{d^2\alpha}{\pi} = \sum_{n,m=0}^{\infty} \frac{|n\rangle\langle m|}{\pi\sqrt{n!m!}} \int_0^{\infty} rdre^{-r^2}r^{n+m} \int_0^{\infty} d\theta e^{i(n-m)\theta}. \tag{2.47}$$

Noting that $\int_0^{2\pi} d\theta e^{i(n-m)} = 2\pi\delta_{nm}$ and $\int_0^{\infty} rdre^{-r^2}r^{2n} = 1$, one can obtain that

$$\int |\alpha\rangle\langle\alpha|\frac{d^2\alpha}{\pi} = 1, \tag{2.48}$$

which proves normalization of the bosonic coherent states.

Bosonic coherent states are minimum uncertainty states

From the relations between the annihilation(creation) operator $a(a^\dagger)$ and the position x and momentum p for the coherent state $|\alpha\rangle$, we get the following equations for the coherent state[56]

$$\langle x\rangle = \sqrt{\frac{\hbar}{2\omega}}\langle\alpha|a + a^\dagger|\alpha\rangle = \sqrt{\frac{\hbar}{2\omega}}(\alpha + \alpha^*), \tag{2.49}$$

$$\langle p\rangle = i\sqrt{\frac{\hbar\omega}{2}}\langle\alpha|a^\dagger - a|\alpha\rangle = i\sqrt{\frac{\hbar\omega}{2}}(\alpha^* - \alpha), \tag{2.50}$$

$$\langle x^2\rangle = \frac{\hbar}{2\omega}(\alpha^{*2} + \alpha^2 + 2\alpha^*\alpha + 1), \tag{2.51}$$

$$\langle p^2\rangle = -\frac{\hbar\omega}{2}(\alpha^{*2} + \alpha^2 - 2\alpha^*\alpha - 1), \tag{2.52}$$

where, ω is the frequency of the respective harmonic oscillator mode and α is a complex number which is the eigenvalue of the annihilation operator a. The uncertainty product thus becomes

$$\Delta p\Delta x = \frac{\hbar}{2}, \tag{2.53}$$

where, $\Delta p = \sqrt{\langle p^2\rangle - \langle p\rangle^2}$ and $\Delta x = \sqrt{\langle x^2\rangle - \langle x\rangle^2}$. Thus the coherent state corresponds to the quantum state having minimum uncertainty product. Herein lies the beauty of the coherent states, that they represent a very good approach to the classical state which can be realized in the quantum domain.

2.5.2 Fermionic coherent state

The formulation of the fermionic coherent states that we follow here is due to Cahill and Glauber[147]. According to them, for any set of Grassmann variables $\gamma = \{\gamma_i\}$, the normalized fermionic coherent state is expressed as a displaced vacuum state

$$|\gamma\rangle = D(\gamma)|0\rangle, \tag{2.54}$$

where, $D(\gamma)$ is the fermionic displacement operator[147] defined as

$$D(\gamma) = e^{a^\dagger\gamma - \gamma^* a} = 1 + (a^\dagger\gamma - \gamma^* a) + (a^\dagger a - \frac{1}{2})\gamma^*\gamma, \tag{2.55}$$

where a and $a^\dagger$ are the spin step down and step-up operators such that $a|1\rangle = |0\rangle$ and $a^\dagger|0\rangle = |1\rangle$, respectively with the anticommutaion relation $\{a, a^\dagger\} = 1$. For any

mode i, γ_i and γ_i^* are Grassmann numbers. Now, using the product formula[147]

$$D(\alpha_i)D(\beta_i) = D(\alpha_i + \beta_i)e^{\frac{\beta_i^*\alpha_i - \alpha_i^*\beta_i}{2}}, \tag{2.56}$$

and the standard result[147]

$$D_k(\lambda_k)|0\rangle_k = (1 - \frac{1}{2}\lambda_k^*\lambda_k)|0\rangle_k + \lambda_k|1\rangle_k, \tag{2.57}$$

and,

$$D_k(\lambda_k)|1\rangle_k = -\lambda_k^*|0\rangle_k + (1 + \frac{1}{2}\lambda_k^*\lambda_k)|1\rangle_k, \tag{2.58}$$

one obtains,

$$|\gamma\rangle = \exp\left(\sum_i (a_i^\dagger\gamma_i - \frac{1}{2}\gamma_1^*\gamma_i)\right)|0\rangle. \tag{2.59}$$

It may be worth emphasizing that in this formula the creation operator $a^\dagger$ stands to the left of the Grassmann number γ_i . Apart from these ordering considerations, this formula takes a form closely analogous to the one that defines bosonic coherent states.

Fermionic coherent state provides an unambiguous description of the fermionic states in terms of number basis. Thus any fermionic state $|\psi\rangle$ can be expressed as[147]

$$|\psi\rangle = \sum_{\{n\}} c(n_1, n_2, ...)a_{n_1}^\dagger a_{n_2}^\dagger ....|0\rangle, \tag{2.60}$$

which in the coherent state representation reads

$$\langle\alpha|\psi\rangle = \exp\left(-\frac{1}{2}\sum_n \alpha_n^*\alpha_n\right) \times \sum_{\{n\}} c(n_1, n_2, ...)\alpha_{n_1}^*\alpha_{n_2}^*.....\alpha_{n_m}^*. \tag{2.61}$$

Here we note that the expression is devoid of any ambiguity or extra minus signs. Since coherent states are dened in terms of bilinear forms in anticommuting variables, there is no need to adopt a standard ordering of the modes.

2.6 Quasiprobability distribution functions

In this section, we have given a very brief description of various quasiprobability distribution functions for both bosonic and fermionic cases.

2.6.1 P-distribution function

The Glauber-Sudarshan $P-$distribution function for bosons was introduced primarily for the description of statistical mixtures of coherent states, which is the closest approach within the quantum theory to the states of the electromagnetic field described by classical theory of optics.

The definition of the $P-$distribution[55] function relies on the fact that the coherent states are not orthogonal, as we have seen and they forms an over-complete basis so that it is possible to expand the density operator ρ as a diagonal sum over the coherent states:

$$\rho = \int d^2\alpha |\alpha\rangle\langle\alpha| P(\alpha). \tag{2.62}$$

The appeal of the $P-$distribution function $P(\alpha)$ is due to a number of reasons. At first, from the very appearance of the Eq.(2.62), it is clear that $\int d^2\alpha P(\alpha) = 1$ which makes $P(\alpha)$ to play the role of a classical probability distribution function. Secondly, the expectation values of operators written in the normal order can be calculated in the way that averages are calculated in the classical statistics, with $P(\alpha)$ playing the role of probability distribution. Thus $\langle a^{\dagger p} a^q\rangle \equiv \int d^2\alpha P(\alpha)\alpha^{*p}\alpha^q$. The most important property in this regard is that in order to define probabilities corresponding to number states, the complete representation requires some non-zero numbers $\rho_{n,m}$ in addition to $\rho_{n,n}$, but if we take refuge to $P-$distribution, it offers a way so that we get $\langle\alpha|\rho|\beta\rangle = \int d^2\lambda e^{-\frac{1}{2}|\lambda-\alpha|^2} e^{-\frac{1}{2}|\lambda-\beta|^2} P(\lambda)$, where we have no need for this to vanish when $\alpha \neq \beta$. Since $e^{-\frac{1}{2}|\lambda-\alpha|^2}$ is not a $\delta-$function, $\langle\alpha|\rho|\alpha\rangle \neq P(\alpha)$, in classical sense. Only when $P(\lambda)$ is sufficiently broad in comparison to the Gaussian filter inside the integral, it approximately represents a probability function. Hence, it is better to use quasi-distribution instead of distribution function for $P(\alpha)$.

2.6.2 Q-distribution function

Another representation that is defined in terms of the characteristic function that gives operator averages in the antinormal order is the $Q-$distribution function.

The $Q-$distribution function $Q(\alpha, \alpha^*)$ is defined as the Fourier transform of the characteristic function for the normal ordered average $\chi_A(z, z^*) \equiv Tr(\rho e^{iza} e^{iz^* a^\dagger})$. It is defined formally as

$$Q(\alpha, \alpha^*) = \frac{1}{\pi^2} \int d^2 z \chi_A(z, z^*) e^{-iz^*\alpha^*} e^{-iz\alpha}. \tag{2.63}$$

The noticeable features one gets for the $Q-$distribution function are: (i) It defines a clear correspondence to the antinormally ordered operator average such that $\langle a^p a^{\dagger p}\rangle = \int d^2\alpha Q(\alpha, \alpha^*)\alpha^{*p}\alpha^q$. (ii) The $Q-$distribution function has a very simple relationship to the coherent states such $Q(\alpha, \alpha^*) = \frac{1}{\pi}\langle\alpha|\rho|\alpha\rangle$. Thus $\pi\langle\alpha|\rho|\alpha\rangle$ is the diogonal matrix element of the density operator considered in the coherent state basis $|\alpha\rangle$ and hence it is directly related to the classical probability of finding the system in the coherent state $|\alpha\rangle$. The relation between the $Q-$ and $P-$distribution function is expressed as[55]

$$Q(\alpha, \alpha^*) = \frac{1}{\pi} \int d^2\lambda e^{-|\lambda-\alpha|^2} P(\lambda). \tag{2.64}$$

2.6.3 Wigner distribution function and non-classicality

The first quasiprobability distribution function for the electromagnetic field which is bosonic in nature was introduced by Wigner[192], to study quantum correlations to the classical statistical mechanics. We will designate the Wigner distribution by $W(\alpha, \alpha^*)$.

We define the Wigner function $W(\alpha, \alpha^*)$ as the Fourier transform of the symmetric characteristic function $\chi_s(z, z^*)$ as

$$W(\alpha, \alpha^*) = \frac{1}{\pi^2} \int d^2 z \chi_s(z, z^*) e^{-iz^*\alpha^*} e^{-iz\alpha}, \tag{2.65}$$

where, $\chi_s(z, z^*) \equiv Tr(\rho e^{iz^* a^\dagger + iza})$. It can be shown that[55, 192]

$$e^{iz^* a^\dagger + iza} = \sum_{n,m=0} \frac{(iz^*)^n (iz)^m}{n!m!} (a^{\dagger n} a^m)_s, \tag{2.66}$$

where, $(a^{\dagger n} a^m)_s$ denotes the operator product written in symmetric order-the average of $(n+m)!/(n!m!)$ possible orderings of n-creation and $m-$annihilation operators.

Wigner function can be alternatively represented[209] in terms of the quantum jump of a system from state $|x'\rangle$ corresponding to position $x' = x - \frac{1}{2}\xi$ to the state $|x''\rangle$ corresponding to $x'' = x + \frac{1}{2}\xi$ through the density operator ρ as

$$W(x, p) = \frac{1}{2\pi\hbar} \int_{-\infty}^{\infty} d\xi \exp(-\frac{i}{\hbar} p\xi) \langle x + \frac{1}{2}\xi | \rho | x - \frac{1}{2}\xi \rangle, \tag{2.67}$$

where, p is the momentum associated with the quantum jump. The most important property is the normalization $\int dx \int dp W(x, p) = 1$ which ensures that x and p are $c-$numbers and not operators. Here, we discuss a remarkable property of the Wigner function in association with the non-classicality of the quantum state. For two field operator having densities ρ_1 and ρ_2 such that $Tr(\rho_1 \rho_2) = 0$, the condition is $\int dx \int dp W_{\rho_1}(x, p) W_{\rho_2}(x, p) = 0$, which implies that either of the two Wigner functions must take upon negative values which is evidently a signature of non-classicality. This surprising feature makes it impossible to interpret the Wigner function as a true probability distribution in a classical sense. Nevertheless, the Wigner function is useful to calculate quantum mechanical expectation values[55]. We carefully state that this condition rigorously holds for two orthogonal states. We also mention that this is closely related to the Hudson-Piquet theorem which states that the only non-negative Wigner function is a Gaussian distribution which is true for coherent states[56, 55]. To illustrate this feature, we consider[55] the expression of the Wigner function $W(x, p)$ for a harmonic oscillator number state $|n\rangle$ as

$$W(x, p) = \frac{2}{\pi} \frac{1}{n!} e^{-2|\alpha|^2} \sum_{k=0}^{n} (-1)^{n-k} \frac{(n!)^2}{(k!)^2 (n-k)!} |2\alpha|^{2k}, \tag{2.68}$$

where, $\alpha = x + ip$. The Eq.(2.68) represents an ordinary, well behaved function but it clearly violates one of the conditions required of a probability distribution i.e., it need not to be positive. This feature is clearly revealed in Fig.(2.3).

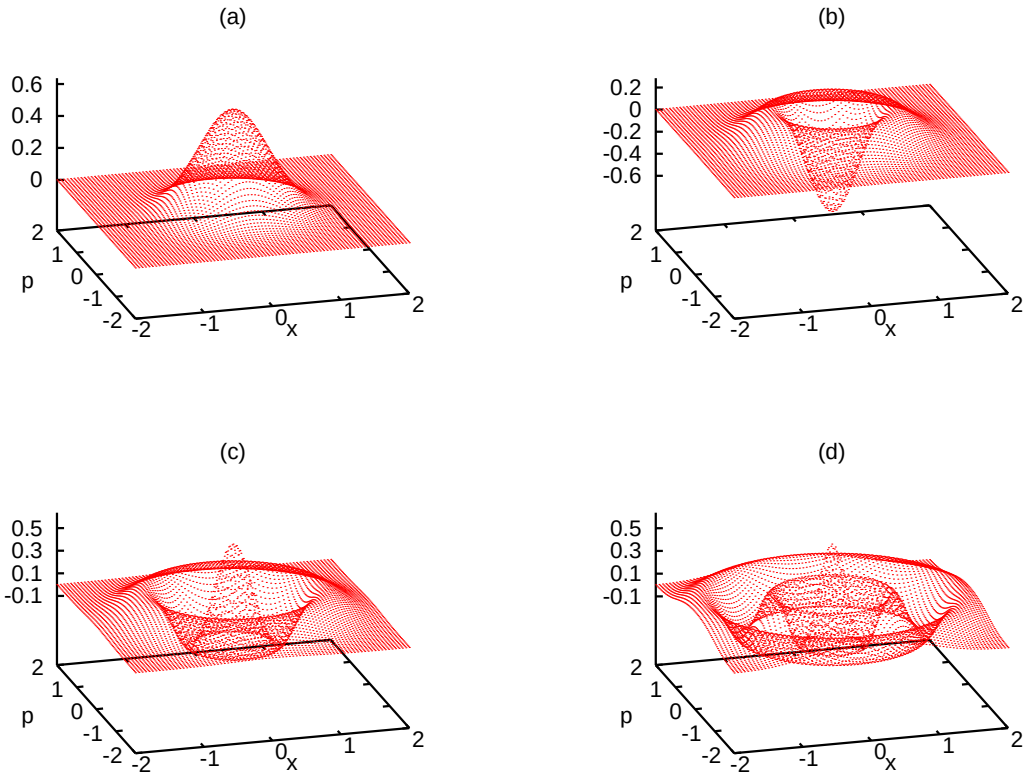

Figure 2.3: 3D plots of the Wigner function $W(x,p)$ for harmonic oscillator Fock states $|n\rangle$.Fig(a) shows the plot for $n = 0$, Fig(b) shows for $n = 1$, whereas Fig(c) and Fig(d) shows the plot for $n = 2$ and $n = 4$ respectively. Here, we can clearly see that for $n \neq 0$ the Wigner function $W(x,p)$ assumes negative value in the phase space indicating signatures of non-classicality.

2.6.4 Wigner function matrix

Wigner function matrix[178] is the extended form of Wigner function to describe the composite system including the electronic degrees of freedom. As the Wigner function is defined for the vibrational degrees of freedom, it cannot describe the entangled electronic motion of a system (molecule) with the vibrational motion. In this context Wigner function matrix is useful for the complete description of the entangled motion[178]. By appropriate measuring techniques[210, 211, 212, 213] the Wigner function matrix can be an index of quantum interference and one can realize the quantum state of a given system. The Wigner function matrix for a superposed state can be expressed as[178],

$$W_{ij}(x,p) = \frac{2}{\pi} Tr\left[\rho|j\rangle\langle i|\hat{D}(\alpha)(-1)^{a^\dagger a}\hat{D}^\dagger(\alpha)\right], \tag{2.69}$$

where, $\hat{D}(\alpha)$ is the Glauber's displacement operator and the electronic flip operator $|j\rangle\langle i|$ gives rise to transition from state $|i\rangle$ to state $|j\rangle$. When the total density operator is expressed as the product of the electronic and vibrational density operators as $\rho = \rho_{el} \otimes \rho_{vib}$, then all of the Wigner function matrix elements become identical in shape irrespective to the electronic indices i, j. They are solely determined by the vibrational Wigner function $W(x,p)$ with the electronic density matrix elements being simple weighting factors. Hence in specific cases, the electronic-vibrational entanglement can be detected by inspecting The Wigner function matrix.

For illustration, we give the expressions of Wigner function matrix elements for an entangled state called the Schrodinger-cat states[74, 214]. It is a quantum superposition of two coherent states, $|\pm\alpha\rangle$ with amplitudes α and $-\alpha$, entangled with the upper and lower electronic states, respectively, expressed as

$$|\psi\rangle = \frac{1}{\sqrt{2}}\left(|\alpha\rangle|2\rangle - |-\alpha\rangle|1\rangle\right). \tag{2.70}$$

The explicit expressions of the Wigner function matrix elements are[178]

$$W_{11}(\beta) = \frac{1}{\pi}\exp(-2|\alpha+\beta|^2), \tag{2.71}$$

$$W_{22}(\beta) = \frac{1}{\pi}\exp(-2|\beta-\alpha|^2), \tag{2.72}$$

$$W_{12}(\beta) = -\frac{1}{\pi}\exp(-2|\beta|^2)\exp(-2(\alpha\beta^* - \alpha^*\beta)). \tag{2.73}$$

For an entangled state, the Wigner function matrix elements are generally of different shape for different electronic indices as expressed in the above equations for the entangled cat state. On the other hand, for a state that can be written as a direct product state, say, of electronic and vibrational degrees of freedom containing no entanglement, the Wigner function matrix elements look all the same independent of the electronic indices. Hence in suitable cases the Wigner function matrix can be an indicator of vibronic entanglement.

Here we will give the detailed derivation of $W_{12}(\beta)$. Other elements are derived similarly. The total density operator is ρ and we take the trace in Eq.(2.69)(with $i = 1, j = 2$) over the vibrational degrees of freedom in the number state ($|n\rangle$) basis and also trace over the electronic degrees of freedom. An important relation which is required in this regard is the matrix element of the displacement operator $D(\alpha)$ in the number state basis. They are given by

$$D_{mn}(\alpha) = \exp(-|\alpha|^2/2)(\alpha)^{m-n}\left(\frac{n!}{m!}\right)^{1/2} L_n^{m-n}(|\alpha|^2), \tag{2.74}$$

where $L_n^{m-n}(|\alpha|^2)$ denotes the associated Laguerre polynomial with m, n being positive integers including zero. The next relation one should know the expressions for the summations containing products of the associated Laguerre polynomials. A general expression is provided as[215],

$$\sum_{k_1=0}^{\infty}\sum_{k_2=0}^{\infty}...\sum_{k_{p-1}=0}^{\infty} A_2^{k_1}A_3^{k_2}...A_p^{k_{p-1}}L_{k_1}^{m-k_1}(\chi_1)L_{k_2}^{k_1-k_2}(\chi_2)...L_{k_{p-1}}^{k_{p-2}-k_{p-1}}(\chi_{p-1})L_n^{k_{p-1}-k_n}(\chi_p)$$

$$= \frac{A_p^n}{A_1^m}\left(\sum_{i=1}^{p}A_i\right)^{m-n}\exp\left[-\sum_{l=1}^{p-1}\frac{\chi_l}{A_l}\sum_{i=l+1}^{p}A_i\right]$$

$$\times L_n^{m-n}\left[\sum_{j=1}^{p}\chi_j+\sum_{l=1}^{p-1}\frac{\chi_{l+1}}{A_{l+1}}\sum_{i=1}^{l}A_i+\sum_{l=1}^{p-1}\frac{\chi_l}{A_l}\sum_{i=l+1}^{p}A_i\right], \tag{2.75}$$

where, $A_j=\prod_{i=1}^{j}A_i$ and A_i and χ_i are independent and, in general, complex. For the calculation of the Wigner function matrix elements, we need the case of $p=2$ of the above expression as given below

$$\sum_{k_1=0}^{\infty}A_2^{k_2}L_{k_1}^{m-k_1}(\chi_1)L_n^{k_1-n}(\chi_2)=A_2^m\left(\frac{1+A_2}{A_2}\right)^{m-n}e^{-\chi_2A_2}L_n^{m-n}\left[\chi_1+\chi_2+\chi_1A_1+\frac{\chi_2}{A_2}\right]. \tag{2.76}$$

For $n=0$, we get

$$\sum_{k_1=0}^{\infty}A_2^{k_1}L_{k_1}^{m-k_1}(\chi_1)=(1+A_2)^me^{-\chi_1A_2}. \tag{2.77}$$

Now we return to the calculation of $W_{12}(\beta)$ for the entangled Schrodinger-cat state given in Eq.(2.70). Taking the trace in Eq.(2.69) we obtain

$$W_{12}(\beta)=-\frac{1}{\pi}\sum_{m=1}^{\infty}\langle m|-\alpha\rangle\langle\alpha|D(\beta)(-1)^{a^\dagger a}D(-\beta)|m\rangle$$

$$=\frac{1}{\pi}e^{-|\alpha|^2}\sum_{m,n}\frac{(-\alpha)^m}{\sqrt{m!}}\frac{(\alpha^*)^n}{\sqrt{n!}}\sum_k(-1)^kD_{nk}(\beta)D_{km}(-\beta)$$

$$=-\frac{1}{\pi}e^{-(|\alpha|^2+|\beta|^2)\sum_{m,n}(-\alpha)^m}\frac{(\alpha^*)^n}{n!}\beta^{n-m}(-1)^m\sum_k L_k^{n-k}(|\beta|^2)L_m^{k-m}(|\beta|^2)$$

$$=-\frac{1}{\pi}e^{-(|\alpha|^2+2|\beta|^2)}\sum_n\frac{(2\alpha^*\beta)^n}{n!}\sum_m\left(\frac{\alpha}{2\beta}\right)^m L_m^{n-m}(4|\beta|^2)$$

$$=-\frac{1}{\pi}e^{-(|\alpha|^2+2|\beta|^2)}\sum_n\frac{(2\alpha^*\beta)^n}{n!}\left(1+\frac{\alpha}{2\beta}\right)^n e^{-2\alpha\beta^*}$$

$$=-\frac{1}{\pi}\exp(-2|\beta|^2)\exp(-2(\alpha\beta^*-\alpha^*\beta)). \tag{2.78}$$

The second step of the above derivation follows from Eq.(2.45) keeping in mind that $\langle n|\alpha\rangle = \exp(-|\alpha|^2/2)\frac{\alpha^n}{\sqrt{n!}}$. The third step uses Eq.(2.74). The fourth and fifth steps use Eq.(2.76) and Eq.(2.77), respectively. The final step follows from simple algebra.

2.6.5 Fermionic quasiprobability distribution functions

For fermionic systems, the $s-$ordered characteristic function $\chi(\xi, s)$ is defined[147] as

$$\chi(\xi, s) = \chi(\xi) \exp\left(\frac{s}{2}\sum_n \xi_n^* \xi_n\right), \tag{2.79}$$

where, the characteristic function $\chi(\xi) = Tr\left[\rho \exp\left(\sum_n \xi_n a_n^\dagger - a_n \xi_n^*\right)\right]$ is the Fourier transform of the density operator ρ and ξ_n and ξ_n^* are Grassmann numbers corresponding to the $n-$th fermion. Incidentally, $\chi(\xi, s)$ is an even function having even parity such that

$$\chi(-\xi, s) = \chi(\xi, s). \tag{2.80}$$

Here, a little digression regrading the ordering parameter s following Ref.[147] is helpful for further understanding. s is a real ordering parameter that runs from -1 for antinormal ordering to 1 for normal ordering. $s = 0$ refers to the symmetrically ordered product of the operator.

The $s-$ordered quasiprobability distribution $W(\alpha, s)$ is the Fourier transform of the function $\chi(\xi, s)$ as

$$W(\alpha, s) = \int d^2\xi \chi(\xi, s) \exp\left(\alpha_n \xi_n^* - \xi_n \alpha_n^*\right). \tag{2.81}$$

As density operators ρ must be physical operators, $W(\alpha, s)$ is also an even function of even parity like $\chi(\xi, s)$. For $s = -1$, we have

$$W(\alpha, -1) = \int d^2\beta \delta(\alpha - \beta)\langle\beta|\rho|-\beta\rangle = \langle\alpha|\rho|-\alpha\rangle, \tag{2.82}$$

where, we have used the relation

$$\delta(\xi - \zeta) \equiv \int d^2\alpha \exp\left(\sum_n [\alpha_n(\xi_n^* - \zeta_n^*) - (\xi_n - \zeta_n)\alpha_n^*]\right). \tag{2.83}$$

From the Eq.(2.82), we get the fermionic analog of the $Q-$distribution function. It is therefore, the weight function that gives the mean values of the antinormally ordered products of creation and annihilation operators in terms of integrals of the corresponding products of Grassmann numbers.

The fermionic analog of the $P-$distribution function is nothing but $W(\alpha, 1)$ which is formally defined[147] as

$$\rho = \int d^2\alpha P(\alpha)|\alpha\rangle\langle-\alpha|. \tag{2.84}$$

The significance of the fermionic $P-$distribution lies in the fact that it can be is formally used to compute average values for the normally ordered product.

2.7 Glauber-Lachs state

In this section, we briefly describe the main features of thermocoherent state of Glauber and Lachs[99]. A thermocoherent state for a bosonic field is a superposition of the thermal and coherent states. The construction of the density operator corresponding to bosonic thermocoherent state involves linear superposition of the thermal and coherent state $P-$distribution functions.

For a thermal state[119] the diagonal density matrix element comes out as

$$\rho_{nn}^{th} = \frac{\bar{n}_T^n}{(\bar{n}_T + 1)^{n+1}}, \tag{2.85}$$

where $\bar{n}_T$ is the average thermal occupation number given by the Bose-Einstein distribution function

$$\bar{n}_T = \frac{1}{e^{\frac{\hbar\omega}{KT}} - 1}, \tag{2.86}$$

and the corresponding quasiprobability function for thermal state is given by

$$P(\alpha)^{th} = \frac{1}{\pi\bar{n}_T} \exp(-\frac{|\alpha|^2}{\bar{n}_T}), \tag{2.87}$$

with ω being the frequency of the respective mode.

Construction of a bosonic thermocoherent state or Glauber-Lachs(GL)-state[99, 216] involves the superposition of the thermal as well as coherent field by using the formula

$$P(\alpha) = \int P_1(\alpha')P_2(\alpha - \alpha')d^2\alpha'. \tag{2.88}$$

The expression for the $P-$distribution of a single mode bosonic thermocoherent field is given by

$$P(\alpha) = \frac{1}{\pi\bar{n}_T^B} \exp(-\frac{|\alpha - \beta|^2}{\bar{n}_T}). \tag{2.89}$$

The resultant expression for the $P-$distribution of a single mode bosonic thermocoherent state is given by

$$P(\alpha)^{GL} = \frac{1}{\pi\bar{n}_T} \exp(-\frac{|\alpha - \beta|^2}{\bar{n}_T}), \tag{2.90}$$

along with the probability of the photon number distribution as[99, 216, 217]:

$$\rho_{nn}^{GL} = \langle n|\rho^{GL}|n\rangle = \frac{\bar{n}_T^n}{(1 + \bar{n}_T)^{1+n}} \exp\left(-\frac{\bar{n}_c}{1 + \bar{n}_T}\right) L_n\left(-\frac{\bar{n}_c}{\bar{n}_T(\bar{n}_T + 1)}\right), \tag{2.91}$$

where, $\bar{n}_T$ and $\bar{n}_c$ are the thermal-average and coherent-average population, respectively and L_n is the Laguerre polynomial[215, 218] expressed as:

$$L_n(x) = \sum_{i=0}^{n} (-x)^i \frac{n!}{(i!)^2(n-i)!}. \tag{2.92}$$

The mean and variance of the average photon number distribution has also been calculated[119], respectively as

$$\bar{n} = \bar{n}_T + \bar{n}_c, \tag{2.93}$$

and

$$\sigma_n^2 = 2\bar{n}_T\bar{n}_c + \bar{n}_c + \bar{n}_T + \bar{n}_T^2, \tag{2.94}$$

where $\bar{n}_c = |\alpha|^2$, the coherent photon population.

Glauber-Lachs(GL)[119, 217, 219] photon distribution of a single mode field interpolates between the Poissonian and thermal distributions. When the coherent-average excitation number $\bar{n}_c$ vanishes, the distribution becomes a thermal one, i.e,

$$\lim_{\bar{n}_c \to 0} \rho_{nn}^{GL} = \frac{\bar{n}_T^n}{(1+\bar{n}_T)^{n+1}}. \tag{2.95}$$

Similarly when the thermal-average excitation number, $\bar{n}_T$ vanishes the distribution becomes Poissonian, i.e,

$$\lim_{\bar{n}_T \to 0} \rho_{nn}^{GL} = e^{-\bar{n}_c} \frac{\bar{n}_c^n}{n!}. \tag{2.96}$$

GL state[219] can be obtained if an external Gaussian pulse of light excites a cavity mode initially in a thermal distribution and then a thermalization takes place before considering the mode exchanges its energy with other system. In the appropriate limits, i.e, for coherent state, $\bar{n}_T = 0$, the variance becomes, $\sigma_n^2 = \bar{n}_c$ and for thermal states, $\bar{n}_c = 0$, the variance becomes $\sigma_n^2 = \bar{n}_T(\bar{n}_T + 1)$. In Equation (2.94), the first term shows the combined effect from the thermal as well as coherent field, while that of the third and fourth term, arise solely due to thermal field.

2.8 Electron transport

When a quantum system is coupled to two electron leads with different electrochemical potential, the electrons will flow through the system in response to the potential difference and a current can be measured for the mesoscopic structure of interest. This section is dedicated to give a very brief overview of the Landauer-Buttiker formula for current associated with the electron transport and also the transport in the Coulomb-Blockade regime. But at first, we have provided a very brief discussion regarding quantum electron transport in general through.

To illustrate, we consider a small device which is a quantum system comprising of only one energy level in the range of interest. The maximum conductance of the

channel is related to the charge of an electron and Planck's constant: $G_0 = \frac{e^2}{h} = 38.7\mu S$. Actually, small channels typically consists of two levels (one for up spin and one for down spin) at the same energy (degenerate levels) making the maximum conductance equal to $G = 2G_0$. This is known as quantum of conductance. It is here carefully noted that the conductance quantum does not mean that the conductance of any system must be an integer multiple of G. Instead, it describes the conductance of two quantum channels (one channel for spin-up and one channel for spin-down). If the probability for transmitting an electron that enters the channel is unity, then transport through the channel is *ballistic*. The term specifically means that the electron transport is devoid of any scattering. On the other hand, if the transmission probability is less than unity, then the conductance of the channel is less than the requisite value. The total conductance of a system thus is equal to the sum of the conductances of all the parallel quantum channels that make up the system[6]. In this regard, one can recall the Landauer formula[5] as $G = \frac{2e^2}{h}T$,

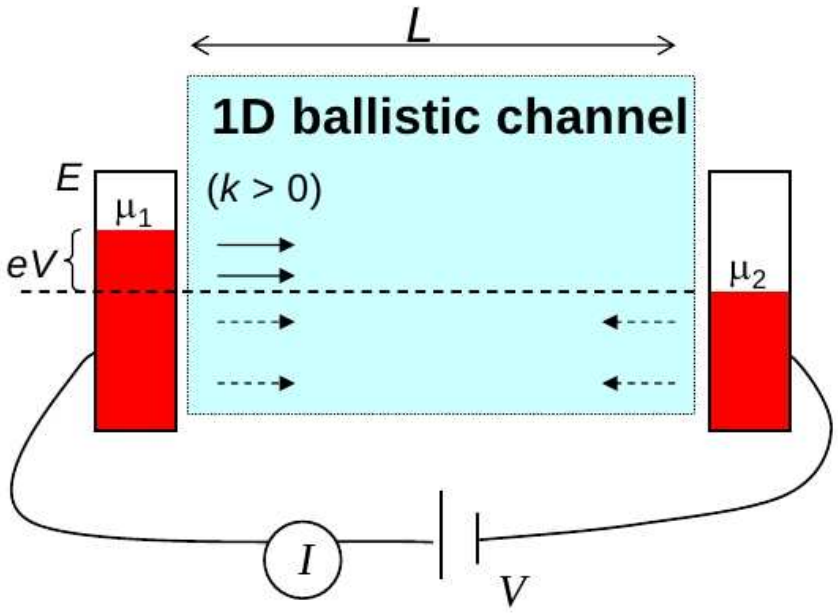

Figure 2.4: Schematic presentation of a system where electron transport in considered through a 1-dimensional channel. The source and sink electron leads are different in respect to the electrochemical potentials.

where T is the transmission probability. It can be shown that at finite temperature, the conductance formula assumes the expression

$$G(E_F, T) = \frac{2e^2}{h} \sum_n f(E_n - E_F), \tag{2.97}$$

where, $f(E_F) = \left[\exp\left(\frac{E-E_F}{KT}\right) + 1\right]^{-1}$ is the Fermi-Dirac distribution function. This formula is not strictly valid to consider molecular conductances. Molecular conductance is largely dependent on the surrounding conditions (e.g., pH, temperature, pressure), as well as the properties of molecule including electron-electron and

electron-nuclear coupling parameters. In the context, of the present thesis as we have primarily considered the molecular electronic transport problem, as an overview we have given a brief discussion of the Landauer-Buttiker formalism which is explicitly considered in the Chapter-5 and the Coulomb-Blockade system whose effect in terms of vibrational modes of the molecular system is considered in the Chapter-6.

2.8.1 Landauer-Buttiker formalism

The flow of current is traditionally considered in terms of the scattering approach, which is also known as Landauer approach. Here, the transport properties of the system are related to its scattering properties, which are assumed to be known from quantum mechanical calculations. In its traditional form, the method is applicable to non-interacting systems in the stationary regime[220]. The derivation we give here essentially follows from Refs.[5, 96, 221].

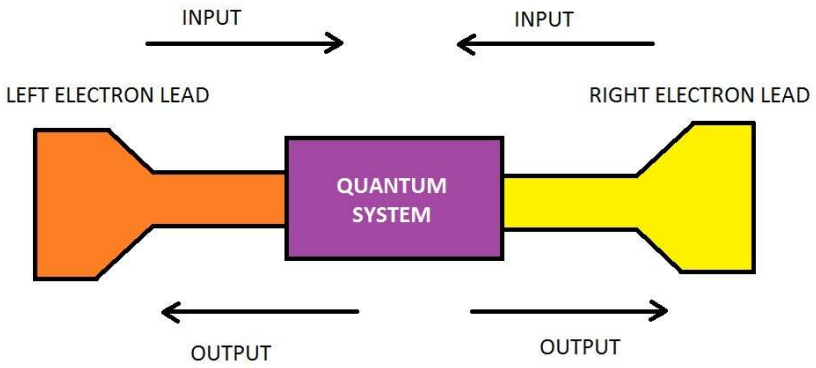

Figure 2.5: Schematic presentation of a system where electron transport in considered as 2-terminal scattering problem. The source and sink electron leads serve as source for input and output noise.

We consider a system connected to reservoirs to be referred to a s "left"(L) and "right"(R) and characterized by a temperature $T_{L,R}$. The distribution functions of electrons in the reservoirs are Fermi distribution functions

$$f_\alpha(E) = \left(\exp\left[\frac{(E-\mu_\alpha)}{KT_\alpha}\right] + 1\right)^{-1}, \{\alpha = L, R\}. \tag{2.98}$$

We consider that the reservoirs(the leads) to be wide enough in comparison to the typical cross-section of the system. The electrons entering and leaving the systems occur through uncorrelated events and the process is thus irreversible although the dynamics is described in terms of Hamiltonian. The average current is thus expressed in terms of the input current proportional to $\langle \tilde{R}^\dagger_{in}(t)\tilde{R}_{in}(t)\rangle$ and the output current proportional to $\langle \tilde{R}^\dagger_{out}(t)\tilde{R}_{out}(t)\rangle$, where $\tilde{R}_{in/out}$ and $\tilde{L}_{in/out}$ are the corresponding

noise operators for the right and left electron reservoirs and in the interaction picture they are expressed as

$$\tilde{R}_{in}(t) = -\sum_j \xi_j e^{-i\omega_j^{(R)} t} c_j(0), \tag{2.99}$$

$$\tilde{R}_{out}(t) = -\sum_j \xi_j e^{-i\omega_j^{(R)}(t-t_f)} c_j(t_f), \tag{2.100}$$

with, $\omega_j^{(R)}$ is the frequency corresponding to the j-th mode of the right electron lead, c_j is the annihilation operator for the right lead and ξ_j is the tunneling of electrons to or from the system. Now, we define the scattering matrix $\bar{S}$ to relate the input and output noise operators[221] as

$$\begin{pmatrix} \tilde{L}_{out}(\omega) \\ \tilde{R}_{out}(\omega) \end{pmatrix} = \bar{S} \begin{pmatrix} \tilde{L}_{in}(\omega) \\ \tilde{R}_{in}(\omega) \end{pmatrix}, \tag{2.101}$$

where,

$$\bar{S} = \frac{2}{\gamma_R + \gamma_L - 2i\omega} \begin{pmatrix} \frac{\gamma_L - \gamma_R}{2} - i\omega & \gamma_L \\ \gamma_R & -\frac{\gamma_L - \gamma_R}{2} + i\omega \end{pmatrix}, \tag{2.102}$$

and

$$\tilde{L}_{in/out}(\omega) = \int_{-\infty}^{\infty} e^{i\omega t} \tilde{L}_{in/out}(t) dt \tag{2.103}$$

$$\tilde{R}_{in/out}(\omega) = \int_{-\infty}^{\infty} e^{i\omega t} \tilde{R}_{in/out}(t) dt. \tag{2.104}$$

The Fourier transform of the average current thus comes out as

$$\langle \hat{I}_R(\omega) \rangle = \frac{1}{\gamma_R} \int_{-\infty}^{\infty} \frac{d\omega'}{2\pi} [\langle \tilde{R}_{out}^{\dagger}(\omega') \tilde{R}_{out}(\omega' + \omega) \rangle - \langle \tilde{R}_{in}^{\dagger}(\omega) \tilde{R}_{in}(\omega' + \omega) \rangle]. \tag{2.105}$$

Noting that $\langle \tilde{R}_{in}^{\dagger}(\omega) \tilde{R}_{in}(\omega + \omega') \rangle = 0$ and $\langle \tilde{L}_{in}^{\dagger}(\omega) \tilde{L}_{in}(\omega' + \omega) \rangle = 2\pi\gamma_L \delta(\omega)$, one obtains the Landauer-Buttiker formula of the average current[96, 221]

$$\langle \hat{I}_R \rangle = \int_{-\infty}^{\infty} \frac{d\omega'}{2\pi} \frac{\gamma_L \gamma_R}{(\frac{\gamma_L + \gamma_R}{2})^2 + \omega'} = \frac{\gamma_L \gamma_R}{\gamma_L + \gamma_R}. \tag{2.106}$$

2.8.2 Coulomb Blockade

The term Coulomb Blockade is used to describe phenomena which show a blockage of transport through a system due to the electrostatic effects. The phenomena of Coulomb blockade can be observed by reducing the dimension of a conducting device. When the device is small enough, electrons inside the device will create a strong Coulomb repulsion preventing other electrons to flow. Thus, the device will no longer follow Ohm's law and the current-voltage relation of the Coulomb blockade looks like a staircase[6]. Even when Coulomb blockade can be used to

demonstrate the quantization of the electric charge, it remains a classical effect and its main description does not require quantum mechanics. However, when few electrons are involved and an external static magnetic field is applied, Coulomb blockade provides the testing ground for a spin blockade (also called Pauli blockade) and valley blockade, which include quantum mechanical effects due to spin-orbital interactions respectively between the electrons.

To exemplify, we consider four multi-electron states which we can designate as 00, 01, 10, and 11. In the neutral state, the system is in either the (10) or the (01) state whose total energy is defined as

$$E(10) = E(01) \equiv E_0. \tag{2.107}$$

The electron-electron interaction energy of a collection of $N-$ electrons is propor-

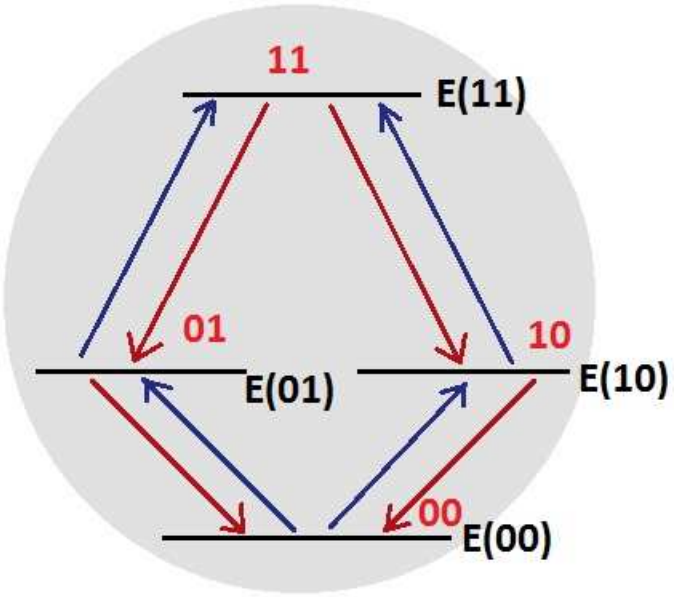

Figure 2.6: Schematic presentation of multi-electron energy levels present in a system between source and sink electron leads

tional to the number of distinct electron pairs. As the number of electron pairs that can be considered from N-electrons is $N(N-1)/2$, the electron-electron interaction U_{ee} is expressed as,

$$U_{ee} = U_{ee}(N) = \frac{U_0}{2} N(N-1), \tag{2.108}$$

where, U_0 is the average interaction energy per pair. U_0 is similar in notion to the single -electron charging energy which can be quiet significant even in nanostructures and is comparable to the thermal energy. The one-electron energy levels ϵ can be expressed as the sum of the "bare" levels $\tilde{\epsilon}$, which is obtained by solving the Schrodinger equation with just the nuclear potential and the self-consistent potential

$\left[\frac{\partial U_{ee}}{\partial N}\right]_{N=N_0}$, such that

$$\epsilon = \tilde{\epsilon} + \left[\frac{\partial U_{ee}}{\partial N}\right]_{N=N_0} = \tilde{\epsilon} + U_0 N_0 - (U_0/2). \tag{2.109}$$

If N_0 be the number of electrons present in the neutral state corresponding to have one of the states 10 or 01 filled, which for the present case happens to have the value $N_0 = 1$. The energy for any one-electron gets its expression as follows

$$E(11) = E_0 + \tilde{\epsilon} + U_{ee}(N_0 + 1) - U_{ee}(N_0) = E_0 + \epsilon + \frac{U_0}{2}, \tag{2.110}$$

$$E(00) = E_0 - \tilde{\epsilon} - U_{ee}(N_0) + U_{ee}(N_0 + 1) = E_0 - \epsilon + \frac{U_0}{2}. \tag{2.111}$$

In this picture, the overall system has different probabilities in one of the multi-electron states and thus the conservation equation reads as

$$1 = P_{00} + P_{01} + P_{10} + P_{11}. \tag{2.112}$$

One can now calculate the individual probabilities by noting that the system continually shuffles among these states under the steady state condition so that there must be no net flow into or out of any state. If the corresponding rate constants are known, then one can express the balance equations as[6]

$$R_{(00\to01)}P_{00} = R_{(01\to00)}P_{01}, \tag{2.113}$$

$$R_{(10\to00)}P_{10} = R_{(00\to10)}P_{00}. \tag{2.114}$$

$$R_{(11\to01)}P_{11} = R_{(01\to11)}P_{01}, \tag{2.115}$$

where, $R_{\alpha\to\beta}$ are the respective rate constant for jump from α-state to the β state, having dimension equal to the inverse time. Thus if γ_1 and γ_2 are quantities having dimensions of energy corresponding to the flow of electron from the system from the source and into the sink electron reservoirs respectively, then the rate constants are explicitly expressed as

$$R_{(00\to01)} = \frac{\gamma_1}{\hbar}f_1^{'} + \frac{\gamma_2}{\hbar}f_2^{'}, \tag{2.116}$$

$$R_{(01\to00)} = \frac{\gamma_1}{\hbar}(1 - f_1^{'}) + \frac{\gamma_2}{\hbar}(1 - f_2^{'}), \tag{2.117}$$

$$R_{(01\to11)} = \frac{\gamma_1}{\hbar}f_1^{''} + \frac{\gamma_2}{\hbar}f_2^{''}, \tag{2.118}$$

$$R_{(11\to01)} = \frac{\gamma_1}{\hbar}(1 - f_1^{''}) + \frac{\gamma_2}{\hbar}(1 - f_2^{''}), \tag{2.119}$$

where, $f_r^{'} = f_0(\epsilon_1 - \mu_r)$ and $f_r^{''} = f_0(\epsilon_2 - \mu_r)$ are the respective Fermi-Dirac distribution functions, with $\{r = 1, 2\}$ and μ_1 and μ_2 are corresponding chemical potentials of the source and sink electron reservoirs respectively. Using these rate constants,

one can arrive at the following balance equations

$$\frac{P_{10}}{P_{00}} = \frac{P_{01}}{P_{00}} = \frac{\frac{\gamma_1}{\hbar} f_1^{'} + \frac{\gamma_2}{\hbar} f_2^{'}}{\frac{\gamma_1}{\hbar}(1 - f_1^{'}) + \frac{\gamma_2}{\hbar}(1 - f_2^{'})}, \tag{2.120}$$

$$\frac{P_{11}}{P_{10}} = \frac{P_{11}}{P_{01}} = \frac{\frac{\gamma_1}{\hbar} f_1^{''} + \frac{\gamma_2}{\hbar} f_2^{''}}{\frac{\gamma_1}{\hbar}(1 - f_1^{''}) + \frac{\gamma_2}{\hbar}(1 - f_2^{''})}. \tag{2.121}$$

Once, we have solved the master equation for the individual probabilities, the source current can be calculated from the relation

$$I = -e \sum_{\beta} (\pm) R_1(\alpha \rightarrow \beta) P_{\alpha}, \tag{2.122}$$

where, $-e$ is the electronic charge, $(+)$ sign refers to the case where β has one more electron than α and $(-)$ sign refers to the case when β has one electron less than α, and R_1 is the part of the total transition rate associated with the source contact. After a straightforward algebra, one arrives at the explicit form of current as

$$I = \left(-\frac{e}{\hbar}\right) [2\gamma_1 f_1^{'} P_{00} - \gamma_1(1 - f_1^{'})(P_{01} + P_{10}) + \gamma_1 f_1^{''}(P_{01} + P_{10}) - 2\gamma_1(1 - f_1^{''}) P_{11}]. \tag{2.123}$$

2.9 Non-adiabatic processes and dimeric interaction

In this section of the overview, we have discussed the basic ideas of non-adiabatic process in the context of electron-vibration entangled states and conical intersection.

For nonadiabatic exciton-vibrational interaction in the dimer aggregate model, the electronic basis consists of two-diabatic electronic states. These states can represent the excitonic states of two conjugated polymer chains with the exciton being on one chain or the other[151]. The localized exciton on each chain is taken to be coupled with a single vibrational mode of the chain with dimensionless normal mode coordinates denoted by $X_i (i = 1, 2)$. The diabatic potential energy (PE) surfaces can be described using a single dimensionless normal coordinate X, constructed from the individual normal mode coordinates as $X = \frac{1}{\sqrt{2}}(X_1 - X_2)$. Here the antisymmetric combination of the coordinates actually couples the excited state diabatic Potential energy surfaces which are given as displaced harmonic oscillators[151]

$$U_1 = \hbar\omega(X + x_0)^2, U_2 = \hbar\omega(X - x_0)^2 \tag{2.124}$$

with the harmonic frequency ω and excited state displacements x_0 being taken equal for identical chains: $X = 0$ is the equilibrium geometry of the ground electronic

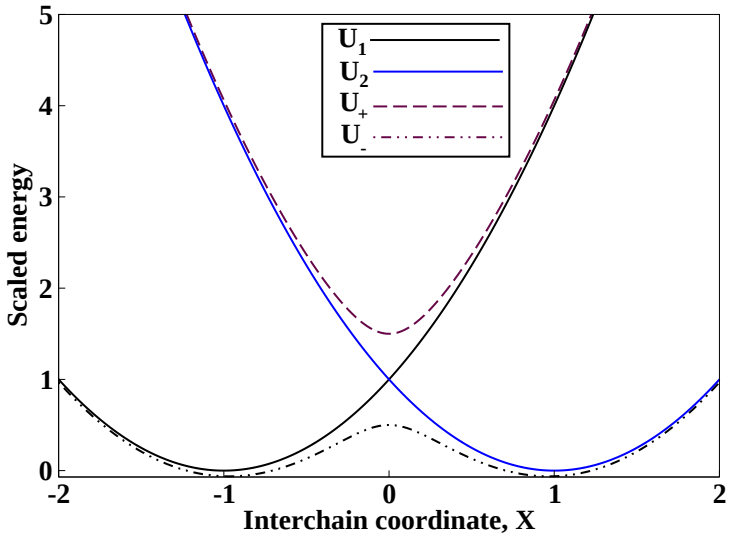

Figure 2.7: Diabatic(solid lines) and adiabatic(dashed lines) potential energy surfaces of the vibronic states of the interchain aggregate plotted as a function of the interchain coordinate, X. Here, the vertical axis represents scaled energy $E/\hbar\omega$.

state. Following the Ref.[151], we write the adiabatic PE surfaces of the molecular dimer as

$$U_{\pm} = \frac{1}{2}\left[(U_1 + U_2) \pm \sqrt{(U_1 - U_2)^2 + 4V^2}\right]. \tag{2.125}$$

Here V is the interaction between the monomer units that mitigates the exciton transfer. If V is taken to be independent of the nuclear coordinates then the adiabatic PE surfaces can not cross for nonzero interchain coupling as shown in Fig.(2.7) along with the diabatic PE surfaces. These are actually PE curves as we are considering a single aggregate coordinate, X. The energy splitting between the adiabatic PE surfaces $\Delta = 2|V|$ is the Davydov splitting of a molecular dimer[151].

Next, we consider a rotational degree of freedom representing the torsional motion of one monomer unit(one polymer chain) with respect to the other for the modeling of positional disorder found in these compounds. We take the interchain coupling to be a function of the torsional coordinate, ϕ as $V = V(\phi)$. As a simple approximation $V(\phi)$ is taken as the point dipole-point dipole interaction of the transition dipoles of the two chain-units. Assuming that the transition dipoles of each chain lie parallel to the long chain axis, ϕ can be taken as the angle between the dipoles which is equivalent to the torsion or dihedral angle between the chains. Now the adiabatic PE surfaces given in Eq.(2.125) become $U_{\pm} = U_{\pm}(X, \phi)$. The two-dimensional nuclear coordinate space now opens the possibility of the intersection of the two adiabatic PE surfaces as discussed in the context of conical intersection(CI) of the molecular PE surfaces in Chapter-7. For example, if we take a co-facial arrangement of the interacting chain-units with parallel transition dipoles, then $V(\phi) \propto \cos\phi$ then a CI of the adiabatic PE surfaces is present at $X = 0, \phi = 90^0$.

Chapter 3

Decoherence without dissipation due to fermionic bath

In this chapter, we have presented an exact solution of a model of a harmonic oscillator coupled to a fermionic environment via a quantum non-demolition type of interaction, which is based based on the formalism of fermionic coherent state of Cahil and Glauber[147]. The model is further utilized to analyze the quantum phase diffusion and linear entropy dynamics in the context of antibunching property of fermionic quantum noise. The rest of the chapter is organised as follows: After giving a short introduction in Section 3.1, in the Section 3.2, we provide an exact analytical solution of the model consisting of a system coupled with fermionic reservoir via QND type of interaction. In the next section, we have applied the theory developed to study the phase distribution pattern and compared our result with traditional bosonic bath case. In Section 3.4, we show the temperature dependence of the time evolution of linear entropy to probe the decoherence behaviour. In Section 3.5, we establish the parallelism between an effective Hamiltonian approach with that of our theory developed in Section 3.2. Finally, the chapter is concluded in Section 3.6.

3.1 Introduction

In the paradigm of decoherence and quantum-to-classical transition[133, 134, 135], regarding the study of quantum open system starting from the Feynmann-Vernon theory[53] which was later popularized by Caldiera and Leggett[54] as quantum Brownian motion, the environment is considered as a collection of a very large number of non-interacting harmonic oscillators. This bosonic description of environmental modes is a natural realisation of most of the open systems that occur with decoherence and dissipation which is evidenced by a large body of literature[55, 57, 58, 75]. A renewed interest in this respect is to study the system-reservoir coupling where no dissipation of energy takes place. This is possible when a system interacts with its environment via Quantum non-demolition(QND) type of

interaction[59, 60, 61, 62]. In this chapter we have studied decoherence from the system-reservoir model where the quantum system is coupled to a fermionic environment instead of a bosonic one. Fermionic environment serves as a theoretical realisation of a bath consisting of two-level systems corresponding to localised modes such as defects, impurities, nuclear and paramagnetic spins [63, 64]. However, the dissipation along with decoherence happens to remain as an integral part of the problem. This stimulates us to propose an exact analytical solution for a model to describe the coherent dynamics of a quantum system interacting with a fermionic reservoir via QND type interaction where no dissipation of energy is taking place.

In this chapter, we have addressed some specific issues regarding dissipationless decoherence model involving the fermionic reservoir. The primary one is to draw an analogy with the dynamics of boson bath case where we have used the close similarity between Ref.[119] and that of Ref.[147] using Grassmann algebra. This is done by providing an exact analytical solution of the reduced density operator for a linear harmonic oscillator coupled to a fermionic reservoir via QND type of coupling. Next we have deduced the dynamics of phase distribution function and also the linear entropy. Finally, in this chapter, we have shown how system-bath dynamics developed can be cast in an equivalent form of a stochastically modulated quantum system by an effective Hamiltonian approach. This corresponds to a fermionic version of the quantum Kubo oscillator.

To put our work in a proper perspective, let us consider a system coupled to infinite number of spin-$\frac{1}{2}$ fermions with characteristic frequencies ω_k. The total Hamiltonian H_T can then be expressed as:

$$H_T = H_s + \sum_k \hbar\omega_k c_+^k c_-^k + H_s \sum_k (c_+^k g_k + g_k^* c_-^k). \tag{3.1}$$

Here, H_s is the system Hamiltonian. The second term is the reservoir Hamiltonian H_R, with the fermions following anticommutation rule $\{c_+^l, c_-^m\}_+ = \delta_{lm}$ and the following algebra:

$$c_+^k c_+^k = c_-^k c_-^k = 0 \tag{3.2}$$

$$[c_+^k, c_+^k c_-^k] = -c_+^k \tag{3.3}$$

$$[c_-^k, c_+^k c_-^k] = c_-^k. \tag{3.4}$$

The third term in Eq.(3.1) is the interaction Hamiltonian H_{int} of QND type, constructed such that $[H_s, H_{int}] = 0$ implying that H_{int} is a constant of motion generated by H_s. g_k and g_k^* are dimensionless interaction coefficients obeying Grassmann algebra. The Grassmann variables satisfy convenient relations like[205]:

$$\{g_i, g_j\}_+ = 0 \tag{3.5}$$

$$\{g_i^*, g_j\}_+ = 0 \tag{3.6}$$

$$\{g_i^*, g_j^*\}_+ = 0. \tag{3.7}$$

We also assume[147] that

$$\{g_k, c_-^k\}_+ = 0. \tag{3.8}$$

Following similar line of treatment as Tameshtit and Sipe[60] which was originally proposed for bosonic bath case, we arrive at

$$\frac{d\rho}{dt} = -\frac{i}{\hbar}[H_s, \rho] - c_{BM}(H_s H_s \rho - 2H_s \rho H_s + \rho H_s H_s) \tag{3.9}$$

with

$$c_{BM} = \frac{\gamma_0 \hbar \omega_0}{4KT} \tag{3.10}$$

where

$$\gamma_0 = Lt_{\omega \to 0} 2\pi g^*(\omega) g(\omega) I(\omega). \tag{3.11}$$

Here, $I(\omega)$ is the spectral density of the bath and we have introduced a high temperature limit along with Born-Markov approximation keeping in mind that $\bar{n}(\omega) \simeq \bar{n}(\omega_0)$. The inverse temperature dependence at finite temperature in comparison to bosonic bath in the Born-Markov limit is an important new feature here.

3.2 Decoherence of a quantum system coupled to a fermionic bath

In this section, we have provided an exact solution of the reduced density operator for an arbitrary system. Using the solution we have derived from a master equation, we have deduced the concomitant survival probability for a harmonic oscillator.

3.2.1 Exact solution

The total Hamilitonian H_T for the system, bath and the interaction can be re-written [see Eq.(3.1)] as:

$$H_T = H_s + \sum_k \hbar \omega_k c_+^k c_-^k + H_s \sum_k (c_+^k g_k + g_k^* c_-^k) + H_s^2 \sum_k \frac{g_k^* g_k}{\hbar \omega_k}. \tag{3.12}$$

However, it is to be noted that the last term on the right hand side of Eq.(3.12) has been added as a counter term in order to make H_T invariant under the unitary transformation defined by

$$U = e^{H_s \sum_k \frac{(c_-^k g_k^* - g_k c_+^k)}{\hbar \omega_k}}, \tag{3.13}$$

and it is evident that

$$U H_T U^{-1} = H_s + \sum_k \hbar \omega_k c_+^k c_-^k. \tag{3.14}$$

A formal solution of Liouville equation can be expressed as

$$\rho(t) = e^{\frac{-iH_T t}{\hbar}} \rho(0) e^{\frac{iH_T t}{\hbar}}, \tag{3.15}$$

where, $\rho(0)$ is the initial joint system-bath density operator and $\rho(t)$ is the same at any time t. Furthermore, we assume that

$$\rho(0) = \rho^{\mathrm{s}}(0)\rho_{\mathrm{B}}(0), \tag{3.16}$$

where, ρ^s is the reduced density operator for system and $\rho_B(0)$ is the equilibrium bath density expressed as

$$\rho_B(0) = \frac{e^{-\sum_k \beta\hbar\omega_k c_+^k c_-^k}}{Tr_B e^{-\sum_k \beta\hbar\omega_k c_+^k c_-^k}}. \tag{3.17}$$

The matrix element in the system space can now be expressed as

$$\rho_{nm} = \sum_{i,j} \langle n|e^{-\frac{itH_T}{\hbar}}|i\rangle \rho_{ij}^s(0)\rho_B(0)\langle j|e^{\frac{itH_T}{\hbar}}|m\rangle. \tag{3.18}$$

Taking trace over the reservoir variables, we obtain

$$\rho_{nm}^s(t) = e^{-\frac{it}{\hbar}(E_n - E_m)} e^{-\frac{it}{\hbar}(E_n^2 - E_m^2)\sum \frac{g_k^* g_k}{\hbar\omega_k}} Tr_B(\rho_B(0) e^{\frac{itH_m}{\hbar}} e^{-\frac{itH_n}{\hbar}}) \rho_{nm}^s(0), \tag{3.19}$$

where,

$$H_n = \sum_k \{\hbar\omega_k c_+^k c_-^k + E_n(c_+^k g_k + g_k^* c_-^k)\} \equiv \sum_k H_n^{(k)}. \tag{3.20}$$

To simplify the above expression, we define

$$H_n^{(k)} = \hbar\omega_k S_+^{k(n)} S_-^{k(n)} - \frac{E_n^2 g_k^* g_k}{\hbar\omega_k}, \tag{3.21}$$

where,

$$S_+^{k(n)} = c_+^k + \frac{E_n g_k^*}{\hbar\omega_k}, \tag{3.22}$$

and

$$S_-^{k(n)} = c_-^k + \frac{E_n g_k}{\hbar\omega_k}. \tag{3.23}$$

$S_+^{k(n)}$ and $S_-^{k(n)}$can be re-expressed as

$$S_+^{k(n)} = D^\dagger(\mu^{(n)}) c_+^k D(\mu^{(n)}), \tag{3.24}$$

and

$$S_-^{k(n)} = D^\dagger(\mu^{(n)}) c_-^k D(\mu^{(n)}), \tag{3.25}$$

where, $\mu_i^{(n)} = \frac{E_n g_k}{\hbar\omega_k}$, with $\mu^{(n)} \equiv \{\mu_i^{(n)}\}$ and fermionic displacement operator[147] $D(\mu^{(n)}) = \prod_i e^{(c_+^i \mu_i^{(n)} - \mu_i^{*(n)} c_-^i)} \equiv \prod_i D_i(\mu_i^{(n)})$. Therefore, one can write

$$e^{\frac{itH_m^{(k)}}{\hbar}} = e^{-\frac{itE_m^2 g_k^* g_k}{\hbar^2\omega_k}} D^\dagger(\mu^{(m)}) e^{it\omega_k c_+^k c_-^k} D(\mu^{(m)}). \tag{3.26}$$

We now introduce a property, whose derivation is shown in the Appendix,

$$e^{ixc_+^k c_-^k} D(\mu) = \prod_{i \neq k} e^{(c_+^i \mu_i - \mu_i^* c_-^i)} \{ e^{(c_+^k \mu_k e^{ix} - \mu_k^* c_-^k e^{-ix})} \} e^{ixc_+^k c_-^k}. \tag{3.27}$$

Again noting that,

$$D_i(\alpha_i) D_i(\beta_i) = D_i(\alpha_i + \beta_i) e^{\frac{\beta_i^* \alpha_i - \alpha_i^* \beta_i}{2}}, \tag{3.28}$$

we obtain,

$$e^{\frac{itH_m^{(k)}}{\hbar}} = e^{-\frac{itE_m^2}{\hbar^2 \omega_k} g_k^* g_k} D_k(\mu_k^{(m)} (e^{it\omega_k} - 1)) e^{i\mu_k^{*(m)} \mu_k^{(m)} \sin(\omega_k t)} e^{it\omega_k c_+^k c_-^k}. \tag{3.29}$$

Therefore, one can write

$$e^{\frac{itH_m^{(k)}}{\hbar}} e^{-\frac{itH_n^{(k)}}{\hbar}} = e^{\frac{it(E_n^2 - E_m^2) g_k^* g_k}{\hbar^2 \omega_k}} e^{\frac{ig_k^* g_k (E_m^2 - E_n^2) \sin(\omega_k t)}{\hbar^2 \omega_k^2}} D_k(\lambda_k), \tag{3.30}$$

where,

$$\lambda_k = (E_m - E_n) \frac{g_k}{\hbar \omega_k} (e^{it\omega_k} - 1), \tag{3.31}$$

and we have used the standard result[147]

$$D_k(\lambda_k) |0\rangle_k = \left(1 - \frac{1}{2} \lambda_k^* \lambda_k \right) |0\rangle_k + \lambda_k |1\rangle_k, \tag{3.32}$$

and,

$$D_k(\lambda_k) |1\rangle_k = -\lambda_k^* |0\rangle_k + \left(1 + \frac{1}{2} \lambda_k^* \lambda_k \right) |1\rangle_k. \tag{3.33}$$

Hence, we have the final solution as follows:

$$\rho_{nm}^s(t) = e^{-\frac{it(E_n - E_m)}{\hbar}} e^{i(E_n^2 - E_m^2)\eta(t)} e^{-(E_n - E_m)^2 \gamma(t)} \rho_{nm}^s(0), \tag{3.34}$$

where,

$$\eta(t) = -\sum_k \frac{g_k^* g_k}{\hbar^2 \omega_k^2} \sin(\omega_k t), \tag{3.35}$$

and,

$$\gamma(t) = 2 \sum_k \frac{g_k^* g_k}{\hbar^2 \omega_k^2} \sin^2 \left(\frac{\omega_k t}{2} \right) (1 - 2\bar{n}_k). \tag{3.36}$$

The temperature dependence in $\gamma(t)$ comes from the term $\bar{n}_k$, which can be identified as the Fermi-Dirac distribution function denoting the average thermal excitation number of the bath. The quantity $\bar{n}_k$ is defined as

$$\bar{n}_k = \frac{1}{e^{\frac{\hbar \omega_k}{KT}} + 1}, \tag{3.37}$$

and,

$$2\bar{n}_k - 1 = -\tanh \left(\frac{\hbar \omega_k}{2KT} \right). \tag{3.38}$$

We now assume the that the bath modes are continuously distributed with a spectral density $J(\omega)$, so that for an arbitrary function $f(\omega)$, we can have the continuum limit as

$$\sum_k \frac{g_k^* g_k}{\hbar^2} f(\omega_k) \longrightarrow \int_0^\infty d\omega J(\omega) f(\omega). \tag{3.39}$$

For a typical choice of Lorentzian distribution of frequency[139], the spectral density $J(\omega)$ assumes the form

$$J(\omega) = \frac{\gamma_0}{\pi} \frac{1}{1+\tau_c^2\omega^2} \tag{3.40}$$

where, γ_0 is strength of the quantum noise and τ_c is the bath correlation time.

One can now find the master equation equivalent to Eq.(3.34) as

$$\dot{\rho}^s(t) = -\frac{i}{\hbar}[H_s, \rho^s] + i\dot{\eta}(t)[H_s H_s, \rho^s] - \dot{\gamma}(t)(H_s H_s \rho^s - 2H_s \rho^s H_s + \rho^s H_s H_s). \tag{3.41}$$

We discuss the implications of these results for the Lorentzian bath. Exact expressions for $\gamma(t)$ and $\dot{\gamma}(t)$ cannot be obtained analytically for all times and at arbitrary temperature and thus we perform numerical integration. However, analytical expressions can be obtained if we consider the the usual approximation of $\bar{n}(\omega) \simeq \bar{n}(\omega_0)$ to make life simple which can however be improved by Taylor series expansion of $\bar{n}(\omega)$ around ω_0. Within this framework, one can write

$$\dot{\gamma}(t) = \frac{\gamma_0}{2} \tanh\left(\frac{\hbar\omega_0}{2KT}\right)(1 - e^{-\frac{t}{\tau_c}}). \tag{3.42}$$

At high temperature, we replace $\tanh(\frac{\hbar\omega_k}{2KT})$ by $\frac{\hbar\omega_k}{2KT}$. Now, in this temperature limit, in a similar spirit as that of Kubo[198] we can investigate two cases. For (a) $\frac{t}{\tau_c} \gg 1$, so that in this limit $\dot{\gamma}(t)$ assumes the Born-Markov(BM) value

$$\dot{\gamma}(t) = c_{BM} = \frac{\hbar\omega_0\gamma_0}{4KT} \tag{3.43}$$

as given in the Sec.3.1.

(b) When $\frac{t}{\tau_c} \ll 1$, $\dot{\gamma}(t)$ assumes the slow-modulation(SM) limiting value which can be written as

$$\dot{\gamma}(t) = c_{SM} = \frac{\hbar\omega_0\gamma_0}{4KT}\frac{t}{\tau_c}. \tag{3.44}$$

It is to be noted that the above results do not depend on the structure of the system Hamiltonian unlike the quantum Brownian motion case corresponding to non-diagonal coupling with the reservoir. Inspite of the marked difference, the results came in a similar form as that of the boson bath case[61]. This feature is a remarkable manifestation of the anticommuting Grassmann variables of the interaction coefficients.

3.2.2 Survival probability

In order to probe the dynamics of decoherence behaviour, we calculate the survival probability in the special case when H_s represents the Hamiltonian for a Harmonic oscillator with $E_n = (n + \frac{1}{2})\hbar\omega_0$. The survival probability, $P(t) = Tr(\rho^s(0)\rho^s(t))$, which is a measure of coherence can be expressed as

$$P(t) = \sum_{m,n} |\rho^s_{m,n}(0)|^2 e^{-it(n-m)\omega_0} e^{i\hbar^2\omega_0^2[(n^2-m^2)+(n-m)]\eta(t)} e^{-\hbar^2\omega_0^2(n-m)^2\gamma(t)}. \tag{3.45}$$

For numerical demonstration, we have assumed that the system is initially in a coherent state so that

$$\rho^s_{n,m}(0) = e^{-|\alpha|^2} \frac{|\alpha|^{n+m}}{\sqrt{n!m!}}. \tag{3.46}$$

In Figure(3.1), we have shown the survival probability for exact dynamics, BM and

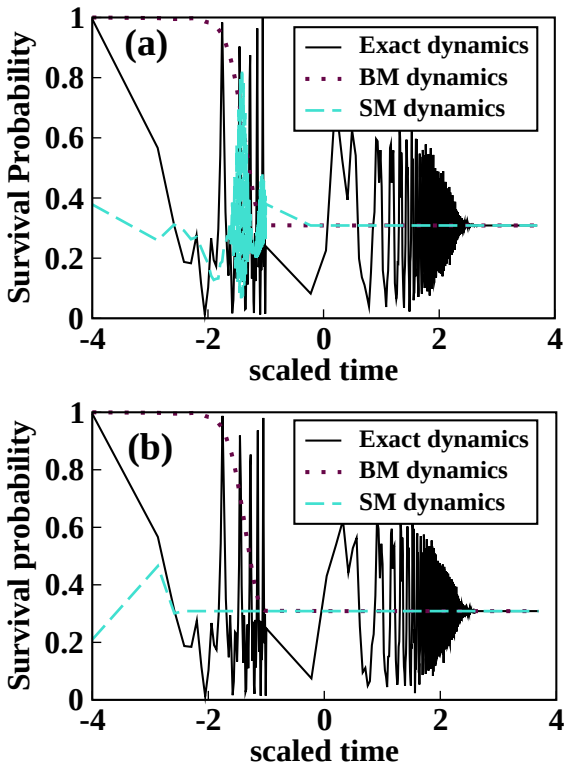

Figure 3.1: Plot of Survival probability against scaled time $\log(\omega_0 t)$ for exact, Born-Markov(BM) and slow modulation(SM) limits. In figure(a), $\tau_c\omega_0 = 10.0$, the exact dynamics is closer to SM than BM. In figure(b), $\tau_c\omega_0 = 0.1$, the exact dynamics is closer to BM than SM.

SM limits, at a fixed low temperature $\frac{KT}{\hbar\omega_0} = 0.01$. In figure(3.1.a), when $\tau_c\omega_0 = 10.0$, the exact dynamics is closer to SM than BM. Whereas, in figure(3.1.b), when $\tau_c\omega_0 = 10.0$, the exact dynamics is closer to BM than SM. This is in conformity with the fact that as $\tau_c \to 0$ the spectral density will be constant throughout the entire range of ω rendering the system to remain exposed over a wider range of bath frequencies

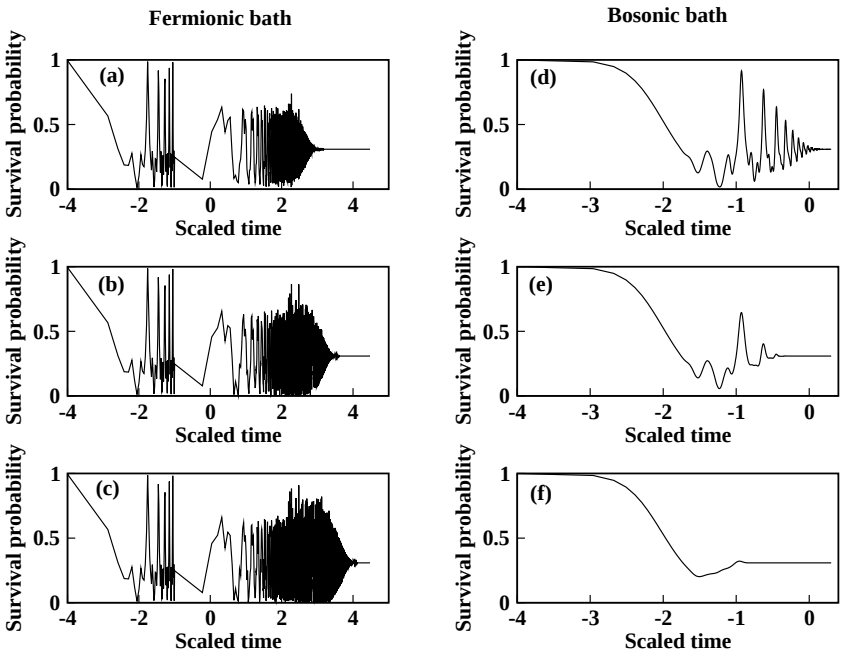

Figure 3.2: Plot of Survival probability against scaled time $\log(\omega_0 t)$ for fermionic and bosonic bath, at a fixed value of $\tau_c\omega_0 = 1.0$ at different scaled temperatures $\frac{KT}{\hbar\omega_0}$. Figure (a),(b) and (c) plots the survival probability for fermionic bath at $\frac{KT}{\hbar\omega_0} = 0.1, 1.0$ and 10.0 respectively. Figure (d),(e) and (f) plots the survival probability for bosonic bath at $\frac{KT}{\hbar\omega_0} = 0.1, 1.0$ and 10.0 respectively. The figure clearly reveals the temperature-assisted survival of coherence in quantum system when it is coupled to fermionic environment compared to the temperature-resisted coherence of the system coupled to bosonic environment.

and we arrive at the expected BM limit. At higher values of τ_c, the system-bath interaction becomes more restricted to a narrower frequency range and we arrive at the SM limit. Here, we find oscillatory decay in the exact dynamics before the survival probability saturates to its asymptotic value $\sum_m |\rho^s_{mm}(0)|^2$ which is purely a quantum feature unlike the bosonic bath case.

In Figure(3.2), we have compared the temperature dependence in the time evolution of the survival probability for a harmonic oscillator system coupled to bosonic and fermionic environments. From Figure(3.2), it is clear that for the same set of bath parameters, the time for decay in survival probability to its asymptotic value differs to a large extent for fermionic bath compared to its bosonic partner. It is also noteworthy to mention that there exists a counterintuitive effect of temperature for the former case. This can be explained on the basis of the fact that at finite temperature, the spectral density function for the spin bath gets modified due to the presence of hyperbolic tangent factor in comparison to the oscillator bath [see Eqs.(3.36) and (3.38)]. As a consequence, it assists coherence at a high temperature.

The numerical results shown in Fig(3.1) and Fig(3.2) assumes that the frequencies of the reservoir modes are in a Lorentizan distribution. The essential features

of a prototype finite bandwidth bath with a Lorentzian distribution is tangible numerically for the model study. The actual distribution of energy level structure of the reservoir modes depend on the practical situation for the particular bosonic and fermionic cases at hand. We have numerically investigated that with a moderate value of $\tau_c\omega_0$, at a low value of the ratio of thermal energy to system characteristic energy, $\frac{KT}{\hbar\omega_0}$ the survival probability plot for exact dynamics will coincide more rapidly with BM and SM results(not shown in diagrams for simplicity). However, increase in the ratio, $\frac{KT}{\hbar\omega_0}$ will promote coherence in the dynamical nature of the system coupled to a fermionic reservoir for all ranges of the parametric value of bandwidth of the bath, $\tau_c\omega_0$.

3.3 Phase diffusion: Harmonic Oscillator system

In this section, we have analysed the phase diffusion pattern for a harmonic oscillator as the system of interest. The master equation can be cast into the respective equivalent equations of quasi-probability distribution functions in a quasi-classical phase space.

Considering a harmonic oscillator as the system of interest, i.e,

$$H_s = \hbar\omega_0 \left(a^\dagger a + \frac{1}{2}\right), \tag{3.47}$$

with $[a, a^\dagger] = 1$, the master equation[see Eq.(3.41)] becomes

$$\dot{\rho^s} = -i\omega_0[a^\dagger a, \rho^s] + i\hbar^2\omega_0^2\dot{\eta}(t)[(a^\dagger a)^2 + a^\dagger a, \rho^s]$$

$$-\hbar^2\omega_0^2\dot{\gamma}(t)[(a^\dagger a)^2\rho^s - 2a^\dagger a\rho^s a^\dagger a + \rho^s(a^\dagger a)^2]. \tag{3.48}$$

The above master equation can be cast into the form of the equation of motion of Glauber-Sudarshan P-distribution function[119, 55]

$$\rho = \int d^2\alpha P(\alpha)|\alpha\rangle\langle\alpha|. \tag{3.49}$$

Noting that $\dot{\eta}(t \to \infty) = 0$, we get the equation of motion for the P-distribution function in $t \to \infty$ limit as

$$\frac{\partial P}{\partial t} = -i\omega_0 \left(\alpha\frac{\partial}{\partial\alpha} - \alpha^*\frac{\partial}{\partial\alpha^*}\right)$$

$$-\hbar^2\omega_0^2\dot{\gamma}\left[\alpha\frac{\partial}{\partial\alpha} + \alpha^*\frac{\partial}{\partial\alpha^*} + \alpha^2\frac{\partial^2}{\partial\alpha^2} + \alpha^{*2}\frac{\partial^2}{\partial\alpha^{*2}} - 2\alpha^*\alpha\frac{\partial^2}{\partial\alpha\partial\alpha^*}\right]. \tag{3.50}$$

Now, after transforming to polar coordinate using $\alpha = re^{-i\theta}$, we get

$$\frac{\partial P}{\partial t} = 2\omega_0\frac{\partial P}{\partial\theta} + 4\hbar^2\omega_0^2\dot{\gamma}(t)\frac{\partial^2 P}{\partial\theta^2}. \tag{3.51}$$

The second term represents the time dependent diffusion on a circle. It is to be noted that, $\dot{\gamma}(t)$ survives both in the high and low temperature limit. Taking into consideration that $\bar{n}(\omega) \simeq \bar{n}(\omega_0)$, we have at $T \to 0$

$$\dot{\gamma}(t) = \frac{\gamma_0}{2} \tag{3.52}$$

and at $T \to \infty$

$$\dot{\gamma}(t) = \frac{\hbar\gamma_0\omega_0}{4KT}. \tag{3.53}$$

Hence, both in the high and low temperature limit, the dynamical behaviour influenced by a fermionic environment can be modelled by a classical stochastic process[61]. This is in sharp contrast to bosonic bath case, where this sort of modelling is possible for only at a very high temperature[136].

In what follows, we numerically evaluate the phase distribution function for harmonic oscillator in an initial coherent state immersed in a fermion bath with QND type interaction. The phase distribution function $P(\theta)$ can be defined as[222]

$$P(\theta) = \frac{1}{2\pi}\langle\theta|\rho|\theta\rangle, (0 \leq \theta \leq 2\pi) \tag{3.54}$$

where the states $|\theta\rangle$ are the eigenstates of the Susskind-Glogower phase operator corresponding to the eigenvalues of unit magnitude and are defined in terms of the number states $|n\rangle$[223] as

$$|\theta\rangle = \sum_{n=0}^{n=\infty} e^{in\theta}|n\rangle. \tag{3.55}$$

Using these relations in Eq.(3.34), we get

$$P(\theta) = \frac{1}{2\pi}\sum_{m,n=0}^{\infty}\frac{|\alpha|^{n+m}}{\sqrt{n!m!}}e^{-|\alpha|^2}e^{-i(m-n)\theta}e^{-i\omega_0(m-n)t}$$

$$\times e^{i(\hbar\omega_0)^2(m-n)(m+n+1)\eta(t)}e^{-(\hbar\omega_0)^2(n-m)^2\gamma(t)}. \tag{3.56}$$

Figure(3.3) depicts the phase distribution pattern for a harmonic oscillator coupled to a fermionic bath via QND type of interaction. From the figure, the following observations can be noted: a) For a fixed value of bath parameter, $\tau_c\omega_0 = 10.0(0.1)$ as in Figure(3.3.a) and (3.3. b) [Figure.(3.3.d) and (3.3.e)], it is evident that with increase in the magnitude of evolution time from 10.0 to 100.0, phase distribution pattern is getting flattened with time. b) Decrease in the bath parameter from $\tau_c\omega_0 = 10.0$ to 0.1 favours diffusion. Lowering in the value of $\tau_c\omega_0$ lowers the temporal correlation amongst the different modes of the fermionic reservoir which effectively increases the exposure of the system to a wider range of bath frequencies resulting an enhancement in diffusion. c) If the bath parameter is kept fixed, decrease in temperature favours diffusion. This is due to effective localisation in system-dynamics at low temperature manifested in terms of dominating temperature dependent hyperbolic tangent factor appearing in $\gamma(t)$[see Eqs.(3.36) and (3.38)]. This sort of temperature resisted diffusion has also been observed earlier[224].

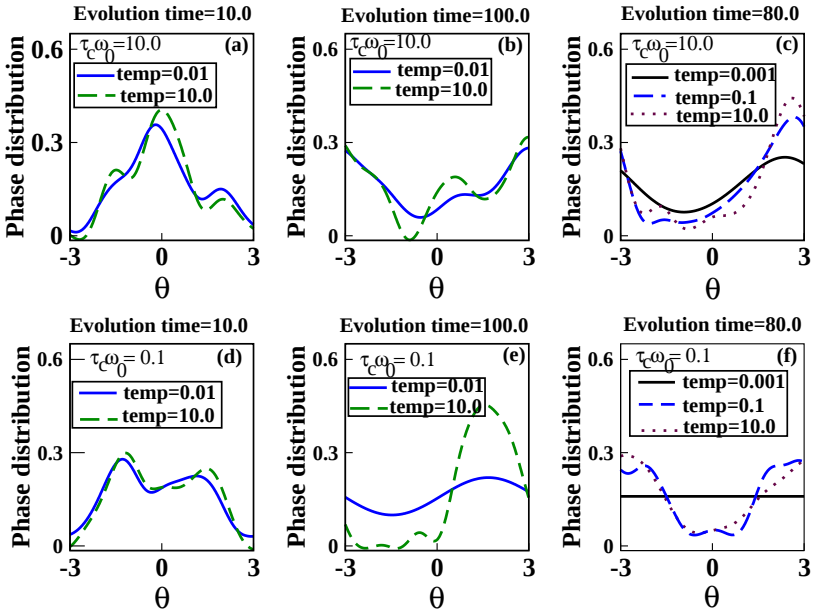

Figure 3.3: Plot of phase distribution $P(\theta)$ against θ for different bath parameters. Figures $(a), (b)$ and (c) depicts the plot for $\tau_c\omega_0 = 10.0$. Figures $(d), (e)$ and (f) depicts the plot for $\tau_c\omega_0 = 0.1$.

3.4 Evolution of linear entropy

The time evolution of linear entropy is a good 'measure of coherence' of the system. Linear entropy $S(t)$ is defined as[58]

$$S(t) = 1 - C(t), \tag{3.57}$$

where,

$$C(t) = Tr[\rho^s(t)]^2. \tag{3.58}$$

$S(t) = 0$ means that the system is initially in a pure state, and $S(t) = 1.0$ means it is in a completely mixed state.

If the system starts from an initial coherent state, i.e,

$$\rho_s(0) = |\alpha\rangle\langle\alpha| = e^{-|\alpha|^2} \sum_{m,n} \frac{|\alpha|^{n+m}}{\sqrt{n!m!}} |n\rangle\langle m|, \tag{3.59}$$

then using Eqs.(3.58) and (3.59) along with Eq.(3.34), we obtain,

$$C(t) = e^{-|\alpha|^2} \sum_{m,n} \frac{|\alpha|^{2(m+n)}}{n!m!} e^{-2(E_n - E_m)^2 \gamma(t)}, \tag{3.60}$$

with $\gamma(t)$ is given by Eq.(3.36). We obtain the values of $C(t)$ under two limiting conditions of temperature. Within the usual approximation of $\bar{n}(\omega) = \bar{n}(\omega_0)$, and at $T \to 0$ limit, we get

$$S(t) = 1 - e^{-|\alpha|^2} \sum_{m,n} \frac{|\alpha|^{2(m+n)}}{n!m!} \exp\left[-2(E_n - E_m)^2 \frac{\gamma_0}{2} \left[t - \tau_c \left(1 - e^{-\frac{t}{\tau_c}}\right)\right]\right]. \tag{3.61}$$

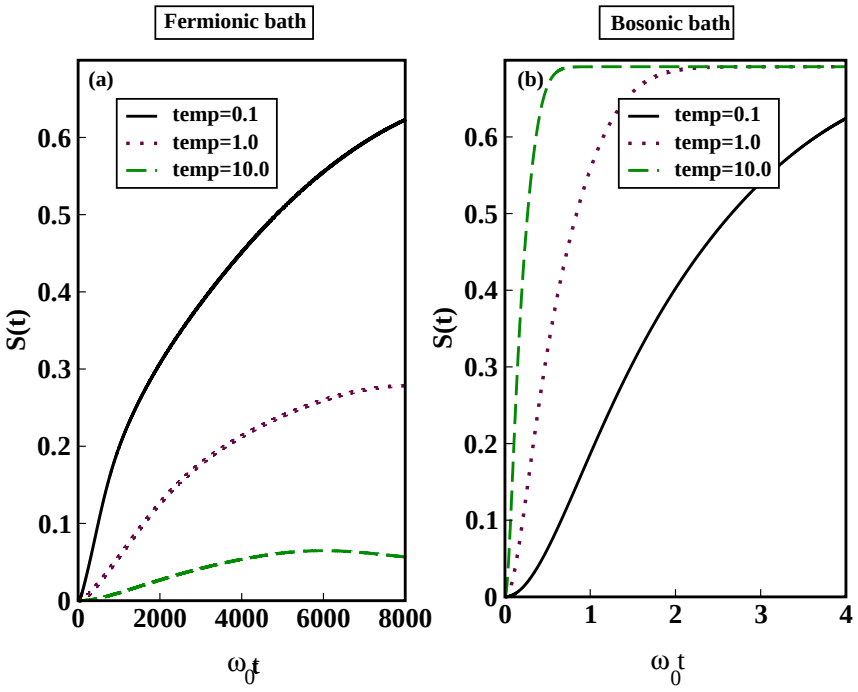

Figure 3.4: Plots to compare the temperature dependence of time evolution of linear entropy $S(t)$. Figure (a) depicts the plot for fermionic bath and figure (b) depicts the plot for bosonic bath. Temperature dependence are not only of opposite nature but also in the fermionic bath case the changes takes place more slowly.

Clearly, in the low temperature limit, the time evolution of linear entropy does not have any temperature dependence.
At high temperature limit, $T \to \infty$, and taking the approximation $\bar{n}(\omega) \simeq \bar{n}(\omega_0)$, we have

$$S(t) = 1 - e^{-|\alpha|^2} \sum_{m,n} \frac{|\alpha|^{2(m+n)}}{n!m!} \exp\left[-2(E_n - E_m)^2 \frac{\hbar\omega_0\gamma_0}{4KT}\left[t - \tau_c(1 - e^{-\frac{t}{\tau_c}})\right]\right]. \tag{3.62}$$

Evidently, in the high temperature limit, with the decrease in temperature, $S(t)$ will attain its asymptotic value, $S(t) = 1$ more rapidly.

In what follows we comparatively show the exact numerical result for the temperature dependence in time evolution of linear entropy among the fermionic and bosonic baths. From figure(3.4), it is clear that with the increase in temperature, in case of fermionic bath, the increment in the linear entropy occurs much slowly. On the contrary, for bosonic bath, increase in temperature favours the increase in the degree of mixedness in the system state thereby suppressing coherent dynamics. In addition, it is also to note that the time-scale in which a system coupled to a fermionic bath decoheres is much larger than that of the harmonic oscillator bath. This is possibly due to the severe restriction in thermally induced excitation for a bath comprising of fermions in comparison to that composed of bosons. It manifests its effect by resisting the decay of coherences at higher temperature and

a much larger time scale for loss of phase coherence.

3.5 Quantum Stochastic oscillator

In this section, we have shown that the exact system-bath dynamics developed in section-3.2 can be cast into an equivalent form of a stochastically modulated quantum system. We have constructed an effective Hamiltonian corresponding to a fermionic version of quantum Kubo oscillator which is distinctly different from the oscillator bath case at high temperature.

From the total Hamiltonian

$$H_T = \hbar\omega_0\left(a^\dagger a + \frac{1}{2}\right) + \sum_k \hbar\omega_k c_+^k c_-^k + \hbar\omega_0\left(a^\dagger a + \frac{1}{2}\right)\sum_k \left(c_+^k g_k + g_k^* c_-^k\right) + \left[\hbar\omega_0\left(a^\dagger a + \frac{1}{2}\right)\right]^2 \sum_k \frac{g_k^* g_k}{\hbar\omega_k}, \tag{3.63}$$

we can have the Heisenberg equation of motion for bath operators as

$$\dot{c_+^k} = i\omega_k c_+^k + i\omega_0 g_k^*\left(a^\dagger a + \frac{1}{2}\right), \tag{3.64}$$

which can be solved to get

$$c_+^k(t) = c_+^k(0)e^{i\omega_k t} - \frac{\omega_0 g_k^*}{\omega_k}\left(a^\dagger a + \frac{1}{2}\right)\left(1 - e^{i\omega_k t}\right). \tag{3.65}$$

Similarly, if we solve the Heisenberg equation of motion for the system operator, we get

$$a(t) = -i\omega_0 a - i\omega_0 K(t)a + 2\hbar^2\omega_0^2 a\dot{\eta}(t)\left(a^\dagger a + \frac{1}{2}\right), \tag{3.66}$$

where $K(t)$, the noise operator can be expressed as

$$K(t) = \sum_k \left(e^{i\omega_k t}c_+^k(0)g_k + g_k^* c_-^k(0)e^{-i\omega_k t}\right), \tag{3.67}$$

and

$$\dot{\eta}(t) = -\sum_k \frac{g_k^* g_k}{\hbar^2\omega_k}\cos(\omega_k t). \tag{3.68}$$

For a fermionic bath at thermal equilibrium, one can find

$$\langle K(t)\rangle = 0. \tag{3.69}$$

To obtain the strength of the fluctuation in fermionic noise, which is real, we calculate the symmetric correlation function as

$$\langle K(t_1)K(t_2) + K(t_2)K(t_1)\rangle = -2\sum_k g_k^* g_k(1 - 2\bar{n}_k)\cos[\omega_k(t_1 - t_2)]. \tag{3.70}$$

From Eq.(3.70), it becomes clear that the magnitude of the fermionic noise fluctuation increases with the decrease in temperature. This is in sharp contrast with the standard observation noted for bosonic environment, in which there is a temperature assisted increase in the magnitude of noise fluctuation. Similar argument can be attributed to the phenomenon of anomalous motional narrowing effect which is observed in the optical spectrum of semiconductor quantum dot[225]. The negative sign appearing in Eq.(3.70) is a result of fermionic antibunching effect[226, 227]. This is in principle a manifestation of the antisymmetric two-particle fermionic wave-function which excludes overlapping wave trains forbidden by Pauli Exclusion principle.

It is to be noted that Eq.(3.66) follows from the effective Hamiltonian as

$$\dot{a}(t) = \frac{i}{\hbar}[H_{eff}(t), a], \tag{3.71}$$

where,

$$H_{eff}(t) = \hbar\omega_0 \left(a^\dagger a + \frac{1}{2}\right)(1 + K(t)) - 2\dot{\eta}(t)\left(a^\dagger a + \frac{1}{2}\right)^2 \hbar^2\omega_0^2. \tag{3.72}$$

Therefore, if one solves the equation

$$\dot{\rho}^s = -\frac{i}{\hbar}\left[H_{eff}(t), \rho^s\right], \tag{3.73}$$

it is possible to arrive at the solution obtained for a stochastically modulated quantum system[61].

3.6 Conclusion

In this chapter, we have given an exact solution to the dissipationless decoherence model of a quantum system coupled to a fermionic bath at thermal equilibrium. In the exact solution, unlike the quantum Brownian case, the decoherence dynamics does not depend on the structure of the system Hamiltonian. We have shown that our result converges to the BM limit under suitable conditions, which is drastically different from the bosonic bath case. We would also like to point out the fact that despite the marked difference of the fermionic displacement operator from the bosonic one, the mathematical structure of the result appears to be quite similar, which is basically a manifestation of the anticommuting Grassmann variables in the interaction terms if one would be interested in understanding any physical role played by the Grassmann variables.

A temperature-assisted suppression of decoherence is found due to the restricted possibility for thermal excitation of the bath degrees of freedom consisting of fermions with two states in contrast to an infinite number of states of the usual oscillator bath.

While calculating the survival probability, we demonstrate that for a fermionic reservoir, there is a delay in the decay of coherences with an increase in temperature. This has also been supported by the temperature dependence of the time evolution of linear entropy. It is shown that the diffusion in phase distribution pattern for a harmonic oscillator leads to a temperature-inhibited diffusion phenomenon. We have also illustrated how the dynamics can be modelled similarly to the classical Kubo stochastic process in both the high and low temperature limits; however, the dephasing and diffusion coefficients are quantum mechanical in origin, stemming from the equilibrium fermionic bath. It is shown that the magnitude of the fermionic noise fluctuation decreases with an increase in temperature. We have demonstrated that a parallel formalism can be developed by an effective Hamiltonian approach to obtain the same result for a stochastically modulated quantum system, and an anomalous motional narrowing is found here with increasing temperature in contrast to the standard quantum Kubo oscillator. A similar feature is found in the motional narrowing in the optical spectrum of the semiconductor quantum dot system[225]. Here a quantum Kubo oscillator is possible to realize from this model due to the antibunching character of the fermionic quantum noise as explicitly shown by the consideration of the non-commutative property of interaction terms obeying the Grassmann algebra.

Appendix

In this section, we have appended the outline of the derivation of Eq.(3.27).

If $D(\mu)$ be the fermionic displacement operator[147], defined by $D(\mu^{(n)}) = \prod_i e^{(c_+^i \mu_i^{(n)} - \mu_i^{*(n)} c_-^i)} \equiv \prod_i D_i(\mu_i^{(n)})$, then we can have

$$e^{ixc_+^k c_-^k} D(\mu) = \prod_{i \neq k} e^{(c_i^k \mu_i - \mu_i^* c_-^k)} \{ e^{ixc_+^k c_-^k} \left[\sum_{n=0}^{\infty} \frac{c_+^k \mu_k - \mu_k^* c_k^k}{n!} \right] e^{-ixc_+^k c_-^k} \} e^{ixc_+^k c_-^k}. \quad (3.74)$$

Following Baker-Hausdorff formula[55], we get

$$e^{ixc_+^k c_-^k}(c_+^k \mu_k - \mu_k^* c_-^k) e^{-ixc_+^k c_-^k} = (c_+^k \mu_k - \mu_k^* c_-^k) + ix[c_+^k c_-^k, (c_+^k \mu_k - \mu_k^* c_-^k)]$$

$$+ \frac{(ix)^2}{2!}[c_+^k c_-^k, [c_+^k c_-^k, (c_+^k \mu_k - \mu_k^* c_-^k)]] + \cdots \quad (3.75)$$

Now, if the bath operators c_+^k and c_-^k obey Eqs.(3.2), (3.3) and (3.4) along with the Grassmann variable μ_k and μ_k^* obeying Eqs.(3.5), (3.6), (3.7) and (3.8), we get

$$[c_+^k c_-^k, c_+^k \mu_k - \mu_k^* c_-^k] = c_+^k \mu_k + \mu_k^* c_-^k \quad (3.76)$$

and

$$[c_+^k c_-^k, c_+^k \mu_k + \mu_k^* c_-^k] = c_+^k \mu_k - \mu_k^* c_-^k. \quad (3.77)$$

Inserting Eqs.(3.76) and (3.77) and into Eq.(3.75), we get

$$e^{ixc_+^k c_-^k}(c_+^k \mu_k - \mu_k^* c_-^k) e^{-ixc_+^k c_-^k} = c_+^k \mu_k e^{ix} - \mu_k^* c_-^k e^{-ix}. \quad (3.78)$$

Now inserting Eq.(3.78) to (3.75), we finally arrive at Eq.(3.27).

Chapter 4

Fermionic bath induced antibunching and coherence in Mollow spectra

In this work, we have derived the modified Bloch equation from the generalized master equation due to the fermionic bath where one needs to consider Grassmann algebra to obtain the similar mathematical structure of the reduced system dynamics, as in the case of a bosonic bath. We have compared our result thoroughly with an experimental result in the temperature dependent emission characteristics within an environment of quantum dots in a Hanburry-BrownTwiss set-up. The entire chapter is organized as follows. After giving a short introduction in the Section 4.1, in section 4.2, we describe dissipative dynamics due to fermionic bath in terms of generalized master equation and construct the modified Bloch equations. The next section is devoted to study the emission characteristics and to probe absorption of the strongly coupled atom-field system. Here, in the first subsection, we show how our results are experimentally viable to explain some features of antibunching character of the emitted photons. In the subsection 4.2.2, we study the Mollow resonance fluorescence of a strongly driven two-level system. In the next subsection, we have studied the absorption characteristics under a weak probe field. Finally we conclude in Section 4.4. A modified quantum fluctuation-dissipation relation for a thermal reservoir composed of spin-1/2 particles is also given as an appendix of the chapter.

4.1 Introduction

The dynamics of dissipation of an open quantum system[54, 55, 57, 75, 58, 56, 69] generally depends on the quantum statistical nature and the energy level structure of the environment degrees of freedom with which the system interacts. The harmonic oscillator description of the environment is useful to explain a large variety of phys-

ical situations[120, 121, 122, 123, 124, 125, 126, 127, 128, 129, 130, 131, 132] such as, spontaneous emission, polaron formation, exciton motion, macroscopic quantum tunneling etc., in atomic physics, condensed matter physics[13] and quantum optics[56]. But, if the environment is considered to be fermionic, a wide range of differences appear in comparison to the bosonic bath case. Most interestibgly, unlike the bosonic case, the dynamic anticorrelations in the noise for a fermionic bath has no classical analog. In the bosonic case, antibunching is usually understood in terms of the constructive and destructive interference of two possible propagation paths that the two particles follow to reach the detector as in the experiment of Hanbury-Brown-twiss[56, 71, 72, 73]. However, if the bath is of fermionic nature which posseses an inherent anticorrelation effect, the emitting atom can be affected in a nontrivial way specially when the effect of bath is magnified at a higher chemical potential. In this context it is reasonable to study how the Mollow resonance fluorescence and probe absorption of the driven system is modified due to fermionic bath at low non-zero temperature and high chemical potential. Enough reports[196, 78, 79, 80] regarding fluorescence from semiconductor quantum dots as well as several experimental reports are also available in the context of the photon antibunching from similar systems. Measurement reveals that the noise correlations are good indicator for the studies of fermi systems[65, 66, 67, 68, 139, 141, 142] composed of electrons or free neutral fermionic atoms which can be modelled by the reservoir to be made up of spin-$\frac{1}{2}$ particles. But to the best of our knowledge the dissipative dynamics of a system coupled to a fermionic reservoir, in a closely similar mathematical structure as that of the bosonic case essentially needs Grassmann algebra, is not well studied in the context of quantum optical phenomena.

In this chapter, we have answered the following questions: (i) How does the antibunching character of in the photon emission from quantum dots differ when the environment is considered fermionic? The analysis has been done after deducing the equation on motion for a simple model 2-level system coupled to a fermionic reservoir under the framework of quantum theory of damping. As the next topic, we have answered the question that (ii) how does the resonance fluorescence and the absorption spectra are affected when the bath is typically fermionic in nature? Finally, we have shown that how the fluctuation-dissipation relation is modified due to system-reservoir interaction and also the role of the Grassmann algebra to get a one-to-one correspondence with the bosonic case.

4.2 The Master Equation and asymptotic solution of a modified Bloch Equation

In this section, we first formulate the generalized master equation for a driven two-level system coupled to a fermionic bath. The dynamics of the reduced system is

derived considering the interaction coefficients of system and bath as Grassmann variables to have similar mathematical structure as in the bosonic bath case.

To put our work in a proper perspective, let us consider a system described by a Hamiltonian,H_S be coupled to a reservoir at thermal equilibrium described by the Hamiltonian,H_B. The total Hamiltonian,H_T can be expressed as

$$H_T = H_S + H_B + V \equiv H_0 + V. \tag{4.1}$$

Here, V represents the interaction between the system and the reservoir in the Schrodinger picture(S.P). In general V assumes the form

$$V = \hbar \sum_k Q_k F_k, \tag{4.2}$$

where Q_k and F_k are the system and the reservoir operators respectively in S.P.

The joint density operator κ for the system and the reservoir obeys the Liouville-von Neumann equation in interaction picture(I.P.) as

$$\frac{\partial \kappa}{\partial t} = -\frac{i}{\hbar}[V(t), \kappa(t)]. \tag{4.3}$$

We assume that the interaction is sufficiently weak so that we can resort to perturbation theory and iterate Eq.(4.3) upto second order in V. Next, we eliminate the bath variables by taking trace in standard procedure[56], thereby obtaining the equation of motion for the reduced density operator, ρ in S.P as

$$\frac{d\rho}{dt} = -\frac{i}{\hbar}[H_S, \rho] - \sum_{i,j} \int_0^t dt' \{[Q_i Q_j^{'} \rho^{'}(t') - Q_j^{'} \rho^{'}(t') Q_i] \langle F_i F_j^{\prime} \rangle_B$$

$$-[Q_i \rho^{'}(t') Q_j^{'} - \rho^{'}(t') Q_j^{'} Q_i] \langle F_j^{'} F_i \rangle_B \}, \tag{4.4}$$

where,

$$Q_j^{'} \rho^{'}(t') = \exp[-\frac{i}{\hbar} H_S(t-t')] Q_j \rho(t') \exp[\frac{i}{\hbar} H_S(t-t')], \tag{4.5}$$

and

$$F_j^{'} = \exp[-\frac{i}{\hbar} H_B(t-t')] F_j \exp[\frac{i}{\hbar} H_B(t-t')]. \tag{4.6}$$

Here we assume that the factorisation $\kappa(t) = s(t)\rho_B(t)$ is valid, where $s(t)$ is the system density operator in I.P and $\rho_B(t)$ is the density operator corresponding to the reservoir at thermal equilibrium.

In our present work, we choose H_S as Hamiltonian for a two-level system with characteristic frequency ω_0 driven by a classical monochromatic light field of frequency ω and coupled to an infinite number of degrees of freedom at thermal equilibrium. The system is characterised by usual Pauli spin operators σ_+, σ_- and σ_z and on the other hand, the reservoir is considered to be composed of infinite number of non-interacting spin-$\frac{1}{2}$ fermions with characteristic frequencies ω_k and reservoir

operators denoted by σ_+^k, σ_-^k and σ_z^k; k being the index for the fermionic bath modes. Within this framework, H_S and H_B assumes the form

$$H_S = \frac{1}{2}\hbar\omega_0\sigma_z, \tag{4.7}$$

$$H_B = \sum_k \hbar\omega_k\sigma_+^k\sigma_-^k. \tag{4.8}$$

The fermions follow the anticommutation rule $\{\sigma_+^l, \sigma_-^m\}_+ = \delta_{lm}$ and the following algebra:

$$\sigma_+^k\sigma_+^k = \sigma_-^k\sigma_-^k = 0 \tag{4.9}$$

$$[\sigma_+^k, \sigma_+^k\sigma_-^k] = -\sigma_+^k \tag{4.10}$$

$$[\sigma_-^k, \sigma_+^k\sigma_-^k] = \sigma_-^k. \tag{4.11}$$

The system-bath interaction is given by

$$V = \sum_k \hbar(g_k^*\sigma_+\sigma_-^k + \sigma_-\sigma_+^k g_k), \tag{4.12}$$

where g_k and g_k^* are dimensionless interaction coefficients obeying Grassmann algebra. The Grassmann variables satisfy convenient relations like[205]:

$$\{g_i, g_j\}_+ = 0 \tag{4.13}$$

$$\{g_i^*, g_j\}_+ = 0 \tag{4.14}$$

$$\{g_i^*, g_j^*\}_+ = 0. \tag{4.15}$$

We also assume that[147]

$$\{g_k, \sigma_-^k\}_+ = 0. \tag{4.16}$$

It is to be noted that the interaction Hamiltonian[see Eq.(4.12)] is expressed under the framework of Rotating Wave Approximation(RWA). The classical driving term in RWA also, can be expressed as

$$V_{ext}(t) = -\frac{\hbar}{2}E_0(\sigma_+ \exp(-i\omega t) + \sigma_- \exp(i\omega t)). \tag{4.17}$$

Therefore, the reduced density operator equation of motion becomes [see Eq.(4.4)]

$$\frac{d\rho}{dt} = -\frac{i}{\hbar}[H_S + V_{ext}, \rho] - \int_0^t dt'\{[\sigma_+\sigma_-^{'}\rho^{'}(t') - \sigma_-^{'}\rho^{'}(t')\sigma_+]\langle\sum_k g_k^*\sigma_-^k e^{-i\omega_k(t-t')}\sigma_+^k g_k\rangle_B$$

$$-[\sigma_+\rho^{'}(t')\sigma_-^{'} - \rho^{'}(t')\sigma_-^{'}\sigma_+]\langle\sum_k e^{-i\omega_k(t-t')}\sigma_+^k g_k g_k^*\sigma_-^k\rangle_B\}$$

$$-\int_0^t dt'\{[\sigma_-\sigma_+^{'}\rho^{'}(t') - \sigma_+^{'}\rho^{'}(t')\sigma_-]\langle\sum_k \sigma_+^k g_k e^{i\omega_k(t-t')}g_k^*\sigma_-^k\rangle_B$$

$$-[\sigma_-\rho^{'}(t')\sigma_+^{'} - \rho^{'}(t')\sigma_+^{'}\sigma_-]\langle\sum_k e^{i\omega_k(t-t')}g_k^*\sigma_-^k\sigma_+^k g_k\rangle_B\}. \tag{4.18}$$

Here, $\langle\cdots\rangle_B$ implies quantum statistical average over the bath coordinates and for any operator X, it is defined as

$$\langle X\rangle_B = \frac{Tr_B X e^{-H_B/KT}}{Tr_B e^{-H_B/KT}}. \tag{4.19}$$

The Bloch equations can then be obtained as:

$$\langle\dot{\sigma}_+\rangle = i\omega_0\langle\sigma_+\rangle + \frac{i}{2}E_0e^{i\omega t}\langle\sigma_z\rangle - \int_0^t dt'\langle\sigma_+(t')\rangle\sum_k g_k^*g_k(1-2\bar{n}(\omega_k))e^{i\omega_k(t-t')}, \tag{4.20}$$

$$\langle\dot{\sigma}_-\rangle = -i\omega_0\langle\sigma_-\rangle - \frac{i}{2}E_0e^{-i\omega t}\langle\sigma_z\rangle - \int_0^t dt'\langle\sigma_-(t')\rangle\sum_k g_k^*g_k(1-2\bar{n}(\omega_k))e^{-i\omega_k(t-t')}, \tag{4.21}$$

$$\langle\dot{\sigma}_z\rangle = iE_0[\langle\sigma_+\rangle e^{-i\omega t} - \langle\sigma_-\rangle e^{i\omega t}]$$
$$- \int_0^t dt'\sum_k 2g_k^*g_k\cos((\omega_0-\omega_k)(t-t'))[1+\langle\sigma_z\rangle(1-2\bar{n}(\omega_k))]. \tag{4.22}$$

In the next step, we introduce the slowly varying operators as ξ_+, ξ_- and ξ_z such that $\xi_+ = \langle\sigma_+\rangle\exp(-i\omega t)$, $\xi_- = \langle\sigma_-\rangle\exp(i\omega t)$ and $\xi_z = \langle\sigma_z\rangle$. The Equations of motion for the Bloch components are now given as:

$$\dot{\xi}_+(t) = i(\omega_0-\omega)\xi_+(t) + \tfrac{i}{2}E_0\xi_z(t)$$
$$- \int_0^t dt'\xi_+(t')\sum_k g_k^*g_k(1-2\bar{n}(\omega_k))\exp[-i(\omega-\omega_k)(t-t')], \tag{4.23}$$

$$\dot{\xi}_-(t) = -i(\omega_0-\omega)\xi_-(t) - \tfrac{i}{2}E_0\xi_z(t)$$
$$- \int_0^t dt'\xi_-(t')\sum_k g_k^*g_k(1-2\bar{n}(\omega_k))\exp[i(\omega-\omega_k)(t-t')], \tag{4.24}$$

$$\dot{\xi}_z(t) = iE_0[\xi_+(t) - \xi_-(t)]$$
$$- \int_0^t dt'\sum_k 2g_k^*g_k\cos((\omega_0-\omega_k)(t-t'))[1+\xi_z(t)(1-2\bar{n}(\omega_k))]. \tag{4.25}$$

We now proceed further taking into consideration of Markov approximation such that the slowly varying variables become $\xi_\pm(t') \simeq \xi_\pm(t)$ and $\xi_z(t') \simeq \xi_z(t)$, we arrive at the equation of motion of Bloch vectors as:

$$\dot{\xi}_+(t) = i\Delta\omega\xi_+(t) + \frac{i}{2}E_0\xi_z(t) - \frac{\gamma}{2}(1-2\bar{n}(\omega_0))\xi_+(t), \tag{4.26}$$

$$\dot{\xi}_-(t) = -i\Delta\omega\xi_-(t) - \frac{i}{2}E_0\xi_z(t) - \frac{\gamma}{2}(1-2\bar{n}(\omega_0))\xi_-(t), \tag{4.27}$$

$$\dot{\xi}_z(t) = iE_0[\xi_+(t) - \xi_-(t)] - \gamma - \gamma(1-2\bar{n}(\omega_0))\xi_z(t), \tag{4.28}$$

where,

$$\gamma = 2\pi g^*(\omega_0)g(\omega_0)P(\omega_0), \tag{4.29}$$

and, $P(\omega_0)$ is the frequency dependent spectral density function at the system frequency $\omega = \omega_0$ along with the detuning parameter $\Delta\omega = \omega_0 - \omega$. This physically corresponds to the possibility of preparation of a thermal bath composed of quantum dots each with two levels having a characteristic size(energy) distribution[228] of a large width ensuring a constancy in the value of the dissipation constant γ. The actual distribution of the energy level structure of the reservoir in fact depends on the practical situation at hand.

We arrive at the asymptotic solution of the Bloch equations as follows:

$$\xi_+(t\to\infty) = \frac{\frac{i}{2}E_0}{\gamma_0 + i\beta}\xi_z(t\to\infty), \tag{4.30}$$

$$\xi_-(t\to\infty) = \frac{-\frac{i}{2}E_0}{\gamma_0 - i\beta}\xi_z(t\to\infty), \tag{4.31}$$

$$\xi_z(t\to\infty) = -\frac{\gamma_0^2+\beta^2}{(1-2\bar{n}(\omega_0))[\frac{E_0^2}{2}+\gamma_0^2+\beta^2]}. \tag{4.32}$$

where $\beta = -\Delta\omega$ and $\gamma_0 = \frac{\gamma}{2}(1-2\bar{n}(\omega_0))$.

From the above deduction, it is evident that the steady state value of the Bloch vector components are only dependent on temperature of the fermion bath for a constant external driving field. The temperature dependence actually comes through the Fermi-Dirac distribution function $\bar{n}(\omega_0)$ which explicitly appears here as $(1-2\bar{n}(\omega_0)) = \tanh(\frac{\hbar\omega_0-\mu}{2KT})$. The presence of this temperature dependent hyperbolic tangent factor was also noted earlier by Caldeira *et.al*[65]. It is evident that due to the presence of this factor, the system reservoir coupling reduces in an effective way. This reduction in the coupling will in turn act as a source to induce coherence within the system dynamics. We[229] have already studied such effects in the context of a system coupled to a spin bath via Quantum non-demolition type of interaction. Here, it would not be out of place, if we mention in this regard that the asymptotic solution of Bloch equations can also be used in the study of quantum transport[221] and to study magnetisation vector dynamics and spin-current damping phenomena[230] in spin polarised fermi liquids.

4.3 Antibunching and Mollow spectra due to a fermionic bath

In this section, we explore the Bloch equation due to fermionic bath to calculate antibunching and the Mollow spectra of the emission and absorption of a strongly driven quantum dot and weakly coupled to a spin reservoir. Few years back, Malko *et.al*[71] reported a temperature dependent measurement of emission characteristics for single pyramidal InGaAs/AlGaAs quantum dots in a Hanburry-Brown Twiss set-up under a low-power excitation intensity. We use the present theory to support the temperature dependence of the antibunching measurements for the quantum dot system.

4.3.1 Second order coherence of the emission spectrum

Here we calculate the second order correlation of the emission intensity in the scattered spectrum. The second order correlation function $G^{(2)}(\tau)$ can be expressed as[56]

$$G^{(2)}(\tau) \propto \langle \sigma_+(0)\sigma_+(\tau)\sigma_-(\tau)\sigma_-(0)\rangle. \tag{4.33}$$

Noting that

$$\sigma_+(\tau)\sigma_-(\tau) = \frac{1}{2} + \frac{1}{2}\sigma_z(\tau), \tag{4.34}$$

we get

$$G^{(2)}(\tau) \simeq \frac{1}{2}\langle \sigma_+(0)\sigma_-(0)\rangle + \frac{1}{2}\langle \sigma_+(0)\sigma_z(\tau)\sigma_-(0)\rangle. \tag{4.35}$$

It is to be noted that,

$$G^{(2)}(0) = 0. \tag{4.36}$$

Let us define

$$R_{++-}(\tau) = \langle \sigma_+(0)\sigma_+(\tau)\sigma_-(0)\rangle, \tag{4.37}$$

$$R_{+z-}(\tau) = \langle \sigma_+(0)\sigma_z(\tau)\sigma_-(0)\rangle, \tag{4.38}$$

$$R_{+--}(\tau) = \langle \sigma_+(0)\sigma_-(\tau)\sigma_-(0)\rangle, \tag{4.39}$$

where, $\sigma_i(0)$ are the steady state components of the Bloch vectors obtained from Eqs.(4.30), (4.31) and (4.32).

Laplace transforms of Eqs.(4.37), (4.38) and (4.39) in matrix representation gives

$$\begin{pmatrix} \gamma_0 + p & -\frac{iE_0}{2} & 0 \\ -iE_0 & 2\gamma_0 + p & iE_0 \\ 0 & \frac{iE_0}{2} & \gamma_0 + p \end{pmatrix} \begin{pmatrix} \bar{R}_{++-}(p) \\ \bar{R}_{+z-}(p) \\ \bar{R}_{+--}(p) \end{pmatrix} = \begin{pmatrix} R_{++-}(0) \\ R_{+z-}(0) \\ R_{+--}(0) \end{pmatrix}, \tag{4.40}$$

with

$$\bar{R}_{ijk}(p) = \int_0^\infty d\tau e^{-p\tau} R_{ijk}(\tau). \tag{4.41}$$

Hence after a straightforward algebra, we get

$$\bar{R}_{+z-}(p) = \frac{D_{\bar{R}_{+z-}(p)}}{D} = -\frac{\langle\sigma_+(0)\sigma_-(0)\rangle\gamma_0 + p}{2(p^2 + 3\gamma_0 p + E_0^2)}, \tag{4.42}$$

with $E_0 \gg \gamma$ and D is the magnitude of the determinant of the corresponding matrix in Eq.(4.40).

Now, we can express

$$\frac{\gamma_0 + p}{(p^2 + 3\gamma_0 p + E_0^2)} \simeq \frac{1}{p + \frac{3\gamma_0}{2} + iE_0} + \frac{1}{p + \frac{3\gamma_0}{2} - iE_0}, \tag{4.43}$$

where, we have applied the approximation that as $\bar{n}(\omega_0)$ varies from 0 to 1, γ_0 is very small and γ_0^2 is even smaller, hence neglected.

Therefore after performing the inverse Laplace transform, we get the normalised second order intensity correlation function

$$g^{(2)}(\tau) = \frac{2G^{(2)}(\tau)}{\xi_+(0)\xi_-(0)} = 1 - \cos(E_0\tau)e^{-\frac{3\gamma_0\tau}{2}}. \tag{4.44}$$

First, we note that, the oscillations appearing in the second order correlation function in Eq.(4.44) is a purely mathematical consequence here due to the presence of the cosine factor having the strength of the incident electric field in its argument[56]. However, in case of experimental observations[71, 73], the oscillations appearing in the second order coherence in photon emission is additionally due to the off-resonant coupling of the classical driving term with that of the particular mode of quantum dot.

We, first of all demonstrate our result by comparing second order coherence for a two-level system coupled to an harmonic oscillator bath and fermion bath. The result is shown in Fig.(4.1) where it is clear that for the same set of bath parameters, the time scale of $g^{(2)}(\tau)$ to reach its asymptotic value differs to a large extent for a fermion bath in comparison to its bosonic partner at finite temperature. It is also worth mentioning that there exists a counter intuitive effect of temperature for the former case. This can be explained on the basis of the fact that at finite temperature, the spectral density function for the fermion bath is effectively modified due to the presence of the hyperbolic tangent factor in comparison to the oscillator bath. The delay in the attainment of asymptotic value of $g^{(2)}(\tau)$ when it is coupled to a fermionic(instead of a bosonic) environment indicates enhancement of antibunching in the emission characteristics. This enhancement is physically caused by the fact that spin bath modes are intrinsically antibunched (a short discussion in this regard in presented in the Appendix). As a consequence, it assists in coherence at a high temperature.

We now explicitly use the result of enhanced antibunching to have a comparison with that of experimentally observed ones. We use the present theory to support the

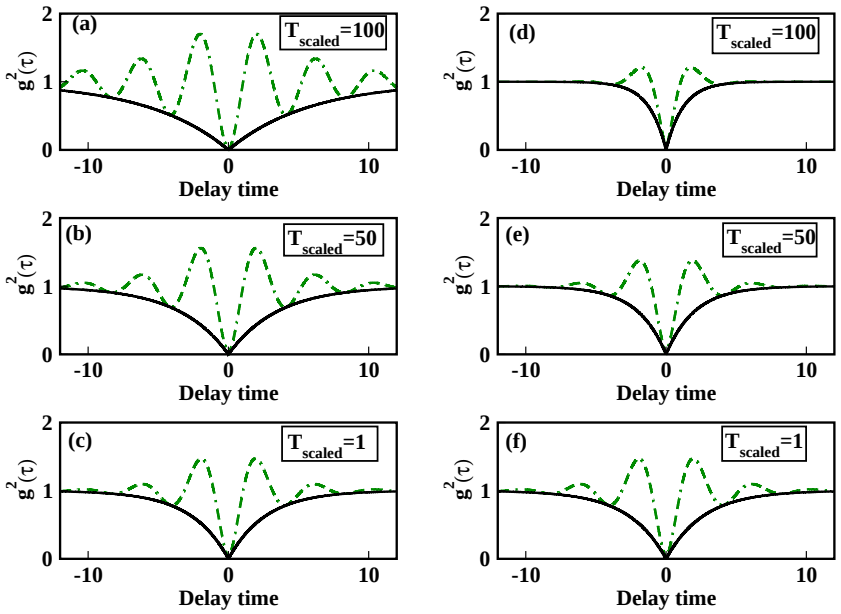

Figure 4.1: Plots of $g^{(2)}(\tau)$ against scaled delay time for fermionic and bosonic baths at a fixed value of $E_0/\gamma = 1.5$ for different values of scaled temperatures $T_{scaled} = KT/\hbar\gamma$. Panels (a) to (c) plot the $g^{(2)}(\tau)$ for the fermionic bath at $KT/\hbar\gamma = 100$, 50 and 1 respectively. The dashed lines represent the actual variation whereas the solid ones do represent their best fits. Panels (d) to (f) plot the $g^{(2)}(\tau)$ for the bosonic bath at $KT/\hbar\gamma = 100$, 50 and 1 respectively. The figure clearly reveals the temperature-assisted enhancement in antibunching in the emission characteristics of the driven two-level system when it is coupled to the fermionic environment. Reversed dependence of temperature is observed when the system is coupled to a bosonic reservoir.

temperature dependence of the antibunching measurements on single quantum dot. Few years back, Malko *et. al*[71] reported a temperature dependent measurement of emission characteristics for single pyramidal InGaAs/AlGaAs QDs in a Hanburry-Brown Twiss set-up under a low-power excitation intensity. The results reported an increase in the decay time from 1.2 ns to 4.0 ns for an increase in the temperature from 10 K to 90 K. In order to correlate this the present theory so far discussed in Section4.2, we set our parameters as $\gamma = 10^9 sec^{-1}$ and $E_0/\gamma = 1.5$ and fix the temperature of the reservoir at 10 K, 30 K, 50 K and 80 K. However a point is to be noted that our theory does not consider any background emission due to absence of any impurity phonon mode in the reservoir leading to a pure antibunching character thereby giving $g^{(2)}(0) = 0$. A more detailed calculation[68] will result an addition of the term γ_{phonon} to γ_0 in order to account for the additional dissipation due to local phonon modes in the bath as impurities. However, in order to accommodate that, we numerically add the value obtained from the experimental data[71] and present our result from a phenomenological point of view.

The result is plotted in Fig.(4.2). From Fig.(4.2), it is clear that a close agreement

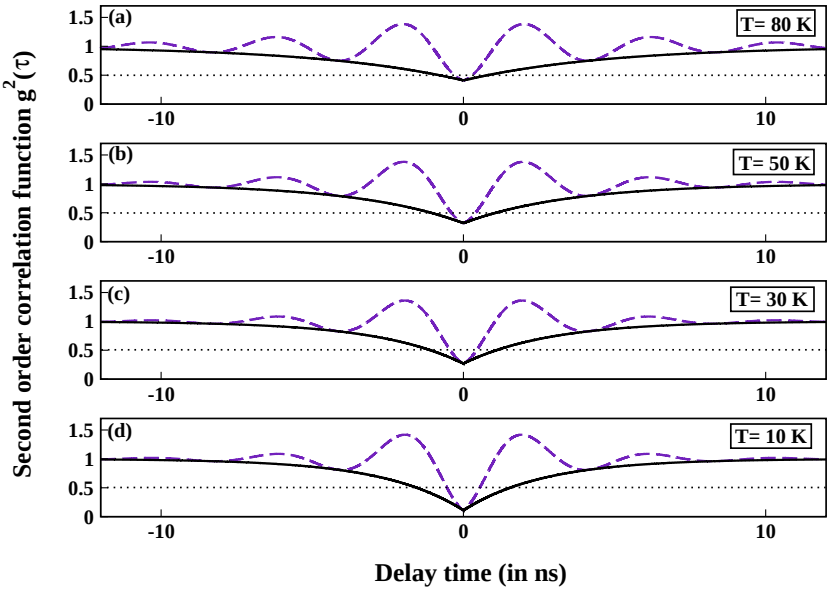

Figure 4.2: Plots of second order correlation $g^{(2)}(\tau)$ against delay time τ in ns for different temperatures in K. The experimental observation of getting background emission is numerically adjusted from the data presented in[71]. The dashed lines represent the actual variation whereas the solid lines represent their best fits. The panels from (a),(b),(c) and (d) present the temperatures as 10 K, 30 K, 50 K and 80 K respectively

between the theory and the experimental observation persists. From the result, it is clear that, with the increase in the reservoir temperature, the antibunching character of the emitted photons increase which is manifested in terms of the increase in the decay time of second order coherence. The so called anomaly in the temperature dependence in the second order coherence in the emission chracteristics lies in the inherent antibunching character of the fermionic noise operators[229]. This is in principle a manifestation of the antisymmetric two-particle fermionic wave-function which excludes overlapping wave trains forbidden by Pauli Exclusion principle. A little digression regarding the coupling mechanism of the quantum dot with that of the fermionic bath would be having a relevance for further understanding. In experimental set up, the quantum dots are prepared on a suitably pre-patterned substrates. This is usually followed by the removal of the substrate using selective chemical etching or by electron beam lithography as the case may be[71, 73]. The possibility of reporting second-order coherence usually depends on the efficiency of the isolation of the single anharmonic quantum system. Therefore, the role of the fermionic bath at a given temperature and chemical potential is played by the additional quantum dots present in the sample during the isolation process. However, the coupling of the specific quantum dot with its neighbour is purely based on the energy conservation consideration. We consider the net effect of excitation of the particular mode in lieu of the de-excitation of the other and vice-versa.

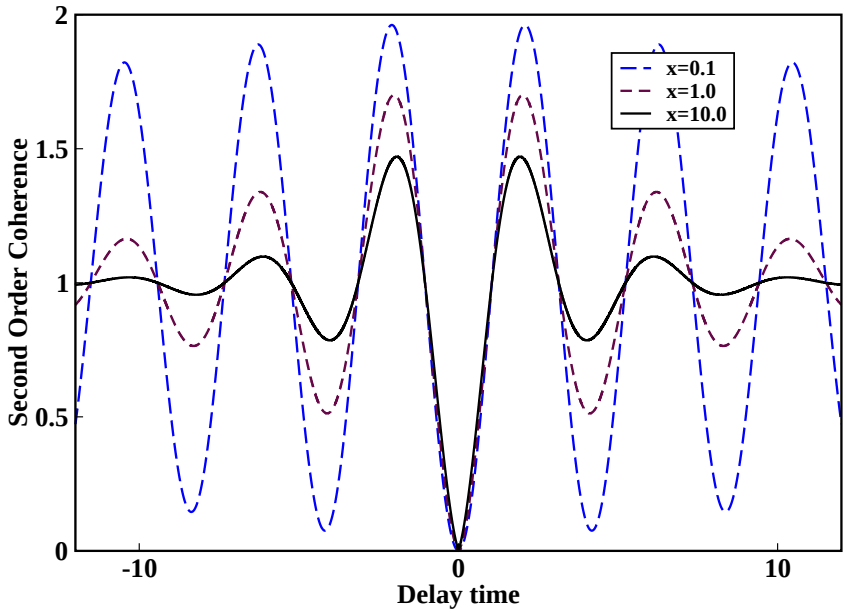

Figure 4.3: Plot of the normalised second order coherence in photon emission from quantum dot $g^{(2)}(\tau)$ against the delay time showing the variation of temperature and chemical potential of the fermion bath in terms of the scaled parameter, $x = \frac{\hbar\omega_0 - \mu}{KT}$. Increase in the scaled parameter, x results suppression of antibunching.

Next, we examine if the bath is considered to be fermionic with a given chemical potential at a given temperature. Here, we see that both temperature and the chemical potential of the reservoir operates together to cause an effective modification in the second-order coherence pattern. We consider $\frac{\hbar\omega_0 - \mu}{KT} = x$ in the Fermi-Dirac distribution function, $\bar{n}(\omega_0)$ and examine the anti-bunching in terms of the scaled parameter x. The result is presented in Fig.(4.3). With the increase in the value of the scaled parameter x from 0.1 to 10.0, the photon antibunching gets supprresed. This is again attributed to the temperature-assisted coherence effect[229] of the reservoir modes.

4.3.2 Resonance Fluorescence Spectrum

Incoherent part of spontaneous emission of a two-level atom irradiated by a continous, monochromatic field is typically known as Resonance Fluorescence. It is usually characterised by a central peak along with two side bands appearing at the strong field-induced Rabi frequency[76]. Strong field Resonance Fluorescence spectrum is defined[76, 231] as

$$S(\nu - \omega_0) = Re\left[\lim_{t\to\infty}\int_0^\infty dt' e^{-i(\nu-\omega_0)t'}\langle\sigma_+(t+t')\sigma_-(t)\rangle\right]. \tag{4.45}$$

An equivalent way to express resonance fluorescence[56] is

$$S(\Delta) = 2Re[\bar{R}_{+-}(-i\Delta)], \tag{4.46}$$

where,

$$\bar{R}_{ij}(p) = \int_0^\infty d\tau e^{-p\tau} R_{ij}(\tau), \tag{4.47}$$

and,

$$R_{+-}(\tau) = \langle \sigma_+(\tau)\sigma_-(0)\rangle. \tag{4.48}$$

In order to evaluate the expression, we follow the standard prescription using regression hypothesis[55]. Without losing any generality, we assume that $\Delta\omega = 0$ for the sake of simplicity of our calculation. As in Section 4.3.1, we get

$$R_{+-}(p) = \frac{D_{\bar{R}_{+-}(p)}}{D}, \tag{4.49}$$

where,

$$D_{\bar{R}_{+-}(p)} = R_{+-}(0)\left[3\gamma_0 p + p^2 + \frac{E_0^2}{2}\right] + \frac{iE_0 R_{z-}(0)}{2}\left[\gamma_0 + p\right], \tag{4.50}$$

and

$$D = [\gamma_0 + p][p^2 + E_0^2 + 3\gamma_0 p], \tag{4.51}$$

within the approximation $E_0 \gg \gamma$.

In the following, we numerically demonstrate the effect of anticommuting nature of the reservoir mode operators in resonance fluorescence spectra in Fig.(4.4). From the traditional Mollow triplet, we see that the position for the appearance of the side peak depends on the strong field induced Rabi frequency. The effect of the anticommuting character of the reservoir modes is studied in terms of the relative magnitudes of the chemical potential and temperature of the thermal bath. For this purpose, we define a scaled parameter $x = \frac{\hbar\omega_0 - \mu}{KT}$ and notice the variations in Fig.(4.4).

From Fig(4.4), it is evident that the fluorescence spectra is appearing typically as a Mollow triplet[76]. A striking feature here is that, with the decrease in x, there is an increase in the height of each of the peaks. For a fixed low value of bath temperature, decrease in x indicates an increase in chemical potential of the bath, which promotes an enhanced coherence effect on the fermionic reservoir modes which in turn produces an increase in intensity of the emission peaks. Since, most of the experiments are performed at low temperature situation, the enhancement in resonance fluorescence by increasing the chemical potential may serve as an alternative tool to increase the fluorescence intensity from a quantum dot.

4.3.3 Absorption spectra

In this section, we analyse the absorption spectrum of a strongly driven two-level system probed by a weak field. The absorption[76, 231] spectrum is given by

$$I(\omega_p - \omega_0) = Re\left[\lim_{t\to\infty}\int_0^\infty e^{-i(\omega_p-\omega_0)t'}\langle[\sigma_-(t+t'),\sigma_+(t)]\rangle dt'\right], \tag{4.52}$$

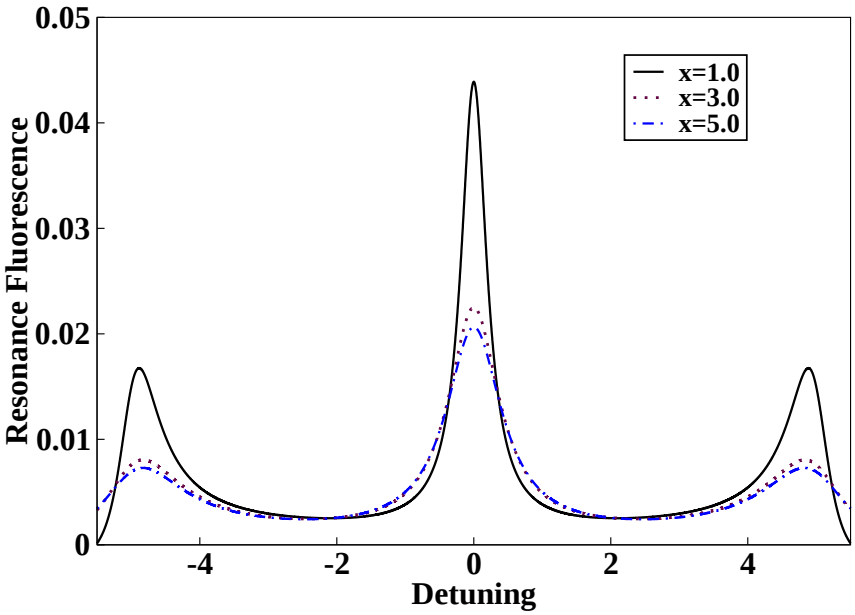

Figure 4.4: The figure shows variation of the resonance fluorescence spectra due to the parametric change in the scaled parameter $x = \frac{\hbar\omega_0 - \mu}{KT}$ for $E_0/\gamma = 4.5$. With the decrease in the value of x, the reseonance fluorescence peak produces enhanced intensity.

where, ω_p is the frequency of the weak probe field. We follow the same line of treatment as that of resonance fluorescence(see the Appendix) at $\Delta\omega = 0$ to get

$$I(\Delta) = \lim_{p \to -i\Delta} 2Re \left[\frac{(\frac{1}{2}(\gamma_0 + p)(2\gamma_0 + p) + \frac{E_0^2}{2})(-2\langle\sigma_z(0)\rangle) - \frac{iE_0}{2}(\gamma_0 + p)(2\langle\sigma_+(0)\rangle)}{D} \right], \tag{4.53}$$

where D is given earlier for $E_0 \gg \gamma$.

For $\bar{n} = 0$, which amounts to $T \to 0$,the bosonic as well as the fermionic bath gives similar result[76, 231, 232]. Here we have plotted the absorption spectra Fig.(4.5) for parameters $E_0/\gamma = 5.0$ for different paramteric values of $x = 1.0$, 3.0 and 5.0 respectively. Change in x causes the change in chemical potential of the bath which effectively modifies the decay rate at a low temperature due to the hyperbolic tangent factor. This induces coherence in the reservoir modes with the decrease in x. The source of this gain is purely thermal in origin and the energy is supplied by the fermionic bath prepared at finite temperature unlike the bosonic bath. A suitable experimental realisation of the observed theoretical result needs preparation of a two-level system(QD) immersed in a sea of spin bath with a characteristic size(frequency) distribution corresponding in a white noise or Markovian limit. The possibility of getting such results however, depend upto what extent the impurity phonon modes in the fermionic bath are properly eliminated

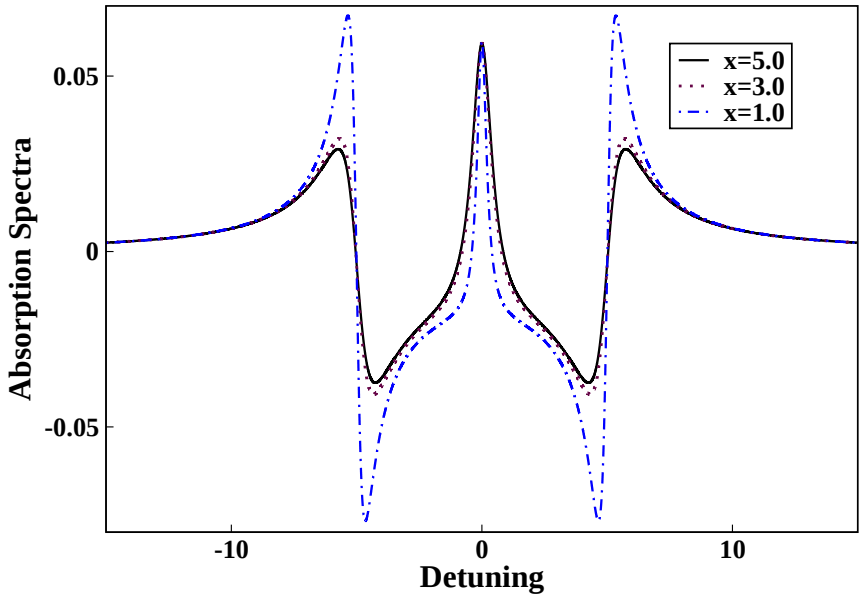

Figure 4.5: Plot of the absorption spectra against the frequency detuning for different parametric values of $x = \frac{\hbar\omega-\mu}{KT}$.

4.4 Conclusion

In the present chapter, we have formulated the equation of motion of the reduced density matrix of a field induced two-level system coupled to a fermionic bath as a modified Bloch equation. Near absolute zero temperature, both for bosonic and fermionic baths, the system dynamics show similar characteristics. However, at a finite temperature, the signature of the two reservoirs becomes distinctly different. This is caused by the presence of the hyperbolic tangent factor appearing in the decay rate. This modifies the system-reservoir coupling in an effective way so that the decay rate does not remain linear with the temperature as well as the chemical potential of the reservoir. It is to be noted that this sort of unique dependence on the system dynamics is an explicit manifestation of the anticommuting Grassmann variables acting as interaction coefficients. It is necessary to implement this to obtain a similar mathematical structure of the reduced system dynamics for both the bosonic and fermionic baths.

An interesting result is an enhancement of antibunching in the photon emission with an increasing temperature from a driven two-level system, as the reservoir has an inherent antibunching property. This is clearly revealed in the Fig.(4.1) where we have demonstrated that, at a finite temperature both for bosonic and fermionic cases, the time scale of $g^{(2)}(\tau)$ to reach its asymptotic value differs to a large extent for a fermionic bath in comparison to its bosonic partner. We have thoroughly compared this feature with an experimental result[71] in the emission characteristics for single pyramidal InGaAs/AlGaAs QDs in a Hanburry-BrownTwiss set-up as shown in the Fig.(4.2). Although the antibunching or anticorrelation considered in this case

is dynamic in origin, this is in principle a manifestation of the antisymmetric two-particle fermionic wave-function, which excludes overlapping of fermions forbidden by the Pauli exclusion principles[70], as is evident from the modified fluctuationdissipation relation. Even if we consider a fermionic bath with a chemical potential at a finite temperature, there is an effective modification in the second order coherence pattern as shown in the Fig.(4.3).

A decrease in the reservoir chemical potential causes an effective reduction in the coupling between the system and the bath. Therefore it should induce a coherence phenomena in the system dynamics. This is indeed reflected in the resonance fluorescence spectrum as depicted in the Fig.(4.4). With a decrease in chemical potential, the peaks appearing in the Mollow triplet are reduced in linewidth, along with an increase in the peak intensity. A similar result was also obtained previously[233] by changing the temperature.

We have again shown that, the chemical potential dependence of the absorption spectra where the side peaks of the absorption, as we can see, generally change with a change in Rabi frequency. But, in the moderately low field regime when the Rabi frequency is low, the appearance of the side peaks rise as a result of chemical potential induced coherence phenomenon rather than a field induced one, as given in the Fig.(4.5). The subsequent gain in the probe frequency is evident from the thermal origin where the energy is fully supplied by the fermionic bath at a non-zero temperature. This is not possible in the bosonic case.

We have explored the crucial role of the Grassmann numbers in the context of thermal bath induced coherence and antibunching. We find that it is necessary to consider that the interaction coefficients are non-commuting with the reservoir operators as well as with the system operators. This leads to the satisfaction of modified fluctuationdissipation relation for a spin bath which has no classical analogue in comparison to its bosonic partner. Here also we should mention that antibunching in the reservoir modes effectively increases the noise correlation time, thereby inhibiting the construction of the traditional Markovian Bloch equation at a high temperature, as the thermalization appears here in a non-trivial way. One should construct the Bloch vector components in steady state domain at a higher temperature in a non-Markovian way, which may become sensitive to the initial values. Moreover, it shows an indication that the prevalent antibunching in the equilibrium fermionic bath or such a noise source can be used as a robust tool for further studies of dynamics of a degenerate Fermi system at a low temperature. We expect the implicit role of the Grassmann numbers will be physically more transparent in many other contexts, for example, in connection with dynamic ordering of electrons and neutral fermionic atoms and dynamic quantum phase transitions.

Appendix: Modified Fluctuation-Dissipation relation with Grassmann variables

In this appendix, we propose a derivation of the Fluctuation-Dissipation relation due to system-bath interaction for fermionic reservoir using Grassmann algebra. To do so we first identify the noise operators in the interaction scheme. From the total hamiltonian as given in the Section3.2, the equation of motion of the reservoir operators, σ_-^k and σ_+^k can be given by,

$$\dot{\sigma_+^k} = i\omega_k\sigma_+^k + ig_k^*\sigma_+, \tag{4.54}$$

$$\dot{\sigma_-^k} = -i\omega_k\sigma_-^k - i\sigma_-g_k, \tag{4.55}$$

where, σ_+ and σ_- are the system operators[see Eqs.(4.7) and (4.8)]. The formal solution of Eqs.(4.54) and (4.55) can be obtained as

$$\sigma_+^k(t) = \sigma_+^k(0)e^{i\omega_k t} + i\int_0^t dt' g_k^*\sigma_+ e^{i\omega_k(t-t')}, \tag{4.56}$$

$$\sigma_-^k(t) = \sigma_-^k(0)e^{-i\omega_k t} - i\int_0^t dt' \sigma_- g_k e^{-i\omega_k(t-t')}. \tag{4.57}$$

Again, the equation of motion for the system operator becomes

$$\dot{\sigma}_+(t) = i\omega_0\sigma_+(t) + i\sigma_z[\frac{E_0}{2}e^{i\omega t} - F_2(t)] + \sigma_z\sum_k\int_0^t dt' g_k^*g_k\sigma_+(t')e^{i\omega_k(t-t')}, \tag{4.58}$$

$$\dot{\sigma}_-(t) = -i\omega_0\sigma_-(t) - i\sigma_z[\frac{E_0}{2}e^{-i\omega t} - F_1(t)] - \sigma_z\sum_k\int_0^t dt' g_k^*g_k\sigma_-(t')e^{-i\omega_k(t-t')}, \tag{4.59}$$

where one can identify the noise operators, $F_1(t)$ and $F_2(t)$ by Eqs.(4.60) and (4.61),

$$F_1(t) = \sum_k g_k^*\sigma_-^k(0)e^{i\omega_k t}, \tag{4.60}$$

$$F_2(t) = \sum_k \sigma_+^k(0)g_k e^{-i\omega_k t}. \tag{4.61}$$

As $\sigma_z(t)$ is a very slowly varying operator compared to that of either $\sigma_+(t)$ or $\sigma_-(t)$, one can consider it parametrically so that the quantum noise operator, $F_1(t)$ or $F_2(t)$ has two roles as it adds a fluctuationg force similarly with the external laser field and a dissipative effect due to the last terms in Eqs.(4.58) and (4.59) and both the fluctuating force and dissipative term would vanish simultaneously as $g_k \to 0$. The noise operators satisfy the following relations,

$$\langle F_1(t)\rangle_B = \langle F_2(t)\rangle_B = 0, \tag{4.62}$$

which confirms the fermionic reservoir to be a Langevin noise source along with

$$Re\langle F_2(t)F_1(t') + F_1(t')F_2(t)\rangle_B = -\sum_k g_k^* g_k \tanh\left(\frac{\hbar\omega_k - \mu}{2KT}\right)\cos[\omega_k(t-t')]. \quad (4.63)$$

Here we have denoted $\langle ...\rangle_B$ as the quantum statistical average over the bath coordinates and it is defined as

$$\langle\chi\rangle_B = \frac{Tr_B \chi e^{-H_{bath}/KT}}{Tr_B e^{-H_{bath}/KT}}, \quad (4.64)$$

where χ is an arbitrary reservoir operator and $H_{bath} = \hbar\sum_k \omega_k \sigma_+^k \sigma_-^k$. The modified Fluctuation-Dissipation relation for fermionic noise operators, show the main signatures as summarised below.

i) In the Eq.(4.63), the noise operator average comes out as symmetric correlation function. The correlation of fluctuation has to be considered in a symmetrized fashion to extract any physical sense from it unlike the bosonic bath case[56].

ii) The negative sign appearing in the Eq.(4.63) is a signature coming from antibunching effect of the fermions. This is in principle a manifestation of the antisymmetric two-particle fermionic wave-function, which excludes overlapping by the Pauli exclusion principle. Experimentally such cases of anticorrelations is also present in the existing literature[70] where noise correlations have been measured for degenerate Fermi gas in a crossed optical dipole trap of ^{40}K atoms. The temperature dependence here comes through the hyperbolic tangent factor which is coming here explicitly due to consideration of anticommuting properties of the interaction coefficients obeying Grassmann algebra which.

iii) The main technical source of such a result comes out from the consideration that the Grassmann numbers are non-commuting with respect to both of the system and the bath operators.

Chapter 5

Fermionic thermocoherent state

In this chapter, on the basis of the fermionic coherent state formalism developed by Cahil and Glauber[147], we have introduced here fermionic thermocoherent state which can be realised physically as a displaced thermal state of fermions and also investigated its relation with the displaced number state of fermions. We have also investigated the nature of the average current through a quantum system and its suppression of noise level to explore the efficiency of electron transport due to thermocoherent character of the source with a thermal sink. The rest of the chapter is organized as follows: After giving a brief outline of the bosonic thermocoherent state in the introduction in Sec. 5.2 we have provided a derivation of the fermionic thermocoherent state as a result of the superposition of the thermal and coherent P-distribution functions for fermions. In the next section, we have established how to relate the thermocoherent state with the displaced thermal state and displaced number states. In Sec. 5.4 we have discussed an application of the fermionic thermocoherent state showing the results of electron transport in the steady state and dynamic regime and the noise spectrum through a single-level quantum system connected to a thermal sink but with a thermocoherent source. Finally the article is concluded in Sec. 5.5.

5.1 Introduction

Electron transport[81, 82, 83, 84, 6] properties of small systems with a discrete energy level structure mostly are dominated by coherent effects. For example, quantum tunneling in a system of self assembled quantum dot array reveals antibunching[85, 86] and near life-time limited line-widths[87]. But coherent control of single electron or electron spin in quantum transport have been used to detect the quantized motion of electrons in nanostructures[88, 12, 5]. A coherent transfer of electrons from the source to sink reservoirs maintained at different chemical potentials[84, 234] have been considered both theoretically[89, 90, 91] and experimentally[92]. A coherent source of electrons[93] can be utilised to inject coherence[93, 94] into thermal electron

source for the suppression of noise[95, 5, 97]. Noise reduction can usually be observed in terms of the interference effects[6, 86, 5] as in the examples of emitted electrons from a carbon nanotube[98] and correlation function of time-dependent amplitude and phase of solid-state single-electron sources[235]. The coherent characteristics are well understood for bosonic systems and and the idea of thermocoherent state in case of light was originally conceived long ago by Lachs[99]. In this chapter, our main objective is to construct a fermionic thermocoherent state similar to the bosonic thermocoherent state on the same footing. Although fermionic coherent states were studied in several contexts[143, 144, 145, 146] Cahil and Glauber[147] in 1999 first systematically introduced fermionic coherent state and the corresponding quasiprobability distribution functions similar to the bosonic coherent state[119]. We have also investigated on the possibility of physical realization of the fermionic thermocoherent state by showing its relation with the displaced thermal state and explored its relation with the displaced number state(DNS). As an immediate application of fermionic thermocoherent state, we have examined its effect on electron transport through a single level quantum system if the source reservoir is maintained in a thermocoherent state with the sink reservoir in thermal state. The motivation is to study the modification of the current noise[56, 55, 148] by introducing some coherent character in the source reservoir. We have also shown its relevance through the effect of reduction of noise which are usually done through a coherent driving mechanism[94] of the system[95, 5] when the two reservoirs are in thermal states.

In this chapter, we have made the studies with respect to the following aspects: (*i*) At first, we have derived the fermionic thermocoherent state by the superposition of thermal and coherent P-distribution function for fermions. (*ii*) Next, we have established a clear cut relation of the fermionic thermocoherent state with displaced thermal state and displaced number state. (*iii*) In what follows, we have addressed the application of fermionic thermocoherent state in the context of electron transport in the steady state as well as in the dynamic regime.

5.2 Fermionic Thermocoherent state

In this section our aim is to formulate a fermionic thermocoherent state using the definition of the fermionic coherent state by Cahill and Glauber[147]. Here it is shown that the mathematical methods that have been used to analyze the properties of the bosonic thermocoherent field and the thermal and coherent limits in quantum optics, have their counterparts for the fermionic field. In particular, using the close analogs of the bosonic coherent states, the displacement operators, the P-representation, and the other operator expansions we have described, the quantum statistical features of the fermionic thermocoherent coherent state are based upon the Grassmann calculus of anticommuting variables.

The normalised fermionic coherent state[147] is defined as

$$|\xi\rangle = D(\xi)|0\rangle, \tag{5.1}$$

with $D(\xi)$ being the spin displacement operators defined as

$$D(\xi) = e^{a^\dagger \xi - \xi^* a} = 1 + (a^\dagger \xi - \xi^* a) + (a^\dagger a - \frac{1}{2})\xi^* \xi, \tag{5.2}$$

where a and $a^\dagger$ are the spin step down and step-up operators defined as $a|1\rangle = |0\rangle$ and $a^\dagger|0\rangle = |1\rangle$, respectively with the anticommutaion relation $\{a, a^\dagger\}_+ = 1$. For any mode i, ξ_i and ξ_i^* are Grassmann numbers for the corresponding mode obeying the following anticommutation relations

$$\{\xi_i, \xi_j\}_+ = 0, \tag{5.3}$$

$$\{\xi_i^*, \xi_j\}_+ = 0, \tag{5.4}$$

$$\{\xi_i^*, \xi_j^*\}_+ = 0. \tag{5.5}$$

We also assume[147] the anticommutation of Grassmann numbers ξ_i and ξ_i^* with the operators a and $a^\dagger$, for example,

$$\{\xi_k, a\}_+ = 0. \tag{5.6}$$

For single mode fermion, the $s-$ordered characteristic function $\chi(\xi, s)$ can be expressed as

$$\chi(\xi, s) = Tr[\rho(1 + (\xi a^\dagger - a\xi^*) + \xi^* \xi \{a^\dagger a\}_s)], \tag{5.7}$$

with $\{a^\dagger a\}_s = a^\dagger a + \frac{1}{2}(s-1)$, where $s = 1$ means normal ordering, $s = -1$ means antinormal ordering and $s = 0$ means symmetrically ordered product and ρ is the density operator.

The $s-$ordered quasiprobability distribution function is again defined as

$$W(\alpha, s) = \int d^2\xi e^{(\alpha\xi^* - \xi\alpha^*)} \chi(\xi, s), \tag{5.8}$$

where α and α^* are also Grassmann numbers.

By analogy with boson, the normally ordered quasiprobability distribution function, $P(\alpha) = W(\alpha, 1)$ is defined as

$$P(\alpha) = -\int d^2\beta e^{-(\alpha-\beta)(\alpha^* - \beta^*)} Q(\beta), \tag{5.9}$$

where the anti-normal ordered quasiprobability distribution function, Q is defined as

$$Q(\beta) = \langle\beta|\rho|-\beta\rangle. \tag{5.10}$$

While deducing Eq.(5.9), we have considered that $a|\beta\rangle = \beta|\beta\rangle$ and $\langle\beta|a^\dagger = \langle\beta|\beta^*$ along with trace formula

$$TrB = \int d^2\beta\langle\beta|B|-\beta\rangle = \int d^2\beta\langle-\beta|B|\beta\rangle, \tag{5.11}$$

and the completeness relation

$$\int d^2\beta|\beta\rangle\langle\beta| = I. \tag{5.12}$$

The single mode fermion density operator for a thermal state can be expressed as[147]

$$\rho = (1-\bar{n}_T)\left(\frac{\bar{n}_T}{1-\bar{n}_T}\right)^{a^\dagger a}, \tag{5.13}$$

where $\bar{n}_T$ is the mean occupation number defined as the Fermi-Dirac distribution function

$$\bar{n}_T = \frac{1}{e^{\frac{\hbar\omega-\mu}{kT}}+1}, \tag{5.14}$$

where, μ is the chemical potential per particle and $\hbar\omega$ is the energy for the respective mode. After having a little algebraic manipulation using Equations (5.10)-(5.14), we have the $Q-$distribution function for a single mode thermal fermionic state as

$$Q(\beta) = \exp\left(\frac{\beta\beta^*}{1-\bar{n}_T}\right). \tag{5.15}$$

The $P-$distribution function of thermal state from Equation(5.9) becomes,

$$P(\alpha) = -\bar{n}_T e^{-\frac{\alpha\alpha^*}{\bar{n}_T}}. \tag{5.16}$$

Now we evaluate the $P-$distribution function for a fermionic coherent state defined by the density operator $\rho = |\alpha_0\rangle\langle-\alpha_0|$ as

$$P(\alpha) = -\int d^2\beta e^{-(\alpha-\beta)(\alpha^*-\beta^*)}\langle\beta|\alpha_0\rangle\langle-\alpha_0|-\beta\rangle = \delta(\alpha-\alpha_0). \tag{5.17}$$

Construction of the above Eq.(5.17) utilizes the formula[147]

$$\langle\beta|\alpha\rangle\langle\alpha|\beta\rangle = e^{-(\beta^*-\alpha^*)(\beta-\alpha)}, \tag{5.18}$$

and the definition[147] of the delta-function,

$$\delta(\xi-\zeta) = \int d^2\alpha e^{\alpha(\xi^*-\zeta^*)-(\xi-\zeta)\alpha^*}. \tag{5.19}$$

We are now in a position to construct the thermocoherent state for a fermionic system by the superposition of the thermal and coherent $P-$distribution functions, $P_1(\alpha_1)$ and $P_2(\alpha_2)$ in terms of the density operator χ as

$$\chi = \int d^2\alpha_2 P_2(\alpha_2)D(\alpha_2)\rho_1 D^\dagger(-\alpha_2), \tag{5.20}$$

where

$$\rho_1 = \int d^2\alpha_1 P_1(\alpha_1)|\alpha_1\rangle\langle -\alpha_1|. \tag{5.21}$$

where $P_1(\alpha)$ and $P_2(\alpha)$, respectively, represent the P-distributions of the thermal and coherent states. Considering the properties of the displacement operators[147]

$$D(\alpha_1)D(\alpha_2) = D(\alpha_1+\alpha_2)e^{\alpha_1^*\alpha_2-\alpha_2^*\alpha_1}, \tag{5.22}$$

and

$$D^\dagger(-\alpha_1)D^\dagger(-\alpha_2) = D^\dagger(-\alpha_2-\alpha_1)e^{\alpha_2^*\alpha_1-\alpha_1^*\alpha_2}, \tag{5.23}$$

the resultant $P-$distribution function comes out as

$$P(\alpha) = \int d^2\alpha_2 P_1(\alpha-\alpha_2)P_2(\alpha_2), \tag{5.24}$$

which gives

$$P(\alpha) = -\bar{n}_T \exp\left(-\frac{(\alpha-\alpha_0)(\alpha^*-\alpha_0^*)}{\bar{n}_T}\right), \tag{5.25}$$

with the corresponding density operator

$$\chi = -\bar{n}_T \int d^2\alpha \exp\left(-\frac{(\alpha-\alpha_0)(\alpha^*-\alpha_0^*)}{\bar{n}_T}\right)|\alpha\rangle\langle -\alpha|. \tag{5.26}$$

In what follows to evaluate the integral, we use the following Fourier transform involving Grassmann calculus[147]

$$\int d^2\xi \exp\left(\alpha\xi^* - \xi\beta^* + \lambda\xi\xi^*\right) = \lambda \exp\left(\frac{\alpha\beta^*}{\lambda}\right). \tag{5.27}$$

Using Eq.(5.26), we calculate the diagonal matrix elements of the thermocoherent density matrix as

$$\langle 1|\chi|1\rangle = \chi_{11} = 1-(1-\bar{n}_T)\exp\left(\frac{\alpha_0\alpha_0^*}{1-\bar{n}_T}\right), \tag{5.28}$$

and

$$\langle 0|\chi|0\rangle = \chi_{00} = -\chi_{11} - \bar{n}_T \int d^2\alpha \exp\left(-\frac{(\alpha-\alpha_0)(\alpha^*-\alpha_0^*)}{\bar{n}_T}\right), \tag{5.29}$$

so that

$$\chi_{00}+\chi_{11} = 1. \tag{5.30}$$

At this point, to have a correspondence of a fermionic thermocoherent state with that of a bosonic one, we evaluate the mean occupation number $\langle n\rangle_{TC}$ for a fermionic thermocoherent state as

$$\langle n\rangle_{TC} = \sum_{n=0,1} n\chi_{nn} = 1-(1-\bar{n}_T)e^{-\frac{\bar{n}_c}{1-\bar{n}_T}} = \bar{n}_T+\bar{n}_c, \tag{5.31}$$

and the mean square occupation number $\langle n^2\rangle_{TC}$ as

$$\langle n^2\rangle_{TC} = \sum_{n=0,1} n^2\chi_{nn} = 1-(1-\bar{n}_T)e^{\frac{-\bar{n}_c}{1-\bar{n}_T}}, \tag{5.32}$$

where $\bar{n}_c = \alpha_0^*\alpha_0$. Hence the variance becomes

$$(\Delta n)^2_{TC} = \langle n^2\rangle_{TC} - \langle n\rangle^2_{TC} = (1-\bar{n}_T)e^{-\frac{\bar{n}_c}{1-\bar{n}_T}}\left[1-(1-\bar{n}_T)e^{-\frac{\bar{n}_c}{1-\bar{n}_T}}\right]. \tag{5.33}$$

In appropriate thermal and coherent limits, Eq.(5.33) gives the following result

$$\lim_{\bar{n}_c\to 0}(\Delta n)^2_{TC} = \bar{n}_T(1-\bar{n}_T), \tag{5.34}$$

and

$$\lim_{\bar{n}_T\to 0}(\Delta n)^2_{TC} = \bar{n}_c. \tag{5.35}$$

Equation(5.35) is exactly similar to the thermocoherent bosonic field in the coherent limit. On the contrary, the fermionic thermocoherent field corresponding to the thermal limit $\bar{n}_c \to 0$[see Eq.(5.34)] is different from the bosonic case by a negative sign. This is due to the fermionic anticorrelation between the particles and the expression is already deduced by Cahill and Glauber[147] for the thermally chaotic fermion field. Such a remarkable similarity in the fermionic domain is essentially a major outcome of the crucial roles played by the Grassmann numbers. This is due to the fact that any polynomial in the Grassmann number should be linear making the higher order terms in the exponential function appearing in Eqs. (5.31) and (5.33) vanish which produces a similar mathematical structure of the moments in the bosonic and fermionic thermocoherent states.

5.3 Fermionic displaced thermal state, displaced number state and fermion added coherent states using displacement operator approach

In the mid-1960s Glauber[216] and Lachs[99] had introduced the bosonic thermocoherent state by the approach of superposition of quasiprability distributions; Filipowicz[219] has also defined it in terms of the displaced thermal state by coherently driving a cavity mode in a thermal equilibrium state. However, in fermionic system these two definitions appear very different as the eigenvalues of the annihilation operator are anticommuting Grassmann numbers and the vacuum state is the only eigenstate of the annihilation operator. Here we have studied the properties of the fermionic thermocoherent state by the approach of the fermionic displacement operator. Using Grassmann algebra we arrive at the fermionic thermocoherent state by unitarily displacing the thermal state and we have shown their relation with the

fermionic displaced number states and the fermion-added coherent state. This approach is subsequently used to study the effect of coherence in the thermal electron transport[95] which is purely quantum mechanical in origin. Here we have shown that it is possible to introduce coherence in the thermal fermion bath modes resulting in a thermocoherent bath by coherently driving a thermal bath followed by equilibration.

5.3.1 Fermionic thermocoherent state as displaced thermal state

The density operator for the fermionic thermal state can be obtained as a steady-state solution of the quantum master equation for a fermionic mode coupled to a thermal fermion bath. The master equation in the Markov limit for the reduced density operator $\rho_T(t)$ is given by

$$\dot{\rho}_T(t) = \hat{L}\rho_T(t), \tag{5.36}$$

where,

$$\hat{L}\rho_T(t) = -\{\frac{\gamma}{2}(1-\bar{n}_T)\left[a^\dagger a\rho_T(t) - a\rho_T(t)a^\dagger\right] + \frac{\gamma}{2}\bar{n}_T[aa^\dagger\rho_T(t) - a^\dagger\rho_T(t)a]$$

$$-\frac{\gamma}{2}\bar{n}_T[a^\dagger\rho_T(t)a - \rho_T(t)aa^\dagger] - \frac{\gamma}{2}(1-\bar{n}_T)[a\rho_T(t)a^\dagger - \rho_T(t)a^\dagger a]\}. \tag{5.37}$$

The unitarily displaced density operator ρ_d can be expressed as

$$\rho_d = D(\alpha)\rho_T D^\dagger(-\alpha). \tag{5.38}$$

Here $D(\alpha)$, the fermionic diplacement operator for single mode fermion is $D(\alpha) = e^{a^\dagger\alpha - \alpha^* a}$. Eq.(5.38) bears a minor dissimilarity of a minus sign with that of displaced thermal state of a harmonic oscillator[236]. The reason for such a structural difference can be traced in the intricate nature of the Grassmann numbers which makes its presence felt in the density operator for fermionic coherent state to be expressed as $\rho = |\alpha\rangle\langle-\alpha|$.

The density operator for the thermal state for a single mode fermion can be obtained from steady state solution of Eq.(5.37)as

$$\rho_T = (1-\bar{n}_T)|0\rangle\langle 0| + \bar{n}_T|1\rangle\langle 1|, \tag{5.39}$$

where $\bar{n}_T$ is the mean occupation number [see Eq.(5.14)].

Keeping the following standard relations[147, 229],

$$D(\alpha)|1\rangle\langle 1|D^\dagger(-\alpha) = -\alpha^*\alpha|0\rangle\langle 0| - \alpha^*|0\rangle\langle 1| + \alpha|1\rangle\langle 0| + |1\rangle\langle 1|(1+\alpha^*\alpha), \tag{5.40}$$

and

$$D(\alpha)|0\rangle\langle 0|D^\dagger(-\alpha) = -\alpha^*|0\rangle\langle 1| + \alpha|1\rangle\langle 0| + |0\rangle\langle 0|(1-\alpha^*\alpha) + \alpha^*\alpha|1\rangle\langle 1|, \tag{5.41}$$

we can get the matrix elements of the density operator for the displaced thermal state as

$$\langle 0|\rho_d|0\rangle = (1-\bar{n}_T)(1-\bar{n}_c) - \bar{n}_T\bar{n}_c, \tag{5.42}$$

and

$$\langle 1|\rho_d|1\rangle = (1-\bar{n}_T)\bar{n}_c + \bar{n}_T(1+\bar{n}_c), \tag{5.43}$$

with $\bar{n}_c = \alpha^*\alpha$. Now, using Eqs.(5.42) and (5.43), we can evaluate the average occupation number for the displaced thermal state for a single mode fermion as

$$\langle n\rangle = \sum_{n=0,1} n\langle n|\rho_d|n\rangle = \bar{n}_T + \bar{n}_c. \tag{5.44}$$

Here, we see that Eq.(5.44) gives the same result as that of Eq.(5.31). Therefore, it is possible to express the fermionic thermocoherent state as displaced thermal state. This is very much similar to the idea of coherently driving a thermal bosonic field to prepare a bosonic thermocoherent state. Again, here we must emphasize that the key role lies in Grassmann algebra which gives such a close one to one correspondence.

5.3.2 Displaced Number States and fermion added coherent state

Here we establish the connection between the fermionic thermocoherent state and displaced number states and fermion-added coherent state as often defined in the bosonic cases. The primary idea is to start from the definition of unitarily displaced fermionic thermal state, which is equivalent to fermionic thermocoherent state and to express the latter as a linear combination of displaced number states.

Following Ref.[147], the displaced number state can be conveniently expressed as

$$|n,\alpha\rangle = D(\alpha)|n\rangle, \tag{5.45}$$

and

$$\langle n,-\alpha| = \langle n|D^\dagger(-\alpha), \tag{5.46}$$

with $n = 0, 1$. Hence, the displaced thermal state can be expressed as

$$\rho_d = (1-\bar{n}_T)D(\alpha)\left(\frac{\bar{n}_T}{1-\bar{n}_T}\right)^{a^\dagger a} D^\dagger(\alpha)\left\{\sum_{m=0,1}|m,\alpha\rangle\langle m,-\alpha|\right\}, \tag{5.47}$$

where $a(a^\dagger)$ is the fermionic annihilation(creation) operator. Defining $\bar{n}_T = 1/(e^\lambda + 1)$, we get

$$\left(\frac{\bar{n}_T}{1-\bar{n}_T}\right)^{a^\dagger a} = 1 - \lambda a^\dagger a. \tag{5.48}$$

The simplified form of Eq.(5.48) is markedly due to the fact that the higher orders of the fermionic operator always vanish which stems from the Pauli Exclusion principle.

Inserting the operator identity $D(\alpha)D^{\dagger}(\alpha) = 1$ twice in Eq.(5.48), we get

$$\left(\frac{\bar{n}_T}{1-\bar{n}_T}\right)^{a^{\dagger}a} = 1 - \lambda(D(\alpha)aD^{\dagger}(\alpha))^{\dagger}D(\alpha)aD^{\dagger}(\alpha). \tag{5.49}$$

We are now in a position to define displaced fermionic operators as

$$D(\alpha)aD^{\dagger}(\alpha) = a - \alpha \tag{5.50}$$

and

$$D(\alpha)a^{\dagger}D^{\dagger}(\alpha) = a^{\dagger} - \alpha^{*}. \tag{5.51}$$

Hence, Eq.(5.47) can be re-expressed as

$$\rho_d = (1-\bar{n}_T)\left(\frac{\bar{n}_T}{1-\bar{n}_T}\right)^{(a^{\dagger}-\alpha^{*})(a-\alpha)} \left\{\sum_{m=0,1} |m,\alpha\rangle\langle m,-\alpha|\right\}. \tag{5.52}$$

Therefore, the fermionic thermocoherent state can be expressed as a mixture of orthogonal states which are basically displaced number states like in the bosonic case[236]. Hence, for a multimode fermionic thermocoherent reservoir, the density operator can be expressed as

$$\rho_{bath}^{TC} = \Pi_k \left[(1-\bar{n}_k)\left(\frac{\bar{n}_k}{1-\bar{n}_k}\right)^{(a_k^{\dagger}-\alpha^{*})(a_k-\alpha)} \left\{\sum_{m_k=0,1} |m_k,\alpha\rangle\langle m_k,-\alpha|\right\}\right]. \tag{5.53}$$

It is be noted that although a reservoir is generally considered as intrinsically incoherent, however, here we have shown that it is possible to make a reservoir which is a partially coherent source of particles. This motivates us to study a simple transport problem involving a single-level system connected to two reservoirs, one of which is in a thermocoherent state.

5.4 Application to electron transport

In this section, we discuss the role of the source reservoir which is in a fermionic thermocoherent state in the context of the electron transport process through a single-level quantum system. For the model of quantum current we consider an arrangement of source-system-sink where the source and the sink are fermionic reservoirs. After giving a brief discussion about the master equation for transport we apply it to build the equation of motion for current. In the next subsection we show the steady-state limit to calculate the Fano factor to probe the current noise spectrum.

5.4.1 Steady state and Dynamic regimes of quantum transport: Modification of Conductance formula

Here we consider a quantum system coupled to both the source and sink of electrons as two fermionic reservoirs. We consider the source bath is in a thermocoherent state and the sink is in a thermal state.

To start with, we consider the total Hamiltonian H_T as

$$H_T = H_s + H_E + H_C + H_{int}, \tag{5.54}$$

where H_s is the system Hamiltonian expressed as

$$H_s = \hbar\omega_0 c^\dagger c, \tag{5.55}$$

H_E is the Hamiltonian of the source or emitter expressed as

$$H_E = \hbar \sum_k \omega_k^E a_k^\dagger a_k, \tag{5.56}$$

H_C is the Hamiltonian of the sink or collector expressed as

$$H_C = \hbar \sum_p \omega_p^C b_p^\dagger b_p, \tag{5.57}$$

and the interaction Hamiltonian H_{int} is expressed as

$$H_{int} = \hbar \sum_k (T_{Ek} c^\dagger a_k + c a_k^\dagger T_{Ek}^*) + \hbar \sum_p (T_{Cp} b_p^\dagger c + c^\dagger b_p T_{Cp}^*). \tag{5.58}$$

In Eqs.(5.55)-(5.58), $c(c^\dagger)$, $a_k(a_k^\dagger)$ and $b_p(b_p^\dagger)$ are the step down(step up) operators for the system, k-th emitter mode and p-th collector mode respectively. The system-lead coupling coefficients $T_{Ek}(T_{Ek}^*), T_{Cp}(T_{Cp}^*)$ are considered to obey Grassmann algebra [see Eqs.(5.3)-(5.6)].

If $\rho_I(t)$ be the density operator for the system in interaction picture and ρ_E and ρ_C represents the density operator for the emitter and collector respectively, then the coarse-grained equation of motion[56] can be expressed as

$$\frac{d\rho_I(t)}{dt} = -\frac{1}{\hbar^2} \int_0^t dt' Tr_R[H_{int}(t), [H_{int}(t'), \rho_I(t') \otimes \rho_E \otimes \rho_C]]. \tag{5.59}$$

Putting the density operators for the emitter and the collector for the fermionic bath from Eq.(5.26) for each of the modes and after performing the Markovian approximation in the Schrodinger picture for weak system-bath coupling, we get

$$\frac{d\rho}{dt} = -i\omega_0[c^\dagger c, \rho] - \frac{1}{2}[(c^\dagger c\rho - c\rho c^\dagger)(\gamma_c(1 - \bar{n}_{TC}^e) - \gamma_e(1 - \bar{n}_{TC}^e))$$

$$-(c^\dagger \rho c - \rho c c^\dagger)(\gamma_e \bar{n}_{TC}^e - \gamma_c \bar{n}_{TC}^c)] - \frac{1}{2}[(cc^\dagger\rho - c^\dagger\rho c)(\gamma_e \bar{n}_{TC}^e - \gamma_c \bar{n}_{TC}^c)$$

$$-(c\rho c^{\dagger} - \rho c^{\dagger}c)(\gamma_c(1-\bar{n}^c_{TC}) - \gamma_e(1-\bar{n}^e_{TC}))], \tag{5.60}$$

where, we have assumed that γ_e and γ_c are the corresponding rate constants for the emitter and collector, respectively[56]. In what follows, we assume that the collector is in purely thermal state with $\bar{n}^c_T = 0$, which physically signifies that the chemical potential of the collector is much smaller than that of the system energy scale i.e., $\hbar\omega - \mu_c \gg KT$, where μ_c is the chemical potential of the collector(sink). From the emitter side, we consider that the transport of electrons through the system is controlled by both the thermal as well as coherent parameter of the emitter(source) bath. In the following analysis, we will show the dependence of current through the system in terms of the scaled parameter, $\frac{\hbar\omega-\mu_e}{KT}$ as well as the coherent parameter, $\bar{n}_c$ of the source reservoir.

First of all, we define the average current as

$$\langle\hat{i}\rangle(t) = \frac{1}{2}[\gamma_c\langle c^{\dagger}c\rangle + \gamma_e\langle cc^{\dagger}\rangle], \tag{5.61}$$

where the occupation number operator averages are calculated

$$\langle c^{\dagger}c\rangle(t) = \frac{\gamma_e\bar{n}^e_{TC}}{2\gamma_e\bar{n}^e_{TC} - \gamma_e + \gamma_c}(1 - e^{-(2\gamma_e\bar{n}^e_{TC} - \gamma_e + \gamma_c)t}) + e^{-(2\gamma_e\bar{n}^e_{TC} - \gamma_e + \gamma_c)t}, \tag{5.62}$$

with,

$$\langle cc^{\dagger}\rangle(t) = 1 - \langle c^{\dagger}c\rangle(t). \tag{5.63}$$

Hence the steady state value of the average current by using Eqs.(5.61), (5.62) and Eq.(5.63) comes out as

$$\langle i\rangle_{ss} = \frac{1}{2}\left[\frac{\gamma_e(\bar{n}^e_T + \bar{n}^e_C)(\gamma_e + \gamma_c) - \gamma_e(\gamma_e - \gamma_c)}{2\gamma_e(\bar{n}^e_T + \bar{n}^e_C) - \gamma_e + \gamma_c}\right] \tag{5.64}$$

as $\bar{n}^e_{TC} = \bar{n}^e_T + \bar{n}^e_C$ and here we have considered that the sink is at zero temperature, i.e., $\bar{n}^c_T = 0$. For the usual thermal source, $\bar{n}^e_{TC} = \bar{n}^e_T$ and when the difference in thermal occupation number of source and sink is unity i,e., if $\bar{n}^e_T = 1$ and $\bar{n}^c_T = 0$ making $\bar{n}^e_T - \bar{n}^c_T = 1$ from the above equation one obtains Landauer conductance formula[3, 6, 96],

$$\langle i\rangle_{ss} = \frac{\gamma_e\gamma_c}{\gamma_e + \gamma_c}. \tag{5.65}$$

However, for the thermocoherent source, i.e., $\bar{n}^e_C \neq 0$, the modified formula of the steady state current becomes

$$\langle i\rangle_{ss} = \frac{1}{2}\left[\frac{\gamma_e\bar{n}^e_C(\gamma_e + \gamma_c) + 2\gamma_e\gamma_c}{2\gamma_e\bar{n}^e_C + \gamma_e + \gamma_c}\right]. \tag{5.66}$$

The steady state current through the system is expressed here in terms of γ_e and γ_c, the rate constants of the flow of electrons from the source and to the sink.

The Landauer conductance formula [see Eq.(5.65)] for the system connected with traditional thermal electron source and sink is modified here by the nonzero coherent average fermion number introduced into the source bath, $\bar{n}_C^e$. The main result in this section is the effective modification of conductance formula coming in Eq.(5.66) due to the thermocoherent state of the emitter through the coherent and thermal population terms.

A few comments are relevant here regarding the formula of quantum electron transport through nanostructures for which various methods have been developed. Foremost is the Landauer-Buttiker formalism[4], which establishes a basic relationship between scattering amplitudes and currents through nanostructures, where the conductance is proportional to the transmission coefficient. Secondly, the non-equilibrium Green's function(NEGF) scheme deals with many body interaction effects in quantum transport. Haug and Jauho[237] applies NEGF formalism to arrive at Landauer formula of conductance[6, 237, 221]. However recently, approaches of quantum optics[55, 238] are also applied to study time dependent transport processes through solid state structures. In the present context, the Landauer formula for conductance which is given here expresses the average of the time dependent current without considering any inelastic scattering processes. Eq.(5.66) carries a signature of coherence in the electron conductance formula coming from the source electron reservoir. This has significant implications on the nature of the noise in current unlike the thermal one in usual tunneling conductance of Landauer type.

In order to investigate the effect of thermocoherent state of the emitter in the electron transport process, we evaluate the steady state current and the transient behavior of current through the quantum system. In Fig.(5.1), we study the steady state behavior of the current in terms of the ratio of the steady state thermocoherent current to the thermal one $\frac{\langle i\rangle_{ss}^{TC}}{\langle i\rangle_{ss}^{T}}$ against the coherent population parameter of the emitter $\bar{n}_c^e$ for different scaled temperatures $\frac{KT}{\hbar\omega_0-\mu_e}$. For a fixed value of the scaled temperature, the ratio $\frac{\langle i\rangle_{ss}^{TC}}{\langle i\rangle_{ss}^{T}}$ increases non-linearly with the increase in the value of the coherence parameter, $\bar{n}_c^e$. It is found that, with the increase in scaled temperature, the increment of the ratio with $\bar{n}_c^e$ shows enhancement. Here, we particularly note that the assigned values of the scaled temperature does not necessarily signify a high temperature limit. This actually suggests that the difference in electrochemical potential between the source and the sink is very high with respect to the thermal energy KT. Fig.(5.1) therefore suggests that, as the energy difference between the system and the Fermi level of the emitter is decreased in comparison to the thermal energy, the steady state value increases and the increase is more prominent for the higher range of coherent parameter. We ascribe this phenomenon to the thermal efficiency of electron transport for coherent character of the source bath.

Next we have considered, the current through the quantum system in its dynamical or transient regime. Figure(5.2) shows the transient current for a fixed value

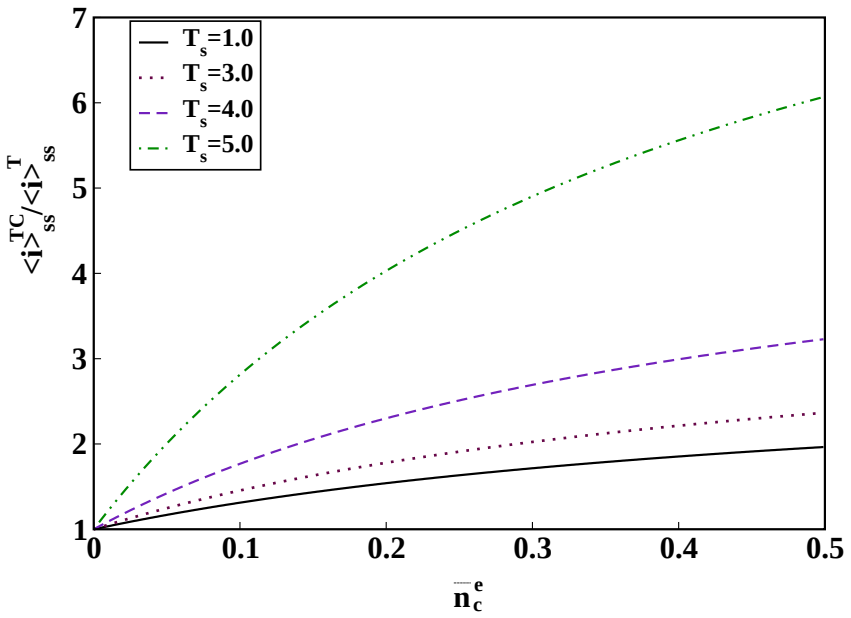

Figure 5.1: Plot of $\frac{\langle i\rangle_{ss}^{TC}}{\langle i\rangle_{ss}^{T}}$ versus, the coherent population of the emitter, $\bar{n}_c^e$ for various scaled temperatures $T_s = \frac{KT}{\hbar\omega_0 - \mu_e}$. Increase in the value of $\frac{KT}{\hbar\omega_0-\mu_e}$ causes an enhancement of the steady state current with the coherent population of the emitter.

of scaled temperature say $\frac{KT}{\hbar\omega_0-\mu_e} = 0.01$ for different parametric values of $\bar{n}_c^e$. We see that the steady current depends on $\bar{n}_c^e$ and in addition to it, the increase in its value causes an increase in the magnitude of steady current. But, the point to be noted here is, for a fixed value of the scaled temperature, the time delay, which is defined as the characteristic time needed for the system to reach the steady state value, decreases. In other words, introduction of coherence in the emitter causes a decrease in the delay time. This is purely a consequence of the quantum nature of the emitter.

We therefore conclude here that the efficiency of transport through the quantum system can be characterized by the magnitude of the delay time which depends strongly on the value of the coherence parameter of the emitter. The more the delay time, the less efficient the transport will be. Thus, the introduction of the coherent character in the emitter enhances the transport efficiency through the device.

5.4.2 Current Noise Spectrum and Fano factor

For the dynamical information about the current and its noise charateristics here we have calculated the noise spectrum and Fano factor from the current-current correlation function. Following Eq.(5.61), we have calculated the equation for the average value of current as

$$\frac{d\langle i\rangle(t)}{dt} = \frac{1}{2}[\gamma_c\gamma_e\bar{n}_c^e + \gamma_e(\gamma_e\bar{n}_c^e - \gamma_e + \gamma_c)] - (2\gamma_e\bar{n}_c^e - \gamma_e + \gamma_c)\langle i\rangle(t). \tag{5.67}$$

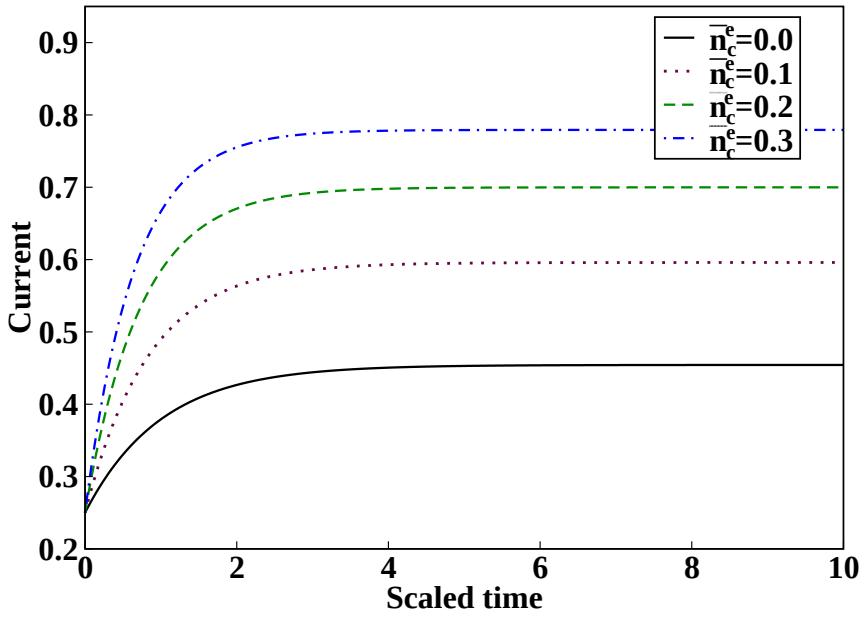

Figure 5.2: Plot of $\langle i\rangle^{TC}(t)$ against scaled time(in units of $(\gamma_e+\gamma_c)^{-1}$) for different parametric values of $\bar{n}_c^e$ at a fixed scaled temperature of $T_s = \frac{KT}{\hbar\omega_0-\mu_e} = 0.01$. Increase in $\bar{n}_c^e$ increases the steady value and also decreases the delay time for the current to reach the magnitude of the steady state.

We use the steady state solution of Eq.(5.67) along with quantum regression theorem[55] (see Appendix) to arrive at the current-current correlation-function as

$$\begin{aligned}\langle i(0)i(\tau)\rangle = \frac{\gamma_e\gamma_c(\bar{n}_c^e+1)+\gamma_e^2(\bar{n}_c^e-1)}{2\gamma_e\bar{n}_c^e-\gamma_e+\gamma_c}\left[1-\frac{\gamma_e\gamma_c(\bar{n}_c^e+1)+\gamma_e^2(\bar{n}_c^e-1)}{2\gamma_e\bar{n}_c^e-\gamma_e+\gamma_c}\right]\\ \times\exp(-(2\gamma_e\bar{n}_c^e-\gamma_e+\gamma_c)\tau)\\ +\left[\frac{\gamma_e\gamma_c(\bar{n}_c^e+1)+\gamma_e^2(\bar{n}_c^e-1)}{2\gamma_e\bar{n}_c^e-\gamma_e+\gamma_c}\right]^2.\end{aligned} \tag{5.68}$$

The Fano factor is defined as

$$F(\omega) = \frac{S(\omega)}{2\langle i(0)\rangle}, \tag{5.69}$$

where $S(\omega)$ is the Fourier transform of the current-current correlation defined as

$$S(\omega) = \int_{-\infty}^{+\infty} e^{i\omega\tau}\langle i(0)i(\tau)\rangle d\tau. \tag{5.70}$$

In what follows, we plot the Fano Factor $F(\omega)$, against the scaled frequency $\frac{\omega}{\gamma_e+\gamma_c}$, for different parametric values of the coherence parameter of the emitter, $\bar{n}_e^c$ and scaled temperature, $\frac{KT}{\hbar\omega_0-\mu_e}$. In Fig.(5.3), we plot the current Fano factor against the scaled frequency, $\frac{\omega}{\gamma_e+\gamma_c}$ for a fixed value of the scaled temperature, $\frac{kT}{\hbar\omega_0-\mu_e} = 0.01$ for different parametric values of the coherent parameter of the emitter, $\bar{n}_c^e$. As the

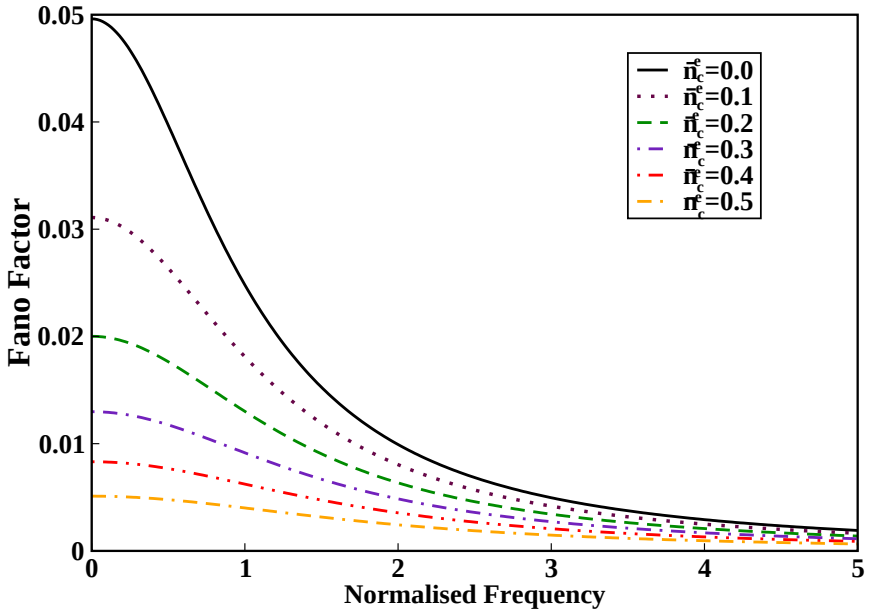

Figure 5.3: Plot of the current Fano factor $F(\omega)$ against normalised frequency $\frac{\omega}{\gamma_e+\gamma_c}$ for a fixed value of the scaled temperature $T_s = \frac{KT}{\hbar\omega_0-\mu_e} = 0.01$ for different paramatric values of the coherent parameter of the emitter $\bar{n}_c^e$. The figure clearly reveals that an increase in the value of coherent parameter results a substantial suppression in noise at a fixed temperature of the emitter.

coherent driving parameter for the emitter increases, the variation pattern becomes more and more flat, revealing that with the increase in coherent population of the emitter results a suppression of current noise. This can be explained on the basis of the fact that, as more and more coherently injected electrons from the emitter tunnels into the system, no further electrons can enter the well until it is drained into the collector. As the emitter as well as collector is assumed to be at a very low temperature and no coherence is present in it, the timescale in which the draining of electrons from the system to the collector takes place will be principally guided by the rate constants γ_e and γ_c along with the thermocoherent state of the emitter. This suppresses the noise which is evident from a decrease in Fano factor.

To conclude the section, we note that the results we show in Fig.(5.3) reveals a quite close qualitative resemblance with that obtained earlier[95], where an increase in the coherent coupling parameter between two quantum systems suppresses the current noise. This evidently gives an indication for an experimental realizability of the thermocoherent bath. An emitter with a suitable thermocoherent state can conveniently be prepared by coupling a system to a fermionic reservoir with a coherent driving followed by thermalizing the entire system at a given low temperature.

5.5 Conclusion

Following the fermionic coherent state formulation of Cahill and Glauber[147], we have introduced a fermionic thermocoherent state. In order to obtain a thermocoherent state, the key element in the derivation is to obtain the quasiprobability P -distribution functions for fermionic thermal and coherent states separately followed by the convolution integration. For the fermionic case the integration is over the anticommuting Grassmann variables which have no classical analog. We have shown that the corresponding average occupation number and the variance gives the appropriate coherent and thermal limits, which puts the fermionic thermocoherent state with the bosonic counterpart on the same footing which is particularly due to the treatment of the Grassmann algebra. We also show that the thermocoherent state can alternately be formulated as a displaced thermal state and subsequently we have shown its connection with the fermionic displaced number state and the fermion-added coherent state. This clearly gives a systematic procedure to introduce coherent character in a thermal fermionic reservoir, which is traditionally considered as an incoherent source of electron.

As an immediate application, we have studied electron transport characteristics of a quantum system connected to a source in a thermocoherent state and a traditional thermal sink. Here we have suggested a modification in the Landauer conductance formula in the present context as a function of thermal and coherent population of the source reservoir. It is found that with the introduction of the coherent character of the emitter, the steady-state current increases and the delay time to reach the steady state decreases which is solely a consequence of the coherent nature of the emitter. Then, we have calculated the current noise spectrum and the Fano factor to monitor the steady-state fluctuation of current. When the emitter is prepared in a thermocoherent state, the noise of the current is suppressed. The suppression of noise in the current reveals a quite close resemblance with the result obtained earlier[95] in the bosonic case using a prepared coherently coupled state of the system instead of introducing coherence in the source as in our case. This evidently gives an indication of an experimental implication of the fermionic thermocoherent source.

Appendix

Here we give a short note on calculating the current-current correlation function using the quantum master equation[55]. In general, a two-time average of two operators $A_1(t)$ and $A_2(t')$ in interaction picture can be expressed as

$$\langle A_1(t)A_2(t')\rangle = Tr_{S+B}[\chi(0)A_1(t)A_2(t')], \tag{5.71}$$

where the total density operator $\chi(t)$ can be expressed as

$$\chi(0) = e^{\frac{iHt}{\hbar}}\chi(t)e^{-\frac{iHt}{\hbar}}, \tag{5.72}$$

with the equations of motion for the operators being expressed as

$$\dot{A}_i(t) = \frac{1}{i\hbar}[A_i, H], \tag{5.73}$$

along with the solution,

$$A_i(t) = e^{\frac{iHt}{\hbar}}A_i e^{-\frac{iHt}{\hbar}}. \tag{5.74}$$

Using Eqs.(5.71) to (5.74), we obtain

$$\langle A_1(t)A_2(t+\tau)\rangle = Tr_s[A_2(0)Tr_B\{\chi_{A_1}(\tau)\}], \tag{5.75}$$

where we define, $t' - t = \tau$ and

$$\chi_{A_1}(\tau) = e^{-\frac{iH\tau}{\hbar}}(\chi(t)A_1(0))e^{\frac{iH\tau}{\hbar}}. \tag{5.76}$$

We now exclude the explicit reference of the reservoir by tracing over the reservoir variables thereby defining the reduced operator $\rho_{A_1}(\tau)$ as

$$\rho_{A_1}(\tau) = Tr_B[\chi_{A_1}(\tau)], \tag{5.77}$$

with,

$$\rho_{A_1}(0) = Tr_B[\chi_{A_1}(0)] = \rho(t)A_1(0). \tag{5.78}$$

We can express an equation of motion for ρ_{A_1} as,

$$\rho_{A_1}(\tau) = e^{L\tau}[\rho(t)A_1(0)], \tag{5.79}$$

where L is a generalized Liouvillean superoperator. After having a little algebra, we can rewrite Eq.(5.75) as

$$\langle A_1(t)A_2(t+\tau)\rangle = Tr_s[A_2(0)e^{L\tau}\rho(t)A_1(0)]. \tag{5.80}$$

For a complete set of system operators $\{K_\mu\}(\mu = 1, 2, 3, \cdots)$ such that for any arbitrary operator O, one can write,

$$Tr_s[K_\mu(LO)] = \sum_\theta M_{\mu\theta}Tr_s(K_\theta O), \tag{5.81}$$

where $M_{\mu\theta}$ are constants. Using Eq.(5.81), we obtain

$$\langle\dot{K}_\mu\rangle = \sum_\theta M_{\mu\theta}\langle K_\theta\rangle, \tag{5.82}$$

which in the matrix form can be expressed as

$$\langle\dot{\mathbf{K}}\rangle = \mathbf{M}\langle\mathbf{K}\rangle. \tag{5.83}$$

Now, using Eqs.(5.80) and (5.83), after a slight algebra we obtain

$$\frac{d}{d\tau}\langle A_1(t)K_\mu(t+\tau)\rangle = \sum_\theta M_{\mu\theta}\langle A_1(t)K_\theta(t+\tau)\rangle, \tag{5.84}$$

a form of quantum regression theorem[55], which is used to calculate the current-current correlation function.

Chapter 6

Electron-vibration entanglement and electron transport in resonating dimers

In this chapter, based on the formulation of master equation for fermionic bath, we have estimated electron transport through a molecular dimer with a vibrational manifold which is coupled to two electron leads. The molecular current is studied both as a function of internal and external bias for a class of molecules as well as the current noise spectra. The rest of the chapter is organized as follows: After providing a brief introduction, in Sec.6.1 we have provided the basic features of our system which is modeled by a dimer chain with two vibrational modes. In the next section, we have depicted the dynamics of the molecule which is coupled to two electron reservoirs in terms of the master equation, rate equation and current through the molecular system. In the subsection 6.3.1, a few examples of molecular dimers are discussed and in the subsection 6.3.2, current through the system is studied as a function of the internal bias and its dependence on the vibrational mode as a function of temperature. In the subsection 6.3.3, the current and the differential conductance behavior of the molecule is studied as a function of the external bias. In the next section, we have deduced explicit expressions for the current noise and studied their dependence on vibrational modes. In Sec. 6.5, we have concluded the chapter.

6.1 Introduction

The coupling of a quantum system with two fermionic reservoirs serves as a theoretical spectroscopic tool to study electron transport dynamics through a molecular system[95, 100]. Inspite of a great deal of theoretical and experimental investigations in the context of electron transport through systems[101, 102, 103, 104, 105, 106, 107, 108], physical insights about coherent dynamics of entangled electron-vibration motion in molecules are very limited in this context. When a molecule is coupled

to two electron reservoirs, the difference in chemical potential of the two reservoirs drives transport of electrons through it. In molecular electronic devices, inelastic effect[109] in the molecular transport junctions along with vibrational effect[16] appears. However, the Coulomb blockade effect plays the most important role and is sufficient enough to explain most of the simplest cases observed in the earlier experiments[111] on quantum dots in terms of simple charging diagrams, which can also be considered in terms of simple rate equations[112]. In this context, it is our interest to do a thorough study on electron transport through molecular systems in terms of the density matrix formalism. For this purpose, we have adopted a quantum system[151, 152] which is consisting of two equivalent resonating structures in terms of a dimer, each of them being described in terms of an electronic basis which is coupled through a vibrational mode. This has also been examined in the context of electron-vibration entanglement in model molecular systems[153, 154] which can provide a physical insight of the quantum dynamics from electron transport through molecules.

In this chapter, we have utilized master equation formalism to study the electron transport process through a molecule coupled to two fermionic reservoirs and included the effect of the vibrational modes characterizing the system on the transport properties under steady state conditions. We have calculated the current through the molecule as a function of internal as well as the external bias voltage and considered the effect of electron-vibration entanglement on both the current-voltage profile as well as on the current versus internal bias profile. We have also calculated the current noise spectrum for electrons flowing through the single molecule junction. For this purpose, we have adopted the formalism of quantum regression in correlation function[55] and calculated the steady state noise fluctuation.

6.2 Resonating dimer between source and sink

To put our work in a proper perspective, we consider a formal quantum transport setup[100] where a system is coupled to both the source(emitter) and sink(collector) of electrons as two fermionic reservoirs with chemical potentials μ_e and μ_c respectively. Electron transports through the system in response to the external bias arising out of difference in chemical potential $V = \mu_e - \mu_c$.

Here, we have considered an interacting resonating dimer as our system. It is modeled in terms of a double well potential surface internally coupled by the parameter, λ_c which also serves as a potential barrier between them. The energy term, $\hbar\lambda_c$ also serves as the tunnelling element between the two electronic states. The system Hamiltonian H_{sys} is constructed following our previous work[152, 151] where we have two independent chains, each of them is described in terms of an

electronic basis with a vibrational manifold. The structure is thus

$$H_{sys} = \sum_{n=\{e,c\}} |n\rangle\langle n| \left(\epsilon_n + \sum_k \hbar\omega_k a_k^\dagger a_k + \hbar g_{nk} \left(a_k^\dagger + a_k \right) \right) + \hbar\lambda_c(|e\rangle\langle c| + |c\rangle\langle e|), \tag{6.1}$$

where, ϵ_n's are the vertical electronic excitation energies relative to the ground state of undimerized system represented by operators $\hat{n}_e = |e\rangle\langle e|$ and $\hat{n}_c = |c\rangle\langle c|$. $a_k^\dagger$ and a_k are creation and annihilation operators, respectively, for k-th vibrational mode with frequency ω_k with g_{nk} being the electron-vibration coupling parameter. Another parameter is the asymmetry between the two states which in an electron transport experiment may be controlled by modulating the gate voltage parameter. We also consider that the energy required to put an additional electron to the molecule is much more than that of λ_c, so that effectively only one additional electron can tunnel through the system at a time.

In order to eliminate the coupling between the electron and vibrational degrees of freedom, we perform a polaron transformation of H_{tot}[152, 239] to consider system dynamics in all regimes of bath strength[240, 241, 242]. We define the polaron transformation using the operator

$$U = \sum_{n=\{e,c\}} |n\rangle\langle n| e^{-\sum_k \frac{g_{nk}}{\omega_k}(a_k^\dagger - a_k)}, \tag{6.2}$$

such that for any system operator O, one can define

$$\bar{O} = U^\dagger O U, \tag{6.3}$$

and after a straightforward but lengthy algebra one can find the transformed system Hamiltonian

$$\bar{H}_{sys} = \sum_{n=\{e,c\}} \bar{\epsilon}_n |n\rangle\langle n| + \sum_k \hbar\omega_k a_k^\dagger a_k + \hbar\lambda_c(|e\rangle\langle c| D(\alpha) + |c\rangle\langle e| D(-\alpha)), \tag{6.4}$$

where $\bar{\epsilon}_n = \epsilon_n - \sum_k \frac{\hbar g_{nk}^2}{\omega_k}$, where the term $\sum_k \frac{\hbar g_{nk}^2}{\omega_k}$ is called Stoke's shift and $D(\alpha) \equiv \prod_k D_k(\alpha_k)$, where $D_k(\alpha_k) = e^{\alpha_k(a_k^\dagger - a_k)}$, with $\alpha_k = \frac{g_{ek} - g_{ck}}{\omega_k}$. For the sake of clarity, we introduce the notation $\bar{H}_{e-e} = \hbar\lambda_c(|e\rangle\langle c| D(\alpha) + |c\rangle\langle e| D(-\alpha))$, where we note that electron-vibration coupling part in Eq.(6.1) has been incorporated into the inter-chain interaction Hamiltonian in terms of Glauber's displacement operator[55] in the polaron frame. It is expressed in terms of localized diabatically coupled electronic bases $|e\rangle$ and $|c\rangle$ where the coupling strength depends on the vibrational coordinates in a complicated way unlike the standard electron transfer picture of linearly coupled diabatic surfaces[153, 154].

Our model is a generalization of the the simplest model system[108] composed of two states without any vibrational degree of freedom called $|e\rangle$ and $|c\rangle$ and are connected through a static tunnel barrier. The effective Hilbert space which becomes

H_{eff} is assumed to be spanned by two many-body states $|e\rangle = |n_e + 1, n_c\rangle$ and $|c\rangle = |n_e, n_c + 1\rangle$ with energies ϵ_e and ϵ_c, corresponding to the lowest energy states for one additional electron in the left and the right state. On the other hand, the empty ground state $|0\rangle = |n_e, n_c\rangle$ has one electron less and n_e electrons in the left and n_c electrons in the right state. Although this state plays a vital role in transport, but there are no superpositions between $|0\rangle$ and the states in H_{eff} by charge super-selection rule[108]. The empty ground state $|0\rangle$ is particularly useful in expressing coherent interaction terms between the molecular system and the leads and also needed to express population conservation criteria. Thus our model additionally considers a vibrational degree of freedom for electron-vibration entanglement.

The total Hamiltonian in the polaron frame can thus be expressed as

$$\bar{H}_{tot} = \bar{H}_{sys} + \bar{H}_e + \bar{H}_c + \bar{H}_{int}, \tag{6.5}$$

where, the emitter Hamiltonian is $H_e = \sum_p \epsilon_p^e b_p^\dagger b_p$ and the collector Hamiltonian is $H_c = \sum_r \epsilon_r^c d_r^\dagger d_r$. H_{sys} is the system Hamiltonian and H_{int} is the interaction Hamiltonian representing system-reservoir interaction. We consider $b_p(b_p^\dagger)$ as the annihilation(creation) operator for the p-th electron in the emitter and that of $d_r(d_r^\dagger)$ is the annihilation(creation) operator for the r-th electron in the collector. The fermions obey the anti-commutation rules $\{b_k^\dagger b_l\}_+ = \delta_{kl}$ and $\{d_k^\dagger d_l\}_+ = \delta_{kl}$. ϵ_p^e and ϵ_r^c are energy of the resonant modes of the emitter and collector fermion(electron) reservoir respectively.

The interaction Hamiltonian is expressed as

$$H_{int} = H_{int}^e + H_{int}^c, \tag{6.6}$$

where, $H_{int}^e = \hbar \sum_p (V_e^p b_p^\dagger |0\rangle\langle e| + V_e^{p*} b_p |e\rangle\langle 0|)$ and $H_{int}^c = \hbar \sum_r (V_c^r d_r^\dagger |0\rangle\langle c| + V_c^{r*} d_r |c\rangle\langle 0|)$, with, $V_e^p(V_e^{p*})$ and $V_c^r(V_c^{r*})$ are the corresponding tunnel matrix elements.

Evidently, in the polaron frame, $\bar{H}_e = H_e$ and $\bar{H}_c = H_c$ as they have contributions only from the electron reservoir degrees of freedom. Under the polaron frame, the system-reservoir interaction Hamiltonian transforms as

$$\bar{H}_{int} = \bar{H}_{int}^e + \bar{H}_{int}^c, \tag{6.7}$$

where,

$$\bar{H}_{int}^e = \hbar \sum_p (V_e^p b_p^\dagger |0\rangle\langle e| e^{-\sum_k \beta_{ek}(a_k^\dagger - a_k)} + V_e^{p*} b_p |e\rangle\langle 0| e^{\sum_k \beta_{ek}(a_k^\dagger - a_k)})$$

and

$$\bar{H}_{int}^c = \hbar \sum_r (V_c^r d_r^\dagger |0\rangle\langle c| e^{-\sum_k \beta_{ck}(a_k^\dagger - a_k)} + V_c^{r*} d_r |c\rangle\langle 0| e^{\sum_k \beta_{ck}(a_k^\dagger - a_k)})$$

with, $\beta_{nk} = \frac{g_{nk}}{\omega_k}$. While deducing the operators in polaron transformed frame, we have used the Baker-Hausdorff formula[55, 56] in addition to the operator algebra $\langle e|e\rangle = \langle c|c\rangle = 1$ and $\langle e|c\rangle = \langle c|e\rangle = 0$ along with $[a_k, a_j^\dagger] = \delta_{kj}$.

6.3 Electron transport through a dimer coupled to two electron reservoirs

In this section we shall provide a master equation under the Born-Markov approximation for fermionic reservoirs and proceed for its solution of the reduced system variables. We shall conclude this section by explicitly considering the rate equation for various matrix elements characterizing the system and give an analytical expression for current through the dimer.

6.3.1 Master equation

The equation of motion for $\chi(t)$, the total density operator in interaction picture for a molecular dimer coupled with two reservoirs is

$$\dot{\chi}(t) = \frac{1}{i\hbar}[\bar{H}_{e-e}(t), \chi(t)] - \frac{1}{\hbar^2}\int_0^t dt'[\bar{H}_{int}(t), [\bar{H}_{int}(t'), \chi(t')]]. \tag{6.8}$$

While expressing $\dot{\chi}(t)$, we assume the tunneling of electrons to or from the molecule to the leads are considered within Born approximation. The damping and the coupling terms are considered to be independent of one another so that $\bar{H}_{e-e}(t)$ appears in the coherent time evolution of the system. This is a reflection of the assumption $\hbar\lambda_c \ll \bar{\epsilon}_n$. The interaction picture description is valid with respect to the free unperturbed Hamiltonian $\bar{H}_0 = \sum_{n=\{e,c\}} \bar{\epsilon}_n |n\rangle\langle n| + \sum_k \hbar\omega_k a_k^\dagger a_k + \sum_p \epsilon_p^e b_p^\dagger b_p + \sum_r \epsilon_r^c d_r^\dagger d_r$. We now invoke the Markov approximation in the sense that the two fermionic baths are always in thermal equilibrium and the total density operator can be approximately factorized as $\chi(t) \simeq \rho(t) \otimes \rho_{res}^e \otimes \rho_{res}^c$, where, $\rho(t)$ is the density operator in interaction picture for the dimer molecule, along with the two vibrational modes and ρ_{res}^e and ρ_{res}^c are the density operators for the emitter and collector electron reservoirs, respectively. We therefore take trace over the reservoir degrees of freedom such that $Tr_{res}\chi(t) = \rho(t)$. The quantum master equation after formal integration within this framework comes out as

$$\begin{aligned}\rho(t) - \rho(0) = &-i\lambda_c \int_0^t dt'[p_{t'} X(\alpha, t'), \rho(t')] - i\lambda_c \int_0^t dt'[p_{t'}^\dagger X(-\alpha, t'), \rho(t')] \\ &- \sum_{n=\{e,c\}} \Big(\frac{\Gamma_{on}}{2}\int_0^t dt'[|0\rangle\langle 0|\rho(t') - 2|n\rangle\langle 0|\rho(t')|0\rangle\langle n| + \rho(t')|0\rangle\langle 0|] \\ &+ \frac{\Gamma_{no}}{2}\int_0^t dt'[|n\rangle\langle n|\rho(t') - 2|0\rangle\langle n|\rho(t')|n\rangle\langle 0| + \rho(t')|n\rangle\langle n|]\Big),\end{aligned} \tag{6.9}$$

where, $X(\alpha, t) = \Pi_k X_k(\alpha_k, t) = \Pi_k e^{\alpha_k(a_k^\dagger e^{i\omega_k t} - a_k e^{-i\omega_k t})}$ and $p_t = |e\rangle\langle c| e^{\frac{it\Delta\bar{\epsilon}}{\hbar}}$, with $\Delta\bar{\epsilon} = \bar{\epsilon}_e - \bar{\epsilon}_c$. The rate constants for electron transport Γ_{0n} and Γ_{n0}(with $n = \{e, c\}$)

here contains the electron-vibration coupling parameters in a little complicated way. The expressions are

$$\Gamma_{0n} = \Gamma_n \Pi_{k=1}^{k=2} \sum_{n_k=-\infty}^{\infty} e^{-\beta_{nk}^2 \coth\left(\frac{\hbar\omega_k}{2k_BT}\right)} e^{\frac{n_k\hbar\omega_k}{2k_BT}}$$

$$\times \bar{f}_n\left(\frac{\bar{\epsilon}_n}{\hbar} - n_k\omega_k\right) I_{n_k}\left(\frac{\beta_{nk}^2}{\sinh(\frac{\hbar\omega_k}{2k_BT})}\right), \tag{6.10}$$

and,

$$\Gamma_{n0} = \Gamma_n \Pi_{k=1}^{k=2} \sum_{n_k=-\infty}^{\infty} e^{-\beta_{nk}^2 \coth\left(\frac{\hbar\omega_k}{2k_BT}\right)} e^{\frac{n_k\hbar\omega_k}{2k_BT}}$$

$$\times \left[1 - \bar{f}_n\left(\frac{\bar{\epsilon}_n}{\hbar} + n_k\omega_k\right)\right] I_{n_k}\left(\frac{\beta_{nk}^2}{\sinh(\frac{\hbar\omega_k}{2k_BT})}\right), \tag{6.11}$$

where, $\bar{f}_n(\omega) = \frac{1}{e^{\frac{\hbar\omega-\mu_n}{k_BT}}+1}$ is the Fermi-Dirac distribution function with $\beta_{ik} = \frac{g_{ik}}{\omega_k}$ and $I_n(z)$ is modified Bessel function of the first kind. The Fermi golden rule decay constants are $\Gamma_n = 2\pi d_n|V_n|^2$, with d_n being the constant density of states in the n-th electron reservoir. While deducing Eqs.(6.10) and (6.11), we have considered a trace operation over the reservoir as well as the vibrational degrees of freedom of the molecule. But this is not reflected in the coherent part of the master equation [see Eq.(6.9)] as $X(\alpha, t)$ consists of vibrational operators a_k and $a_k^\dagger$. This turns out to be physically reasonable as we have already considered that the excitonic coupling term, $\hbar\lambda_c$ and the damping terms to be independent of each other on the basis of time scale separation. To arrive at analytical solution of the master equation, we follow the technique to rewrite the equation as a closed set of simultaneous integral equation[107, 108]. We define number operators as $n_n = |n\rangle\langle n|(n = \{e, c\})$ and the time dependent coherent operators as $\bar{p} = p_t X(\alpha, t)$, where various system operator expectation values are defined as $\langle O\rangle_t = Tr(O\rho(t))$. With all these notations, the equation of motion comes out as

$$\langle n_e\rangle_t - \langle n_e\rangle_0 = -i\lambda_c \int_0^t dt'(\langle\bar{p}\rangle_{t'} - \langle\bar{p}^\dagger\rangle_{t'}) + \Gamma_{oe}\int_0^t dt'[1 - \langle n_e\rangle_{t'} - \langle n_c\rangle_{t'}]$$

$$-\Gamma_{eo}\int_0^t dt'\langle n_e\rangle_{t'}, \tag{6.12}$$

$$\langle\bar{p}\rangle_t - \langle\bar{p}\rangle_0 = -i\lambda_c\int_0^t dt' F(t-t')e^{\frac{i(t-t')\Delta\bar{\epsilon}}{\hbar}}\langle n_e\rangle_{t'} + i\lambda_c\int_0^t dt' F^*(t-t')e^{\frac{i(t-t')\Delta\bar{\epsilon}}{\hbar}}\langle n_c\rangle_{t'}$$

$$-\frac{1}{2}(\Gamma_{eo}+\Gamma_{co})\int_0^t dt' F(t-t')e^{\frac{i(t-t')\Delta\bar{\epsilon}}{\hbar}}\langle\bar{p}\rangle_{t'}, \tag{6.13}$$

$$\langle n_c\rangle_t - \langle n_c\rangle_0 = i\lambda_c\int_0^t dt'(\langle\bar{p}\rangle_{t'} - \langle\bar{p}^\dagger\rangle_{t'}) + \Gamma_{oc}\int_0^t dt'[1 - \langle n_e\rangle_{t'} - \langle n_c\rangle_{t'}]$$

$$-\Gamma_{co}\int_0^t dt'\langle n_c\rangle_{t'}, \tag{6.14}$$

where,

$$F(\tau)=\sum_{n_1,n_2=-\infty}^{\infty} C_{n_1}C_{n_2}e^{-i\tau(n_1\omega_1+n_2\omega_2)}, \tag{6.15}$$

with,

$$C_{n_k}=e^{-\alpha_k^2(1+2N_k)}\left(\frac{1+N_k}{N_k}\right)^{\frac{n_k}{2}} I_{n_k}(2\alpha_k^2\sqrt{N_k(1+N_k)}), \tag{6.16}$$

where the thermal average occupation number for the vibrational mode is expressed as $N_k=\frac{1}{e^{\frac{\hbar\omega_k}{KT}}-1}$ and $\alpha_k=\frac{g_{ek}-g_{ck}}{\omega_k}$. While deducing the equations of motion [see Eqs.(6.12)-(6.14)], we have assumed[107] the factorization for terms like $\langle n_e X(\alpha,t)X^\dagger(\alpha,t')\rangle_{t'}=\langle n_e\rangle_{t'}\langle X(\alpha,t)X^\dagger(\alpha,t')\rangle_{t'}$. This amounts to the physical situation that we are not interested in the back-action effects of the tunneling electrons through the system on the vibrational modes, so that the vibrational modes are considered to remain in thermal equilibrium at all times. Some basic steps of the derivation regarding the vibrational correlation function $F(\tau)$ is outlined in Appendix-A.

6.3.2 Rate equation and current through the system

In the stationary state, the average current through the molecule is expressed as the rate[107, 108] of tunneling of the electrons from the left electron reservoir to the system,

$$\langle\hat{I}\rangle_t=\frac{\partial}{\partial t}\langle n_e\rangle=-i\lambda_c\left(\langle\bar{p}\rangle_t-\langle\bar{p^\dagger}\rangle_t\right). \tag{6.17}$$

The details of derivation of the expression for the average value of current through the molecule is provided in Appendix-B. In this section we only provide the final expression of current. The analytical expression of the average steady-state current is given as

$$\begin{aligned}\langle\hat{I}\rangle_{t=\infty}=&\frac{2\lambda_c^2\Gamma_{eo}\Gamma_{oc}}{\Delta}Re\left\{\bar{C}_2(0)\left(1+\frac{1}{2}\left(\Gamma_{eo}+\Gamma_{co}\right)\bar{C}_1(0)\right)\right\}\\&-\frac{2\lambda_c^2\Gamma_{oe}\Gamma_{co}}{\Delta}Re\left\{\bar{C}_1(0)\left(1+\frac{1}{2}\left(\Gamma_{eo}+\Gamma_{co}\right)\bar{C}_1^*(0)\right)\right\},\end{aligned} \tag{6.18}$$

where,

$$\begin{aligned}\Delta=&\left[(\Gamma_{eo}+\Gamma_{oe})(\Gamma_{co}+\Gamma_{oc})-\Gamma_{oc}\Gamma_{oe}\right]\left|1+\frac{1}{2}(\Gamma_{eo}+\Gamma_{co})\bar{C}_1(0)\right|^2\\&+2\lambda_c^2[\Gamma_{oe}+\Gamma_{eo}+\Gamma_{oc}]Re\left[\bar{C}_2(0)\left\{1+\frac{1}{2}(\Gamma_{eo}+\Gamma_{co})\bar{C}_1(0)\right\}\right]\\&+2\lambda_c^2[\Gamma_{oc}+\Gamma_{co}+\Gamma_{oe}]Re\left[\bar{C}_1(0)\left\{1+\frac{1}{2}(\Gamma_{eo}+\Gamma_{co})\bar{C}_1^*(0)\right\}\right].\end{aligned} \tag{6.19}$$

In Eqs.(6.18) and (6.19), we have defined $\bar{C}_1(s) = L[F(t)e^{\frac{it\Delta\bar{\epsilon}}{\hbar}}]$ and $\bar{C}_2(s) = L[F(t)e^{\frac{-it\Delta\bar{\epsilon}}{\hbar}}]$, where $L(f(t)) = \int_0^\infty dt e^{-st} f(t)$. This is an analytical result of the current due to vibrationally induced dimeric coupling.

Our result is a modification of the previously obtained expressions[107, 108] in the sense that the expression accommodates all possible effects arising out of the vibrational modes present in the molecule[151]. Furthermore, the previous results [107, 108] were presented in the limit of infinite bias voltage $V \longrightarrow \infty$ which presumes the thermal average number occupation for the emitter and collector to be 1 and 0, respectively. Additionally our result does not assume that the polaron transformation operator [see Eq.(6.2)] renders the H_{int} unchanged which is an oversimplification for studying the current-voltage characteristic curves. This has generated explicit dependence of the vibrational mode dynamics in the rate constants of tunneling electron through the molecule. Under the approximation of having no vibrational mode in the system and considering the infinite bias limit, one can easily obtain similar expression for average current[108]

$$\langle \hat{I} \rangle_{t=\infty} = \lambda_c^2 \frac{\Gamma_c}{\left(\frac{\Gamma_c}{2}\right)^2 + \left(\frac{\Delta\bar{\epsilon}}{\hbar}\right)^2 + \lambda_c^2\left(2 + \frac{\Gamma_c}{\Gamma_e}\right)}, \tag{6.20}$$

which is Lorentzian about $\Delta\bar{\epsilon}$.

6.4 Numerical results

In this section, we have depicted the characteristic of molecular current as a function of internal as well as external bias for a class of resonating dimeric structures. For the sake of presenting our numerical result, we have considered the parameters of pyridine and also some other systems of diverse photophysical importance as our model molecular system. Here we have assumed that the electronic states are coupled to each other through a single vibrational mode, though in general many modes can contribute to the coupling. Extension to the multimode case is straightforward and is not important for qualitative understanding. The essential features of the electron-vibration interaction in molecular system can be described by basic one-mode model with appropriately chosen effective vibrational parameters and is a good approximation for some important molecular properties like shape, central frequency and intensity of the characteristic intervalence electronic transition[153].

6.4.1 Examples of a few molecular dimers

We have considered a few examples of model chemical systems[243, 244, 245, 246, 247] to demonstrate a general trend in the electron transport properties through it when coupled to two electron reservoirs. We have adopted five model chemical dimer

systems with examples like pyridine, PRC(the bacterial photosynthetic reaction radical cation), B-N-B, Creutz-Taube ion and benzene. Although they belong to diverse chemical nature as evidenced by their wide range of inter-valence to mixed valence compounds where, the double degenerate electronic state is coupled through the vibrational degree of freedom. The degeneracy of the electronic states can be lifted by introduction of asymmetry in terms of gate voltage for a quantum transport setup. For example pyridine, which is well known for solution processing in inkjet printing and is favorable for making cost-effective organic light-emitting diodes and recognized in various domains of molecular electron transport starting from the study of electron transport through pyridine-based single molecule junctions[243], to study and identify the vibrational signatures in the differential conductance[244] spectra. Pyridine has also been utilized for designing and synthesis of normal[244] as well as tripodal[245] anchor to construct a single molecule junction with a metal electrode. Pyridines are also employable as a switch molecule to study single molecule conductances[246]. Next to pyridine, we consider the PRC(bacteriochlorophyll-a dimer cation) which is an example of the mixed valence complex. Such systems are simulated to study photon-induced electron transport between molecular entities that are rigidly embedded within a lipid membrane and separated from each other by well-defined distances[247]. The hint to study PRC cation came from the usefulness of Dendritic Porphyrin, Porphyrin Dimer, and Porphyrin-C60 Dyad to prepare supramolecular photovoltaic cells. Next, we have considered Creutz-taube which forms a paradigm in electron transport through biological system[153]. Finally we consider the B-N-B species for a model case study.

The metal-dimer-metal contacting scheme where the two electronic states coupled by an effective vibrational mode are shown in Fig.(6.1) along with five sample molecular systems coupled through resonating dimeric structures. Vibrational frequencies $\hbar\omega$ and tunnel coupling parameters $\hbar\lambda_c$ given in the Table.(6.1)[153]. These systems differ in terms of the vibrational frequency ω and inter-chain interaction λ_c.

MOLECULAR SYSTEMS	$\hbar\omega$**(cm**$^{-1}$**)**	$\hbar\lambda_c$**(eV)**	$\lvert\lambda_c/\omega\rvert$**(eV-cm)**
Benzene	1564	-9.5	0.00607
Pyridine	1620	-0.33	0.0003
CT	800	0.35	0.0004
PRC	980	-0.13	0.0001
BNB	1800	-0.36	0.0002

Table 6.1: Vibrational frequencies $\hbar\omega$ and tunnel coupling parameters $\hbar\lambda_c$ adopted from Ref.[153]

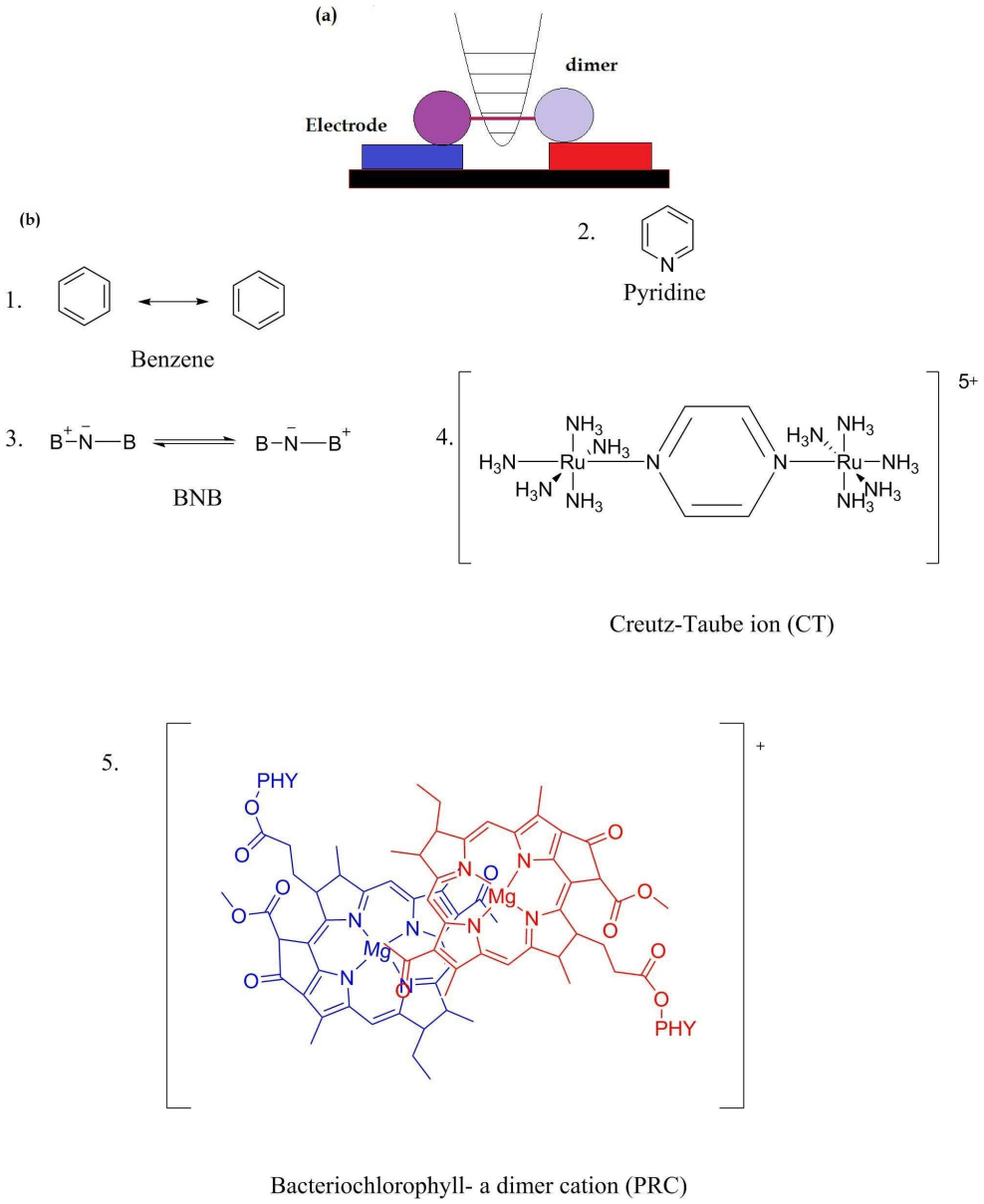

Figure 6.1: (a) The metal-dimer-metal contacting scheme where the two electronic states coupled by an effective vibrational mode. (b) Five sample molecular systems coupled through resonating dimeric structures.

6.4.2 Current as a function of internal bias

In this section, we have analyzed the current through the system as a function of the internal bias in eV, which is the energy difference between the left and right molecules, $\Delta\bar{\epsilon} = \bar{\epsilon}_e - \bar{\epsilon}_c$ constituting the system. The internal bias can be experimentally realized in terms of gate voltage. The infinite bias limit is expressed as $\bar{f}(\frac{\bar{\epsilon}_e}{\hbar}) = 1$ and $\bar{f}(\frac{\bar{\epsilon}_c}{\hbar}) = 0$, which is considered to present this result. In the figure(6.2), we have plotted molecular current against the internal bias expressed in eV. Here we have considered that the two vibrational modes have a common frequency such

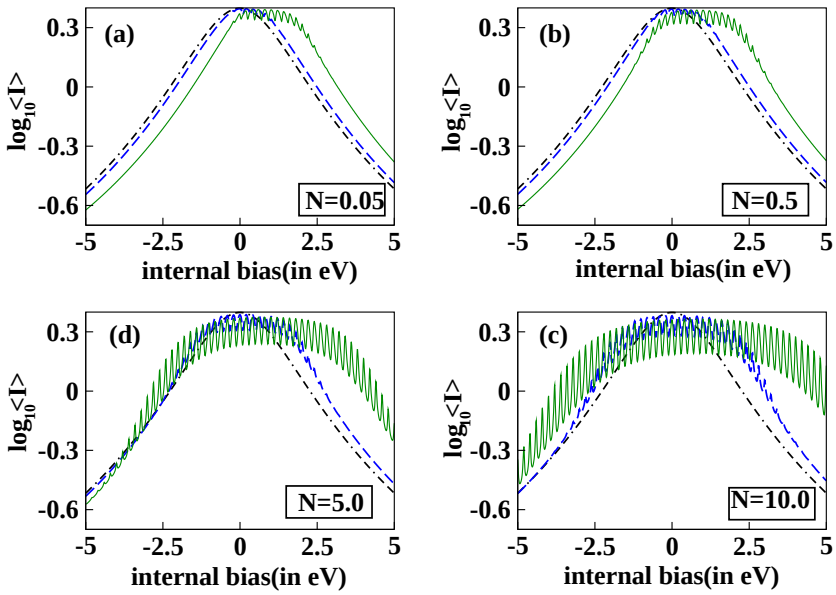

Figure 6.2: Plots of the variation of $\log_{10}\langle I\rangle$ ($\langle I\rangle$ in pA) against internal bias expressed in eV. The temperature is expressed in terms of average thermal occupation number $N = \frac{1}{e^{\frac{\hbar\omega}{KT}}-1}$ and it is changed parametrically[(a)-(d)]. The variation is shown for different degrees of electron-vibration coupling, g. In each of the figures, the black double dashed dotted line corresponds to $g = 0.0$, the blue dashed line corresponds to $g = 0.25\omega$ and the green bold line corresponds to $g = \omega$.

that $\omega_1 = \omega_2 = \omega = 1620cm^{-1}$, which is the characteristic value for pyridine molecule[153] and the electron-vibration coupling matrix elements $g_{11} = g_{22} = g$ and $g_{12} = g_{21} = 0$. The tunneling rate constants are $\Gamma_e = \Gamma_c = 0.03$ meV. We have explicitly considered the ratio g/ω for presenting our results. The coupling between the two electronic states is $\hbar\lambda_c = -0.33$ eV for pyridine dimer[153]. As the internal bias varies, the current spectrum is clearly revealed. When the electron-vibration coupling is switched off, the current is typical of a Lorentzian profile centering about $\Delta\bar{\epsilon}$ which is evident from Eq.(6.20). For non-zero electron vibrational coupling constants, the current shows spikes when the energy bias $\Delta\bar{\epsilon}$ becomes equal to the vibrational mode resonant frequency and its multiples. The result shows a close resemblance with that obtained earlier[108], with a notable difference that our model dimer system does not incorporate any separate vibrational damping mechanism, instead it is comprised of two independent vibrational degrees of freedom coupled to the electronic modes of the system. The spikes corresponding to the positive values of $\Delta\bar{\epsilon}$ refers to excitation of the vibrational modes due to the tunneling of electrons from the left to right electron lead through the system. On the contrary, spikes corresponding to the negative values of $\Delta\bar{\epsilon}$ corresponds to de-excitation of vibrational modes due to electron tunneling. Interestingly, in the limit of very low temperatures, the vibrational emission is suppressed, which suggests that in this low temperature limit, vibrational modes can only absorb energy which is emitted by

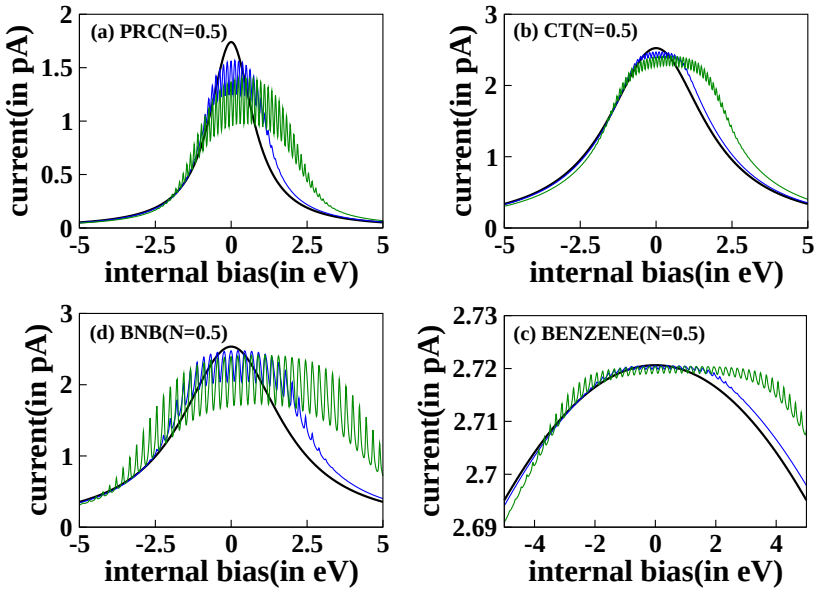

Figure 6.3: Plots of the variation of $\langle I \rangle$ (in pA) against internal bias expressed in eV. The temperature is expressed in terms of thermal average occupation number $N = \frac{1}{e^{\frac{\hbar\omega}{KT}}-1}$ and it is kept fixed at $N = 0.5$. The variation is shown for different degrees of electron-vibration coupling g for (a)PRC(Bacteriochlorophyll-a dimer cation)[$\omega = 980\ cm^{-1}$, $\hbar\lambda_c = -0.13$ eV], (b)CT(Creutz-Taube ion)[$\omega = 800\ cm^{-1}$, $\hbar\lambda_c = 0.35$ eV], (c)Benzene[$\omega = 1564\ cm^{-1}$, $\hbar\lambda_c = -9.5$ eV] and (d)BNB[$\omega = 1800\ cm^{-1}$, $\hbar\lambda_c = 0.36$ eV]. In each of the figures, the black line corresponds to $g = 0.0$, the blue line corresponds to $g = 0.25\omega$ and the green line corresponds to $g = 0.5\omega$.

the tunneling electrons. As the temperature is increased, the vibrational emission becomes more and more active due to higher energy content inducing decoherence in the system which was not present earlier[108]. Hence in our discussion, we will prefer to employ a low temperature approximation which is also relevant from experiments with single molecule junction[155]. A little more digression at this point would be more helpful for further discussions. The vibrational correlation functions C_{n_k} enters via factorisation assumption in the expression for current through the molecule. But for a single vibrational mode, the applicability of such factorisation is not unquestionable. However, for small coupling constants g, we expect that such approximations would work well and existence of finite vibrational damping which is not considered here, should come into play.

In the figure(6.3), we have plotted the current vs internal bias profiles for four different molecular systems(bacteriochlorophyll-a dimer cation[PRC], Creutz-Taube ion[CT], Benzene and BNB) at a constant temperature corresponding to the bosonic occupation number $N = 0.5$. The data is explicitly given in the Table(6.1)[153]. These systems differ in terms of the vibrational frequency ω and inter-chain interaction λ_c. As the parameters are varied in terms of molecules, we observe that the sensitivity of the current-internal bias profile towards the vibrational mode decreases

for molecules having more inter-chain interaction energy terms. But here we note that, the vibrational frequency plays the deciding role. As the vibrational frequency ω decreases, the sensitivity of the current towards the vibrational mode will increase. Thus, there is a compromise between the strength of inter-chain interaction and the frequency of the vibrational mode to detect the vibrational structure of the molecule in terms of the conductance spectra which should be true also from experimental point of view. Here, it is very much relevant to mention that the additional resonances occurring in the current-internal bias profile can serve the purpose of a marker of vibrational modes present in the system.

6.4.3 Current as a function of external bias

In this subsection, we have analyzed the current-voltage($I-V$) characteristics and the differential conductance profile ($\frac{dI}{dV}-V$) for different electron-vibration coupling constants in case of pyridine just as a typical example in fig.(6.4). The parameters considered in figure(6.4) are kept the same as that in the figure(6.2). The two vibrational modes have a common frequency such that $\omega_1 = \omega_2 = \omega$ such that $\hbar\omega = 1620\ cm^{-1}$ and the electron-vibration coupling matrix elements $g_{11} = g_{22} = g$ and $g_{12} = g_{21} = 0$. The tunneling rate constants are $\Gamma_e = \Gamma_c = 0.03$ meV. In addition we have considered a $\hbar\omega = 10KT$ which suggests a low temperature approximation along with $\Delta\bar{\epsilon} = 0.0$. Additionally, we have also assumed for simplicity that $\mu_e = V/2$ and $\mu_c = -V/2$ and it would not qualitatively affect our result. As the external bias voltage $V = \mu_e - \mu_c$ is increased, the current asymptotically reaches its saturation. But the feature one can note is that, as the electron-vibration coupling parameters are switched on, the current shows a typical Coulomb blockade pattern.

This is specifically due to the single electron transport mechanism which suggests that only one electron will be able to reside in the molecule at a time. The increase in the value of conductance should occur for external bias equal to the vibrational resonant frequencies or its multiple. But the system being much less sensitive towards the external bias, it is not possible to characterize the vibrational mode from the current-external bias profile. The electron vibrational coupling thereby continues to provide additional channel for electron transport by inducing steps in the $I-V$ characteristic curves. For finite bias voltages, before reaching the saturation, one can note that the current is suppressed by electron-vibration coupling. This can be explained on the basis of the fact that, switching on the vibrational modes will dissipate the energy required for transport and hence suppresses the molecular current. Similar feature was also obtained earlier[248]. The same feature is also reflected from the differential conductance plot where we see that conductance peaks corresponding to the steps in the $I-V$ plot.

The dependence of the conductance profile on the vibrational modes are also

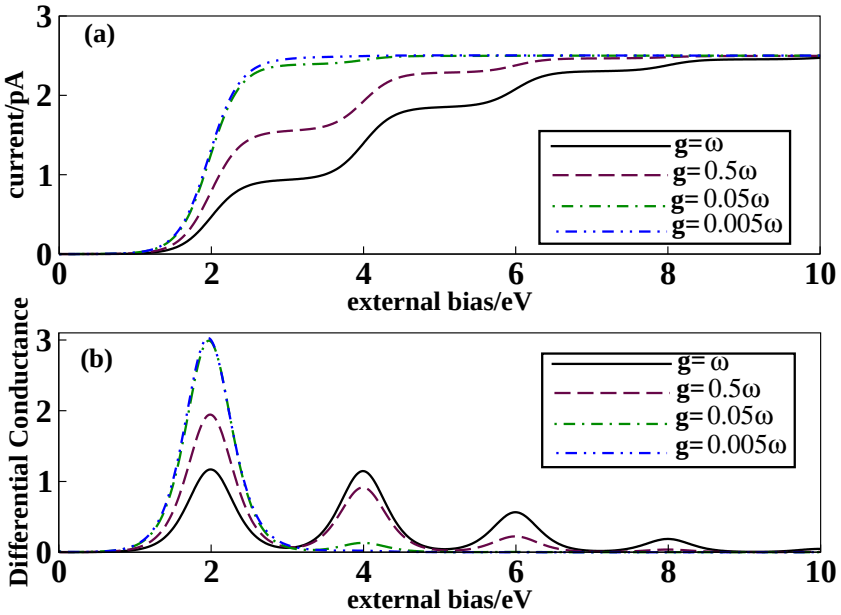

Figure 6.4: Plot of variation of current(in pA)[in (a)] and differential conductance $\frac{dI}{dV}$[in (b)] with external bias(in eV) for different electron-vibration coupling parameters. The other parameters are kept same as that in figure(6.2) and we have considered a low temperature situation such that $\hbar\omega = 10KT$.

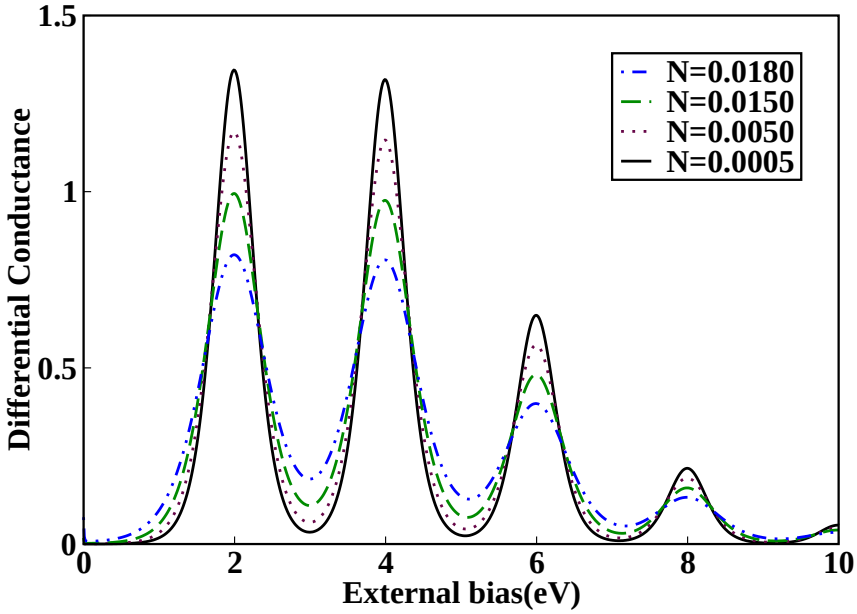

Figure 6.5: Plot of variation of differential conductance $\frac{dI}{dV}$ with external bias(in eV) for different temperatures. The electron-vibration coupling parameter $g = \omega$ where we have considered temperature parametrically. With the increase in temperature, a decrease in height and broadening of the peaks are observed.

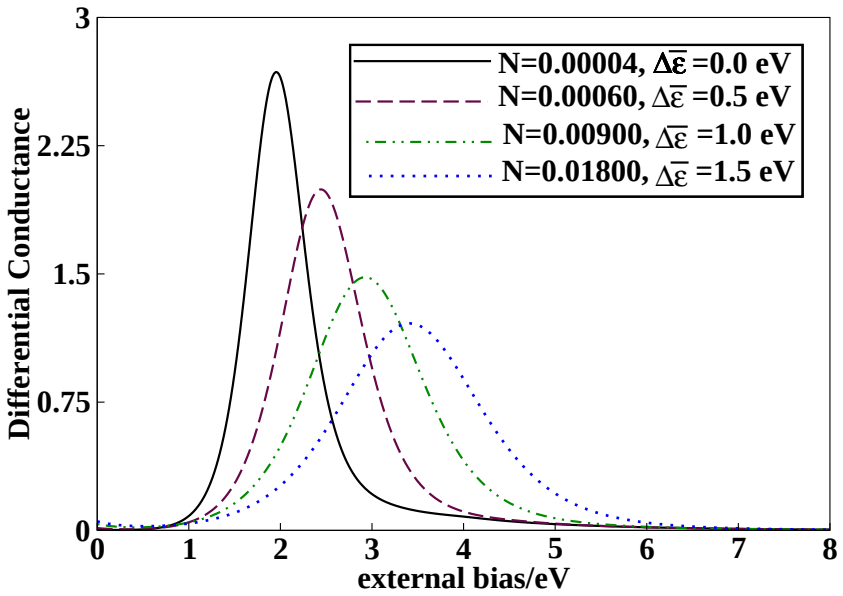

Figure 6.6: Plot of variation of differential conductance$\frac{dI}{dV}$ with external bias(in eV) for different temperatures and $\Delta\bar{\epsilon}$. The electron-vibration coupling parameter $g = 0.0025\omega$ where we have considered temperature parametrically. With increase in temperature, a decrease in height and broadening of the peaks are observed. In addition, change in the internal bias $\Delta\bar{\epsilon}$ also causes a shift in the peak position

studied with temperature as a parameter in the figure(6.5). Under the assumption of a low temperature with $\hbar\omega = 10KT$, the tunneling electrons can emit phonons during the conduction process. But with the increase in temperature, the vibrational absorption process becomes more and more dominant resulting gradual disappearance of the resonances in the differential conductance plot in the regime of strong electron-vibration coupling. This is clearly revealed in the figure(6.5). With the increase in temperature, a decrease in height and broadening of the peaks are observed which suggests change in thermal distribution of the electrons in the leads[155]. We here also note that no temperature dependent shift in the conductance peaks are observed[155] due to no change in gate voltage. With the change in the internal bias in the limit of very small electron-vibration coupling constant, $g = 0.0025\omega$, the conductance curve shifts its peak position with simultaneous broadening which we have shown in Fig.(6.6)[155].

6.5 Current-current correlation for molecule

In this section, we calculate the current-current correlation function and noise spectrum for the electron transport through the molecular dimer coupled to two electron reservoirs and analyze the dependence of the vibrational modes on the noise spectrum.

We first derive the equations of motion for the molecular variables directly from

Eqs.(6.12)-(6.14). While deriving the requisite expressions, we have assumed that the rate constant of the electron transport into(or from) the molecule from(or into) the electron reservoirs is independent of the electron-vibration coupling parameters g_{nk}'s. This approximation is reasonable in the infinite bias limit[$\bar{f}(\frac{\bar{\epsilon}_e}{\hbar}) = 1$ and $\bar{f}(\frac{\bar{\epsilon}_c}{\hbar}) = 0$] as the vibrational dependence of the rate constants will appear in an average way. Thus one can obtain

$$\frac{\partial}{\partial t}\langle n_e\rangle_t = -i\lambda_c[\langle\bar{p}\rangle_t - \langle\bar{p^\dagger}\rangle_t] + \Gamma_e[1 - \langle n_e\rangle_t - \langle n_c\rangle_t], \tag{6.21}$$

$$\frac{\partial}{\partial t}\langle n_c\rangle_t = i\lambda_c[\langle\bar{p}\rangle_t - \langle\bar{p^\dagger}\rangle_t] - \Gamma_c\langle n_c\rangle_t, \tag{6.22}$$

$$\frac{\partial}{\partial t}\langle\bar{p}\rangle_t = -i\lambda_c\langle n_e\rangle_t P_1(t) + iT_c\langle n_c\rangle_t P_2(t) - \frac{\Gamma_c}{2}\langle\bar{p}\rangle_t P_1(t), \tag{6.23}$$

where,

$$P_1(t) = \sum_{n_1}\sum_{n_2}[e^{-i(n_1\omega_1+n_2\omega_2-\frac{\Delta\bar{\epsilon}}{\hbar})t} - 1], \tag{6.24}$$

and,

$$P_2(t) = \sum_{n_1}\sum_{n_2}[e^{i(n_1\omega_1+n_2\omega_2+\frac{\Delta\bar{\epsilon}}{\hbar})t} - 1]. \tag{6.25}$$

While deducing the above set of equations, [see Eqs.(6.21)-(6.23)] we have used relation of time-derivative of convolution as $\frac{\partial}{\partial t}\int_0^t dt' f_1(t-t')f_2(t') = \int_0^t dt' f_1'(t-t')f_2(t')$. A very brief outline leading to the Eqs.(6.24) and (6.25) is given in Appendix C. Now we recast the equations of motion in terms of the time dependent expectation value of current [see Eq.(6.17)] and $\langle J\rangle_t = -i\lambda_c(\langle\bar{p}\rangle_t + \langle\bar{p^\dagger}\rangle_t)$. Thus in matrix notation one can obtain,

$$\begin{bmatrix} \langle\dot{n}_e\rangle_t \\ \langle\dot{I}\rangle_t \\ \langle\dot{J}\rangle_t \\ \langle\dot{n}_c\rangle_t \end{bmatrix} = \mathbf{M}\begin{bmatrix} \langle n_e\rangle_t \\ \langle I\rangle_t \\ \langle J\rangle_t \\ \langle n_c\rangle_t \end{bmatrix} + \begin{bmatrix} \Gamma_e \\ 0 \\ 0 \\ 0 \end{bmatrix}, \tag{6.26}$$

where,

$$\mathbf{M} = \begin{bmatrix} -\Gamma_e & 1 & 0 & -\Gamma_e \\ -2\lambda_c^2 Re[P_1(t)] & -\frac{\Gamma_c}{2}Re[P_1(t)] & -\frac{i\Gamma_c}{2}Im[P_1(t)] & 2\lambda_c^2 Re[P_2(t)] \\ -2\lambda_c^2 Im[P_1(t)] & -\frac{i\Gamma_c}{2}Im[P_1(t)] & -\frac{\Gamma_c}{2}Re[P_1(t)] & 2\lambda_c^2 Im[P_2(t)] \\ 0 & -1 & 0 & -\Gamma_c \end{bmatrix}.$$

The square matrix possesses time-dependent elements in terms of $P_1(t)$ and $P_2(t)$. Interestingly, both of them are composed of system frequency terms ω_1, ω_2 and $\frac{\Delta\bar{\epsilon}}{\hbar}$. Therefore, $P_1(t)$ and $P_2(t)$ are supposed to be much slowly varying functions than $\langle n_e\rangle_t, \langle n_c\rangle_t, \langle I\rangle_t$ and $\langle J\rangle_t$. Thus it is physically reasonable to replace $P_i(t)$'s by their time averages P_i's, where $P_i = \gamma\int_0^\infty dt P_i(t)e^{-\gamma t}$, where $e^{-\gamma t}$ is the corresponding

distribution with arbitrarily small value of γ, which has a dimension of frequency. Thus the matrix equation [see Eq.(6.26)] can be expressed as

$$\frac{\partial}{\partial t}\begin{bmatrix}\langle\delta n_e\rangle_t\\ \langle\delta I\rangle_t\\ \langle\delta J\rangle_t\\ \langle\delta n_c\rangle_t\end{bmatrix} = \mathbf{M}'\begin{bmatrix}\langle\delta n_e\rangle_t\\ \langle\delta I\rangle_t\\ \langle\delta J\rangle_t\\ \langle\delta n_c\rangle_t\end{bmatrix}, \tag{6.27}$$

where,

$$\mathbf{M}' = \begin{bmatrix} -\Gamma_e & 1 & 0 & -\Gamma_e \\ -2\lambda_c^2 Re[P_1] & -\frac{\Gamma_c}{2}Re[P_1] & -\frac{i\Gamma_c}{2}Im[P_1] & 2\lambda_c^2 Re[P_2] \\ -2\lambda_c^2 Im[P_1] & -\frac{i\Gamma_c}{2}Im[P_1] & -\frac{\Gamma_c}{2}Re[P_1] & 2\lambda_c^2 Im[P_2] \\ 0 & -1 & 0 & -\Gamma_c \end{bmatrix},$$

$$P_1 = \gamma\sum_{n_1,n_2} C_{n_1}C_{n_2}[\frac{\gamma(\gamma+1)+\omega_{n_1,n_2}^2}{\gamma(\gamma^2+\omega_{n_1,n_2}^2)} - i\frac{\omega_{n_1,n_2}}{\gamma(\gamma^2+\omega_{n_1,n_2}^2)}], \tag{6.28}$$

and,

$$P_2 = \gamma\sum_{n_1,n_2} C_{n_1}C_{n_2}[\frac{\gamma(\gamma+1)+\omega_{n_1,n_2}'^2}{\gamma(\gamma^2+\omega_{n_1,n_2}'^2)} + i\frac{\omega_{n_1,n_2}'}{\gamma(\gamma^2+\omega_{n_1,n_2}'^2)}], \tag{6.29}$$

with $\omega_{n_1,n_2} = n_1\omega_1 + n_2\omega_2 - \frac{\Delta\bar{\epsilon}}{\hbar}$ and $\omega'_{n_1,n_2} = n_1\omega_1 + n_2\omega_2 + \frac{\Delta\bar{\epsilon}}{\hbar}$. In the Eq.(6.27), we have introduced fluctuation operators such that for any operator O, the corresponding fluctuation operator is $\delta O = O - \langle O\rangle_{ss}$, where $\langle O\rangle_{ss}$ is the corresponding steady state expectation value. We now apply the quantum regression theorem[100, 55] to calculate the current noise spectra $G(\Omega)$ which can be deduced from the current-current correlation $f(t) = \langle\delta I(0)\delta I(t)\rangle$ through the Fourier transform

$$G(\Omega) = \int_0^\infty dt e^{-i\Omega t} f(t). \tag{6.30}$$

We also note

$$G(\Omega) = \bar{F}(i\Omega), \tag{6.31}$$

where, $\bar{F}(s)$ is the Laplace transform of $f(t)$. After performing a straightforward algebra, one thus obtains an explicit expression of $\bar{F}(s)$ as

$$\bar{F}(s) = \frac{1}{X}\sum_{i=1}^{i=4} A^{(i)} f_i, \tag{6.32}$$

where,

$$\begin{aligned} X = {} & (s+\Gamma_e)(s+\Gamma_c)\left\{\left(s+\frac{\Gamma_c}{2}Re(P_1)\right)^2 + \left(\frac{\Gamma_c Im(P_1)}{2}\right)^2\right\} \\ & -i\Gamma_c\lambda_c^2(s+\Gamma_e)Im(P_1)Im(P_2) + 2\lambda_c^2 Re(P_2)\left\{s+\frac{\Gamma_c}{2}Re(P_1)\right\} \\ & -(s+\Gamma_e+\Gamma_c)\left[-2\lambda_c^2 Re(P_1)\left(s+\frac{\Gamma_c}{2}Re(P_1)\right) + i\Gamma_c\lambda_c^2(Im(P_1))^2\right]. \end{aligned} \tag{6.33}$$

The quantities $A^{(i)}$ are defined as

$$A^{(1)} = -(s+\Gamma_c)\left\{2\lambda_c^2 Re(P_1)\left(s+\frac{\Gamma_c}{2}Re(P_1)\right) - i\Gamma_c\lambda_c^2(Im(P_1))^2\right\}, \tag{6.34}$$

$$A^{(2)} = (s+\Gamma_c)(s+\Gamma_e)\left(s+\frac{\Gamma_c}{2}Re(P_1)\right), \tag{6.35}$$

$$A^{(3)} = -(s+\Gamma_c)(s+\Gamma_e)\left(\frac{i\Gamma_c}{2}Im(P_1)\right), \tag{6.36}$$

$$A^{(4)} = (s+\Gamma_e)\left\{-i\Gamma_c\lambda_c^2 Im(P_1)Im(P_2) + 2\lambda_c^2 Re(P_2)\left(s+\frac{\Gamma_c}{2}Re(P_1)\right)\right\}$$
$$+\Gamma_e\left\{2\lambda_c^2 Re(P_1)\left(s+\frac{\Gamma_c}{2}Re(P_1)\right) - i\Gamma_c\lambda_c^2 Im(P_1)\right\}^2. \tag{6.37}$$

The quantities f_i-s are expressed as

$$f_1 = i\lambda_c\langle\bar{p}^\dagger\rangle_{ss} - \langle I\rangle_{ss}\langle n_e\rangle_{ss}, \tag{6.38}$$

$$f_2 = \lambda_c^2[\langle n_e\rangle_{ss} + \langle n_c\rangle_{ss}] - \langle I\rangle_{ss}^2, \tag{6.39}$$

$$f_3 = \lambda_c^2[\langle n_e\rangle_{ss} - \langle n_c\rangle_{ss}] - \langle I\rangle_{ss}\langle J\rangle_{ss}, \tag{6.40}$$

$$f_4 = -i\lambda_c\langle\bar{p}\rangle_{ss} - \langle I\rangle_{ss}\langle n_c\rangle_{ss}. \tag{6.41}$$

Keeping these expressions in our mind, we have plotted the fano factor associated with the current noise for electron transport through the molecule in figure(6.7). In figure(6.7),we have plotted the fano factor, $G(\Omega)$ against scaled frequency, Ω/ω, where we have considered that the two vibrational modes have the same frequency $\omega_1 = \omega_2 = \omega$. While presenting our result, we have considered a low temperature situation such that the thermal average population of the bosonic mode is $N = 0.05$. This low temperature corresponds to only absorption of photons due electrons tunneling through the dimer. The value of $\Delta\bar{\epsilon}/\hbar\omega = 1.0$ and the tunneling rate constants in figure(6.7) are such that $\Gamma_e = \Gamma_c = 0.1\omega$. From the figure(6.7), it is clear that increase in the electron-vibration coupling parameter increases the fano factor. The interesting feature we obtain here is that switching on the electron-vibration coupling parameter g promotes more and more coherent tunneling of electrons through the molecule and a decrease in width of the spectra and thus the noise of the current decreases. It is relevant here to compare the coherence induced noise suppression of current which can be found earlier in fermionic[100] and bosonic[95] bath cases.

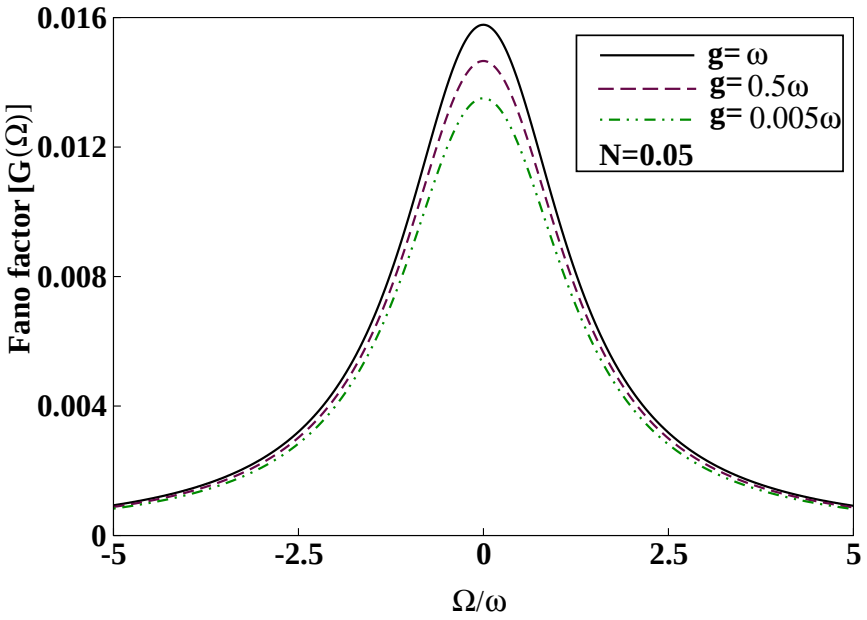

Figure 6.7: Plot of the fano factor, $G(\Omega)$ against scaled frequency Ω/ω. The electron-vibration coupling parameters are such that $g/\omega = 1, 0.5, 0.05, 0.005$. The temperature is kept low such that thermal average occupation number of the vibrational mode is $N = 0.05$. The value of $\Delta\bar{\epsilon}/\hbar\omega = 1.0$ and the tunneling rate constants are such that $\Gamma_e = \Gamma_c = 0.1\omega$.

6.6 Conclusion

In the present chapter, we have formulated the approach for the quantum transport of electrons between two electron leads which are fermionic in character to explore the electron-vibration entanglement in a class of resonating dimeric structures. The dimer is comprised of two electronic states with a common ground state with a vibrational manifold. The electron-vibration coupling shows its effect felt in the transport set up and when it is switched-off, the expression of current resembles with that obtained previously[108] along with the additional features in the case of external bias.

We have numerically calculated average current as a function of the internal as well as external bias in the steady state domain. For that purpose, we have first taken pyridine as a prototypical example for electron-vibration entanglement [153, 243]. We have obtained that the current shows spikes when the energy bias becomes equal to the vibrational mode resonant frequency and its multiples. We have also shown that only in the low temperature limit, the vibrational modes can absorb energy due to the tunneling of electrons from the left lead to the right lead through the molecule. The study is also extended by comparing the current- internal bias profile for different molecules with different molecular parameters. Here, we have shown that their is an interplay between the tunneling matrix element and the vibrational frequency for obtaining vibrational signatures in the current-internal bias profile.

Here additional peaks can clearly identify the vibrational signatures which can be of potential application in electron transport spectroscopy of single molecules. While investigating current as a function of the external bias voltage we get two principal results. First, introduction of electron-vibration coupling suppresses the noise level in molecular current and secondly, the electron vibration coupling also provides additional channel for electron transport thereby inducing additional steps in the $I-V$ characteristics, which is also further evidenced in the differential conductance plot. With the increase in temperature, a clear identification of broadening of the peaks are possible for the differential conductance profile within the interplay of gate voltage and electron-vibration coupling.

We have also considered the current noise spectrum and Fano factor to monitor the steady state fluctuation of the molecular current. When the electron-vibration coupling parameter is gradually decreased, there is a suppression of current noise. This suppression in current noise is quite similar to that obtained earlier[100], where incorporation of a coherent signal in the bath suppresses the noise. Thus vibrationally coupled resonating structures of dimers of conjugated electron rich molecule is the basic testing ground to probe the vibrational mode in electron transport spectroscopy.

Appendix A

In this appendix, we have provided a brief outline of the deduction leading to the expression of $F(\tau)$ given in Eq.(6.15). This will be followed by calculation of the correlation function appearing in Eq.(6.16). For the sake of clarity we consider the single bosonic mode case.

For single vibrational mode(say k-th mode), the time dependent operator in the interaction picture can be expressed as

$$X_k(\alpha_k, t) = e^{it\omega_k a_k^\dagger a_k} e^{\alpha_k(a_k^\dagger - a_k)} e^{-it\omega_k a_k^\dagger a_k}. \tag{6.42}$$

When the operators in the exponential term are expanded, using Baker-Hausdorff formula, we recast Eq.(6.42) as

$$X_k(\alpha_k, t) = \sum_{n=0}^{\infty} \frac{\alpha_k^n}{n!} (a_k^\dagger e^{i\omega_k t} - a_k e^{-i\omega_k t}). \tag{6.43}$$

The time dependent vibrational operator thus can be expressed as

$$X(\alpha_k, t) = e^{\alpha_k(a^\dagger e^{i\omega_k t} - a e^{-i\omega_k t})}. \tag{6.44}$$

Thus, the one-mode two-time bosonic correlation function can be expressed as

$$\langle X(\alpha_k, t) X^\dagger(\alpha_k, t') \rangle = e^{-\alpha_k^2(1-e^{-i\omega_k(t-t')})} \langle e^{z^* a_k^\dagger} e^{-z a_k} \rangle, \tag{6.45}$$

where, $z = \alpha_k(e^{i\omega_k t} - e^{-i\omega_k t'})$ and while deducing Eq.(6.45), we have considered the Baker-Hausdorff formula[56]. The correlation function is $\langle e^{z^* a_k^\dagger} e^{-z a_k} \rangle$
$= Tr_{ph}[\rho_{ph} e^{z^* a_k^\dagger} e^{-z a_k}]$, where the vibrational density operator is $\rho_{ph} =$
$(1 - e^{-\frac{\hbar\omega_k}{k_B T}}) e^{-\frac{-\hbar\omega_k a_k^\dagger a_k}{k_B T}}$. After a straightforward algebra[56], we arrive at

$$\langle e^{z^* a_k^\dagger} e^{-z a_k} \rangle = (1 - e^{-\frac{\hbar\omega_k}{k_B T}}) \sum_{n=0}^{\infty} e^{-\frac{n\hbar\omega_k}{k_B T}} L_n(|z|^2), \tag{6.46}$$

where $L_n(|z|^2)$ is the Laguerre polynomial of order n. We now use the generating function $\sum_{n=0}^{\infty} L_n(x) h^n = \frac{e^{-\frac{xh}{(1-h)}}}{1-h}$ and arrive at the expression

$$\langle X(\alpha_k, t) X^\dagger(\alpha_k, t') \rangle = e^{-\alpha_k^2(1-e^{-i\omega_k \tau})} e^{-|z|^2 N_k}, \tag{6.47}$$

where $N_k = \frac{1}{e^{\frac{\hbar\omega_k}{k_B T}} - 1}$. We now expand the exponential terms and algebraically manipulate the vibrational correlation function to finally get

$$\langle X(\alpha_k, t) X^\dagger(\alpha_k, t') \rangle = e^{-\alpha_k^2(1+2N_k)} \sum_{n=0}^{\infty} \left(\frac{1+N_k}{N_k} \right)^{\frac{n}{2}} I_n(2\alpha_k^2 \sqrt{N_k(1+N_k)}). \tag{6.48}$$

Appendix B

Here, we have provided the basic outlines of getting the expression for average current through a dimer molecule having two vibrational modes. At first we take Laplace transform of the equations of motion[see Eqs.(6.12,6.13,6.14)] such that for any time dependent function $f(t)$, we define the Laplace transformed function as $\bar{F}(s) = L[f(t)] = \int_0^\infty dt e^{-st} f(t)$. We have also applied the convolution property such that $\bar{G}(s)\bar{H}(s) = L[g(t-t')h(t')]$. On explicit evaluation of the Laplace transformation of the two-time vibrational correlation function, it can be expressed as

$$\bar{C}_1(s) = \sum_{n_1=0}\sum_{n_2=0} C_{n_1} C_{n_2} \frac{1}{s + i(n_1\omega_1 + n_2\omega_2 - \frac{\Delta\bar{\epsilon}}{\hbar})} \tag{6.49}$$

and

$$\bar{C}_2(s) = \sum_{n_1=0}\sum_{n_2=0} C_{n_1} C_{n_2} \frac{1}{s + i(n_1\omega_1 + n_2\omega_2 + \frac{\Delta\bar{\epsilon}}{\hbar})}, \tag{6.50}$$

with, $C_{n_k} = e^{-\alpha_k^2(1+2N_k)}(\frac{1+N_k}{N_k})^{\frac{n_k}{2}} I_{n_k}(2\alpha_k^2\sqrt{N_k(1+N_k)})$[see Eq.(6.16)]. Additionally, we have applied the final value theorem $\lim_{t\to\infty} f(t) = \lim_{s\to 0} s\bar{F}(s)$ to obtain the steady state values of $\langle n_e\rangle$, $\langle n_c\rangle$, $\langle\bar{p}\rangle$ and $\langle\bar{p}^\dagger\rangle$. After performing the Laplace transform, Eqs.(6.12,6.13,6.14) appear as

$$(\Gamma_{oe} + \Gamma_{eo})\langle n_e\rangle_\infty + i\lambda_c\langle\bar{p}\rangle_\infty - i\lambda_c\langle\bar{p^\dagger}\rangle_\infty + \Gamma_{oe}\langle n_c\rangle_\infty = \Gamma_{oe}, \tag{6.51}$$

$$i\lambda_c\bar{C}_1(0) + [1 + \frac{1}{2}(\Gamma_{eo} + \Gamma_{co})\bar{C}_1(0)]\langle\bar{p}\rangle_\infty - i\lambda_c\bar{C}_2^*(0)\langle n_c\rangle_\infty = 0, \tag{6.52}$$

$$-i\lambda_c\bar{C}_1^*(0)\langle n_e\rangle_\infty + [1 + \frac{1}{2}(\Gamma_{eo} + \Gamma_{co})\bar{C}_1^*(0)]\langle\bar{p^\dagger}\rangle_\infty + i\lambda_c\bar{C}_2(0)\langle n_c\rangle_\infty = 0, \tag{6.53}$$

$$\Gamma_{oc}\langle n_e\rangle_\infty - i\lambda_c\langle\bar{p}\rangle_\infty + i\lambda_c\langle\bar{p^\dagger}\rangle_\infty + (\Gamma_{oc} + \Gamma_{co})\langle n_c\rangle_\infty = \Gamma_{oc}. \tag{6.54}$$

Now after rearranging the equations, we adopt matrix notation to represent the set of four simultaneous linear algebraic equation as

$$\begin{bmatrix} \langle n_e\rangle_\infty \\ \langle\bar{p}\rangle_\infty \\ \langle\bar{p}^\dagger\rangle_\infty \\ \langle n_c\rangle_\infty \end{bmatrix} = \mathbf{P}^{-1} \begin{bmatrix} \Gamma_{oe} \\ 0 \\ 0 \\ \Gamma_{oc} \end{bmatrix}, \tag{6.55}$$

where, $\mathbf{P} = \begin{bmatrix} \Gamma_e & i\lambda_c & -i\lambda_c & \Gamma_{oe} \\ i\lambda_c\bar{C}_1(0) & 1 + \frac{1}{2}\Gamma_{ec}\bar{C}_1(0) & 0 & -i\lambda_c\bar{C}_2^*(0) \\ -i\lambda_c\bar{C}_1^*(0) & 0 & 1 + \frac{1}{2}\Gamma_{ec}\bar{C}_1^*(0) & i\lambda_c\bar{C}_2(0) \\ \Gamma_{oc} & -i\lambda_c & i\lambda_c & \Gamma_c \end{bmatrix}$, with $\Gamma_e = \Gamma_{oe} + \Gamma_{eo}$, $\Gamma_c = \Gamma_{oc} + \Gamma_{co}$, $\Gamma_{ec} = \Gamma_{eo} + \Gamma_{co}$ to obtain the steady state solution for average current given in Eq.(6.18).

Appendix C

In this Appendix, we have outlined the basic steps for obtaining the expressions for $P_1(t)$ and $P_2(t)$ in Eqs.(6.24 and (6.25). We principally show the steps to get $P_1(t)$. The steps to find $P_2(t)$ follows naturally. Following Eq.(6.15), we denote

$$F_1(t-t') = F(t-t')e^{\frac{i(t-t')\Delta\bar{\epsilon}}{\hbar}} = \sum_{n_1,n_2=-\infty}^{\infty} C_{n_1}C_{n_2}e^{-i(n_1\omega_1+n_2\omega_2-\frac{\Delta\bar{\epsilon}}{\hbar})(t-t')}. \tag{6.56}$$

Now using the formula for derivative of convolution

$$\frac{\partial}{\partial t}\int_0^t dt' F_1(t-t')\langle n_e\rangle_{t'} = \int_0^t dt' F_1'(t-t')\langle n_e\rangle_{t'}. \tag{6.57}$$

and keeping in mind that $L\{f(t-t')g(t)\} = L\{f(t)\}L\{g(t)\}$, one obtains

$$L\left\{\int_0^t dt' F_1'(t-t')\langle n_e\rangle_{t'}\right\} = \sum_{n_1,n_2} C_{n_1}C_{n_2}\left(\frac{[-i(n_1\omega_1+n_2\omega_2-\frac{\Delta\bar{\epsilon}}{\hbar})]}{s+i(n_1\omega_1+n_2\omega_2-\frac{\Delta\bar{\epsilon}}{\hbar})}\right)\bar{\langle n_e\rangle}(s), \tag{6.58}$$

where, $L\{f(t)\} = \int_0^\infty dt e^{-st}f(t) = \bar{f}(s)$. Now after carrying out the inverse Laplace transform, one obtains $\int_0^t dt' F_1'(t-t')\langle n_e\rangle_{t'} = L^{-1}\{\langle\bar{n}_e\rangle(s)\bar{f}_1(s)\}$, where $\bar{f}_1(s) = \sum_{n_1,n_2} C_{n_1}C_{n_2}\left(\frac{[-i(n_1\omega_1+n_2\omega_2-\frac{\Delta\bar{\epsilon}}{\hbar})]}{s+i(n_1\omega_1+n_2\omega_2-\frac{\Delta\bar{\epsilon}}{\hbar})}\right)$. Thus we find

$$L^{-1}\{\langle\bar{n}_e\rangle(s)\bar{f}_1(s)\} = \int_0^t dt'\langle n_e\rangle_t \sum_{n_1,n_2} C_{n_1,n_2}e^{-i\left(n_1\omega_1+n_2\omega_2-\frac{\Delta\bar{\epsilon}}{\hbar}\right)(t-t')}, \tag{6.59}$$

where, $C_{n_1,n_2} = C_{n_1}C_{n_2}\left[-i\left(n_1\omega_1+n_2\omega_2-\frac{\Delta\bar{\epsilon}}{\hbar}\right)\right]$. After performing a short piece of algebra, one thus obtains

$$\int_0^t dt' F_1'(t-t')\langle n_e\rangle_{t'} = \langle n_e\rangle_t P_1(t). \tag{6.60}$$

Chapter 7

Electron transport in a molecule due to quantum entanglement and conical intersection

In this chapter, to find the effect of electron-vibration entanglement and conical intersection in a molecule, we have studied cis-trans isomerization in a molecule in an electron transport setup with electronic source and sink composed of fermions. Here, we show that the vibronic coupling introduces quantum entanglement and non-classicality which is typically enhanced in the CI point which is supported from Wigner function and other measures of entanglement. The layout of the rest of the chapter is as follows: After providing a brief introduction in the section 7.1, in the section. 7.2, we have discussed the Hamiltonian and its features for a molecule having conical intersection. In this section, the system-electron lead couplings are also discussed in the context of molecular electron transport. The next section is devoted to deduce the master equation involved for a molecule coupled to two electronic reservoir in a quantum transport setup, where explicit rate expressions for the electron-vibration entangled states matrix elements are provided. Section 7.4, which is dedicated for numerical results and discussion is subdivided into two subsections. The subsection 7.4.1 is dedicated to calculate the Von-Neumann entropy, the uncertainty product as a function of ϕ. We have also calculated the Wigner quasiprobability distribution function and the Wigner function matrix, respectively for the vibrational mode present in the molecule put in the transport setup. In the subsection 7.4.2, we have calculated the current as a function of the torsion angle(ϕ) characterizing the system and also as a function of vibronic coupling. Finally in section 7.5, we have concluded the chapter.

7.1 Introduction

Several unexpected phenomena like radiationless relaxation of excited electronic states, photoinduced unimolecular decay and isomerization processes of polyatomic molecules appears in the molecular dynamics if we consider going beyond the Born-Oppenheimer approximation[113, 114]. Vibronic coupling, which is an an essential idea behind *conical intersection*(CI) between electronic states is uniquely utilized to describe the mechanistic pathway and its underlying features in molecular system in non-adiabatic regime[115, 116, 117, 118]. Due to the added complexity of the non-adiabatic dynamics, the effect of quantum entanglement among various degrees of freedom in a molecule on its observables is not easy to understand in comparison to the entanglement between two spatially separated objects. Among several non-adiabatic reactions and processes, the cis-trans isomerization is a prominent example which is investigated[156] for rotations about C=C bonds using specially designed femtosecond laser pulses and it has been a subject of longstanding research interest [157, 158, 159, 160, 161, 162]. This isomerization forms the leading step in many photophysical processes of biological importance namely vision[163, 164]. In this regard, it is noteworthy that such systems are also used to produce light-induced ion pumping which plays vital role in producing photomemories and light triggered switches[165]. Generally the theoretical characterization of the CI point in such systems involve study of phase space quasiprobability distribution functions namely the Wigner distribution function[166], Among other measures von-Neumann entropy[167] and ATAS technique[168] are also utilized popularly from the joint density matrix. Experimental features of CI are performed by several techniques[169, 170, 171, 172, 173, 174, 175] including ultrafast electron diffraction studies[176]. Extensive studies on the measurement of electron-vibration entanglement of trapped atoms and ions[177, 178] have also been done. Whereas, most of the theoretical studies are based on the wave-packet propagation of the CI, our aim has become to study the non-classicality and entanglement in a molecule in an electron transport setup.

In this chapter, we have addressed the following issues: At first we have probed the conical intersection CI point present in a molecular system by theoretically measuring the electron transport through it when put in between two electron reservoirs. When a molecule is connected to two electronic leads with a difference in the chemical potential, electrons will flow[101, 102, 103, 104, 105, 106, 107, 108] within it in response to the potential difference. The current-voltage profile of the molecule in such a case should bear some signature of the electronic-nuclear entanglement, if any present in the system. Driven by this motive, we have theoretically calculated the molecular electron current by using the quantum master equation formalism following our previous work on system coupled with fermionic reservoir[100] and

provided an indication of the presence of the conical intersection and a measure of the entanglement in the molecular system. In addition, we have also calculated the traditional measures like von-Neumann entanglement entropy, the uncertainty product and the Wigner distribution function to identify and locate the CI point present in the molecule. For that purpose, we have considered the variation of non-classicality and entanglement in the molecular states by treating the torsional coordinate parametrically and it is important to explore the nature of entanglement and non-classicality when the molecule behaves as a junction for electron transport.

7.2 Model molecular system with conical intersection

To put our work in a proper perspective, we consider a formal quantum transport setup[108] where a system is coupled to both the source(emitter) and sink(collector) of electrons as two fermionic reservoirs with chemical potentials, μ_e and μ_c, respectively. Electron transports through the system in response to the external bias arising out of the difference in chemical potential, $V = \mu_e - \mu_c$. The total Hamiltonian can thus be expressed as

$$H_{tot} = H_{sys} + H_e + H_c + H_{int}, \tag{7.1}$$

where, the emitter Hamiltonian is $H_e = \sum_p \epsilon_p^e b_p^\dagger b_p$ and the collector Hamiltonian is $H_c = \sum_r \epsilon_r^c d_r^\dagger d_r$. H_{sys} is the system Hamiltonian and H_{int} is the interaction Hamiltonian representing system-reservoir interaction. We consider $b_p(b_p^\dagger)$ as the annihilation(creation) operator for the p-th electron in the emitter and that of $d_r(d_r^\dagger)$ is the annihilation(creation) operator for the r-th electron in the collector. The fermions obey the anti-commutation rules $\{b_k^\dagger b_l\}_+ = \delta_{kl}$ and $\{d_k^\dagger d_l\}_+ = \delta_{kl}$. ϵ_p^e and ϵ_r^c are energy of the resonant modes of the emitter and collector fermion(electron) reservoir respectively.

The construction of H_{sys} is considered following the Ref.[249] and Domcke *et.al.*,[250] where the system consists of two diabatic[162, 250] electronic states $|i\rangle (i = 1, 2)$ corresponding to cis and trans isomer of the molecule coupled with a single vibrational mode. Additionally we consider the existence of torsional motion of the molecule representing torsion of the molecule across a double bond say a carbon-carbon double bond associated with the electronic excitation. The system Hamiltonian can thus be expressed as

$$H_{sys} = \sum_{i=1}^{2} |i\rangle \left(E_i(\phi) + (-\frac{\hbar^2}{2I}\frac{\partial^2}{\partial\phi^2}) + \hbar\omega a^\dagger a \right) \langle i| + \hbar\lambda(a + a^\dagger)(|1\rangle\langle 2| + |2\rangle\langle 1|), \tag{7.2}$$

where, ϕ is the torsion angle, $E_i(\phi)$ is the torsional potential energy for the i-th state which is a function of ϕ. I is the reduced moment of inertia of torsion, $a^\dagger(a)$

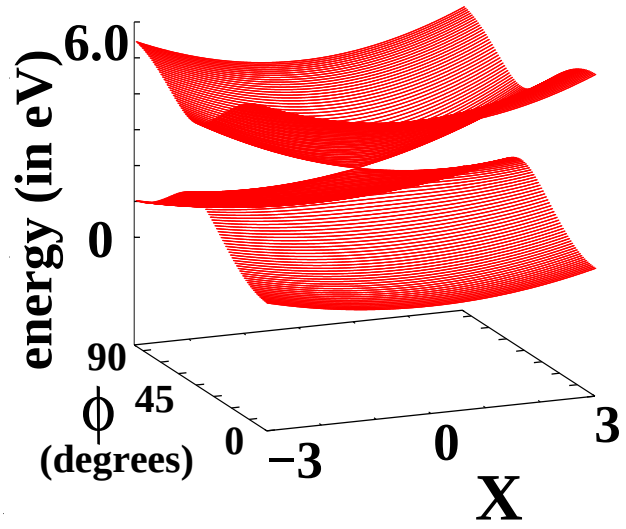

Figure 7.1: The adiabatic PESs of a model molecular system plotted as a function of the dimensionless normal coordinate X and torsion angle ϕ. The vertical axis represents energy of the two diabatic states in arbitrary units. A conical intersection is present at ($X = 0$, $\phi = 48.2^o$).

is the creation (annihilation) operator for the vibrational degree of freedom having frequency ω and λ is the vibronic coupling constant having dimension of frequency. The torsional potential energies are expressed as

$$E_1 = \frac{1}{2}V_0\left(1 - \cos(2\phi)\right)$$

and

$$E_2 = E - \frac{1}{2}V_0\left(1 - \cos(2\phi)\right).$$

The system-electron reservoir interaction Hamiltonian is expressed following the Ref.[100] as

$$H_{int} = H^e_{int} + H^c_{int}, \tag{7.3}$$

where, $H^e_{int} = \hbar\sum_p(V^p_e b^\dagger_p|0\rangle\langle e| + V^{p*}_e b_p|e\rangle\langle 0|)$ and $H^c_{int} = \hbar\sum_r(V^r_c d^\dagger_r|0\rangle\langle c| + V^{r*}_c d_r|c\rangle\langle 0|)$, with, $V^p_e(V^{p*}_e)$ and $V^r_c(V^{r*}_c)$ are the corresponding tunnel matrix elements. In this system, the two adiabatic potential energy surfaces exhibit a conical intersection(CI) at $\phi = 48.2^o$. At other values of ϕ, the degeneracy is lifted. A little digression at this point would not be irrelevant for further discussions. The bare electronic states$|1\rangle$ and $|2\rangle$ are connected through a tunnel barrier which couples among them through the position operator $(a + a^\dagger)$ and characterized by λ. The effective Hilbert space which becomes H_{eff} =span$(|1\rangle, |2\rangle)$ is assumed to be spanned by two many-body states $|1\rangle = |n_1 + 1, n_2\rangle$ and $|2\rangle = |n_1, n_2 + 1\rangle$ with energies E_1 and E_2, both of them being dependent on ϕ. The empty ground state $|0\rangle = |n_1, n_2\rangle$ has one electron less and n_1 electrons in the left and n_2 electrons in the right state. Although this state

plays a vital role in transport, but there are no superpositions between $|0\rangle$ and the states in H_{eff} [108]. As it is evident, the vacuum state $|0\rangle$ particularly useful in expressing coherent interaction terms between the molecular system and the leads and also needed to express the population conservation criteria.

7.3 Master equation for transport through electron-vibration entangled states

In this section we shall formulate a Born-Markov master equation for the fermionic reservoirs of source and sink[100] and proceed towards its formal solution. This section shall be concluded by explicitly considering the rate equation for various electron-vibration entangled density operator matrix elements characterizing the molecular system.

The equation of motion for the total density operator in interaction picture $\chi(t)$ for a molecule coupled with two electron reservoirs is

$$\frac{\partial\chi(t)}{\partial t} = \frac{1}{i\hbar}[H_{int}(t) + H_{e-e}(t), \chi(t)], \tag{7.4}$$

where, $H_{int}(t)$ is interaction Hamiltonian in the interaction picture, and

$$H_{e-e}(t) = \hbar\lambda(a^\dagger e^{i\omega t} + ae^{-i\omega t})(|1\rangle\langle 2|e^{\frac{it\epsilon}{\hbar}} + |2\rangle\langle 1|e^{-\frac{it\epsilon}{\hbar}}), \tag{7.5}$$

where $\epsilon = E_1 - E_2$.

While expressing the equation of motion for the total density operator in the interaction picture, we assume the following:(i)The tunneling of electrons to or from the molecule to the leads is considered upto its second order(Born Approximation), which amounts to neglecting the back-action effects by tunneling on the electrons on the reservoirs. (ii) The damping and the coupling terms are considered to be independent of one another so that $H_{e-e}(t)$ appears in the coherent time evolution of the system. (iii) The interaction picture description is valid with respect to the free unperturbed Hamiltonian $H_0 = \sum_{i=\{1,2\}} E_i|i\rangle\langle i| + \hbar\omega a^\dagger a + \sum_p \epsilon_p^e b_p^\dagger b_p + \sum_r \epsilon_r^c d_r^\dagger d_r$. Thus finally, we have

$$\dot{\chi}(t) = \frac{1}{i\hbar}[H_{e-e}(t), \chi(t)] - \frac{1}{\hbar^2}\int_0^t dt'[H_{int}(t), [H_{int}(t'), \chi(t')]]. \tag{7.6}$$

We now invoke the Markov approximation in the sense that the two electron reservoirs are always in thermal equilibrium and the total density operator can be approximately factorized as $\chi(t) \simeq \rho(t)\otimes\rho_{res}^e\otimes\rho_{res}^c$, where, $\rho(t)$ is the density operator for the molecule, along with the vibrational mode and ρ_{res}^e and ρ_{res}^c are the density operators for the emitter and collector electron reservoirs respectively. We therefore take trace over the reservoir degrees of freedom such that $Tr_{res}\chi(t) = \rho(t)$. After

a straightforward but lengthy process following Ref.[100], we finally arrive at the Born-Markov master equation,

$$\frac{\partial \rho}{\partial t} = -\frac{i}{\hbar}[H_{int}(t), \rho] + D(\rho), \tag{7.7}$$

where,

$$D(\rho) = -\frac{\Gamma_1}{2}(|0\rangle\langle 0|\rho - 2|1\rangle\langle 0|\rho|0\rangle\langle 1| + \rho|0\rangle\langle 0|)$$
$$-\frac{\Gamma_2}{2}(|2\rangle\langle 2|\rho - 2|0\rangle\langle 2|\rho|2\rangle\langle 0| + \rho|2\rangle\langle 2|), \tag{7.8}$$

and we have assumed that the external bias arising out of the difference in chemical potential between the two reservoirs is infinitely large and Γ_1 (and Γ_2) are the rate constants for tunneling of electrons to (or from) the molecule from (or to) the electron reservoir.

7.4 Numerical Exploration

This section is dedicated to outline the numerical scheme that we have adopted to present our result for characterization of the conical intersection point for a molecule and estimate the entanglement present in terms of the Von-Neumann entropy, uncertainty product, Wigner distribution function and finally in terms of the molecular electronic current due to its coupling with an emitter and collector electron reservoir at different chemical potentials.

For the purpose of presenting our result in subsequent subsections, we define the electron-vibration entangled density operator matrix elements[107] as $\rho^{i,j}_{n,m} = \langle n, i|\rho|j, m\rangle$ where, $i, j = 0, 1, 2$ refers to the electronic states and n, m refers to vibrational states.

The matrix elements obey the following coupled differential equations:

$$\frac{\partial \rho^{0,0}_{n,m}}{\partial t} = -i\omega(n-m)\rho^{0,0}_{n,m} - \Gamma_1\rho^{0,0}_{n,m} + \Gamma_2\rho^{2,2}_{n,m}, \tag{7.9}$$

$$\frac{\partial \rho^{1,1}_{n,m}}{\partial t} = -i\omega(n-m)\rho^{1,1}_{n,m} - i\lambda[(\sqrt{n+1}\rho^{2,1}_{n+1,m} + \sqrt{n}\rho^{2,1}_{n-1,m})$$
$$-(\sqrt{m}\rho^{1,2}_{n,m-1} + \sqrt{m+1}\rho^{1,2}_{n,m+1})] + \Gamma_1\rho^{0,0}_{n,m}, \tag{7.10}$$

$$\frac{\partial \rho^{1,2}_{n,m}}{\partial t} = -i\left[\frac{\epsilon}{\hbar} + \omega(n-m) + \frac{\Gamma_2}{2i}\right]\rho^{1,2}_{n,m} - i\lambda[(\sqrt{n+1}\rho^{2,2}_{n+1,m} + \sqrt{n}\rho^{2,2}_{n-1,m})$$
$$-(\sqrt{m}\rho^{1,1}_{n,m-1} + \sqrt{m+1}\rho^{1,1}_{n,m+1})], \tag{7.11}$$

$$\frac{\partial \rho^{2,1}_{n,m}}{\partial t} = i\left[\frac{\epsilon}{\hbar} - \omega(n-m) - \frac{\Gamma_2}{2i}\right]\rho^{2,1}_{n,m} - i\lambda[(\sqrt{n+1}\rho^{1,1}_{n+1,m} + \sqrt{n}\rho^{1,1}_{n-1,m})$$
$$-(\sqrt{m}\rho^{2,2}_{n,m-1} + \sqrt{m+1}\rho^{2,2}_{n,m+1})], \tag{7.12}$$

$$\frac{\partial \rho^{2,2}_{n,m}}{\partial t} = -(i\omega(n-m)+\Gamma_2)\rho^{2,2}_{n,m} - i\lambda[(\sqrt{n+1}\rho^{1,2}_{n+1,m} + \sqrt{n}\rho^{1,2}_{n-1,m}) \\ -(\sqrt{m}\rho^{2,1}_{n,m-1} + \sqrt{m+1}\rho^{2,1}_{n,m+1})], \tag{7.13}$$

where, $\epsilon = E_1(\phi) - E_2(\phi)$. These equations are in principle not exactly solvable, so that we resort to solve the system of equations numerically under the steady state condition. Here, we mention that while deducing these equations, we have considered that the emitter and the collector electron reservoirs are present under infinite difference in the chemical potential. In the stationary state, the time derivatives are zero and thus we obtain a linear set of algebraic equations which we have solved iteratively. In order to get a physically reasonable numerical solution, the boson space has to be truncated at a finite number[107] along with the normalization condition $\sum_n \rho^{0,0}_{n,n} + \rho^{1,1}_{n,n} + \rho^{2,2}_{n,n} = 1$. The particular feature one should note is that, it is not possible to employ any factorization approximation like $\rho \simeq \rho_{el} \otimes \rho^b$, where the '$el$' and '$b$' respectively refers to electronic and vibrational degrees of freedom, under strong conditions of electron-vibration entanglement. We have numerically solved the set of linear simultaneous differential equations [see Eqs.(7.9)-(7.13)] coming from the master equation [see Eq.(7.7)] under steady state condition. The values of the parameters of the Hamiltonian in the Eq.(7.2) are taken from the work of Seidner *et.al.,*[250]. We have considered $V_0 = 4.5$ eV and $E = 5.0$ eV in the expressions of torsional potentials. The value of the reduced moment of inertia, I is taken in such a way that it corresponds to an energy value of 0.01 eV. The frequency of the coupling of vibrational mode is $\omega = 0.17$ eV and the vibronic coupling constant, λ is changed parametrically in the range between ω and 2ω. As a consequence, the torsional motion becomes slowly varying compared to the vibrational motion and hence ϕ can be considered parametrically. The tunneling rate constants are fixed at a value of $\Gamma_1 = \Gamma_2 = 0.13$ meV. This suggests that the energy associated with the tunneling rates to and fro for the molecule to the electronic reservoir is smaller than electronic and vibrational energies of the molecule.

In what follows, we have calculated different parameters like Von-Neumann entropy, Wigner function, the uncertainty product and finally the molecular current for the purpose to quantify entanglement and non-classicality in case of a molecule put in a transport setup with conical intersection.

7.4.1 Characterization of conical intersection through entanglement and non-classicality

In this subsection, we have quantified entanglement in terms of Wigner function in phase space with reference to the CI point. We have also utilized Wigner function matrix elements to estimate non-classicality. The dependence of entanglement and non-classicality on CI can also be understood from the Von-Neumann information

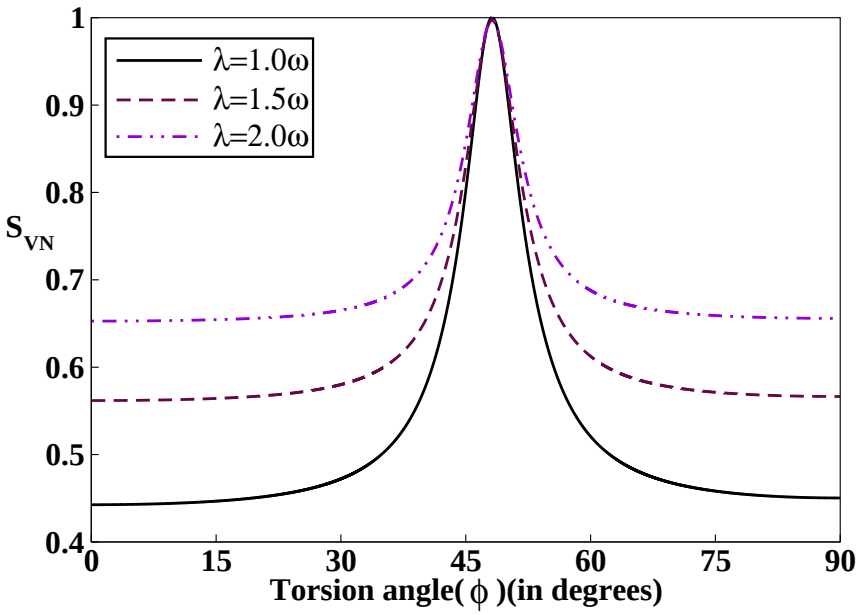

Figure 7.2: Plot of S_{VN} against ϕ for different parametric values of λ, the vibronic coupling. S_{VN} maximizes for $\phi = 48.2$. Increase the λ increases the overall electron-vibration entanglement (SE).

entropy and uncertainty product, which we have studied in this section.

Von-Neumann entropy

Here, we aim to analyze the role of electron-vibration entanglement for a molecule put in a proper electron transport setup in terms of the von-Neumann entropy of entanglement S_{VN}. The entanglement between the electronic and vibrational degrees of freedom of the composite states of the molecule concerned can be expressed using the von-Neumann entropy of entanglement[251] as

$$S_{VN} = -Tr_{el}(\rho_{el} \log_2 \rho_{el}), \tag{7.14}$$

where ρ_{el} is the reduced density operator for the electronic degrees of freedom such that $\rho_{el} = Tr_{vib}\rho$. For the unentangled states, the entropy is zero and for the maximum entangled state, it has an entropy 1.

In the fig.(7.2), we have shown the variation of the Von-Neumann entanglement entropy S_{VN} against the torsion angle ϕ in degrees for different parametric values of the vibronic coupling parameter λ. With increase in the torsion angle ϕ, S_{VN} remains almost constant upto a certain ϕ for a fixed λ. But from $\phi \approx 30^o$ there is a sharp rise in the curve upto the CI point i.e., $\phi = 48.2^o$ indicating maximum electron-vibration entanglement. At the CI point S_{VN} becomes almost equal to its maximum possible value indicating a maximally entangled state which is independent of the coupling strength, λ. For all other values of λ, the entanglement measure, S_{VN} is higher for higher λ. For the torsion angle ϕ far from that corresponding to

CI, the small finite value of S_{VN} suggests another source of entanglement which comes through the vibronic coupling parameter λ. We designate this as *persistent entanglement*(PE). At the CI, the energy asymmetry almost vanishes so that S_{VN} maximizes indicating introduction of ϕ-dependent entanglement called *sensitive entanglement*(SE). In between these two extremities, a clear interplay of both types of entanglement can be well noted in the molecular system.

Uncertainty product

In this part, we have studied the uncertainty product $\Delta X.\Delta P$ for the vibrational state of the molecule involved in electron transport. The variances $(\Delta X)^2 = \langle X^2\rangle - \langle X\rangle^2$ and $(\Delta P)^2 = \langle P^2\rangle - \langle P\rangle^2$ for the dimensionless position coordinate X and its conjugate momentum P are first expressed in terms of the electron-vibration entangled state for the molecule. In this regard, one can define[107, 56] them as

$$X = \frac{(a + a^\dagger)}{\sqrt{2}}, P = \frac{i(a^\dagger - a)}{\sqrt{2}}, \tag{7.15}$$

where, $a(a^\dagger)$ is the bosonic annihilation(creation) operator for the vibrational mode in the molecule. The position and momentum variances are explicitly expressed in terms of the density operator ρ^b, for the vibrational mode, as

$$(\Delta X)^2 = \frac{1}{2}Tr_{el}\sum_n[\sqrt{n(n-1)}\rho_{n,n-2} + (2n+1)\rho_{n,n} + \sqrt{(n+1)(n+2)}\rho_{n,n+2}]$$
$$-\frac{1}{2}[Tr_{el}\sum_n(\sqrt{n}\rho_{n,n-1} + \sqrt{n+1}\rho_{n,n+1})]^2, \tag{7.16}$$

$$(\Delta P)^2 = \frac{1}{2}Tr_{el}\sum_n[-\sqrt{n(n-1)}\rho_{n,n-2} + (2n+1)\rho_{n,n} - \sqrt{(n+1)(n+2)}\rho_{n,n+2}]$$
$$-\frac{1}{2}[Tr_{el}\sum_n(-i\sqrt{n}\rho_{n,n-1} + i\sqrt{n+1}\rho_{n,n+1})]^2, \tag{7.17}$$

where, $\rho_{n,m} = \langle n|\rho^b|m\rangle$.

In the fig.(7.3), we have calculated the uncertainty product as a function of the torsion angle ϕ for different vibronic coupling strengths varying from $\lambda = \omega$ to $\lambda = 2\omega$. From the fig.(7.3), one can observe that the uncertainty product $\Delta X.\Delta P$ starts to deviate from the minimum uncertainty value of 0.5 to attain its maximum at $\phi = 48.2^o$. We note that this is particularly due to the minimum uncertainty product corresponding to the coherent state[107, 249]. As the torsion angle ϕ approaches the conical intersection point, the deviation from 0.5 magnitude starts. But the extent of the deviation depends on the vibronic coupling constant, λ. For $\lambda = \omega$ the deviation

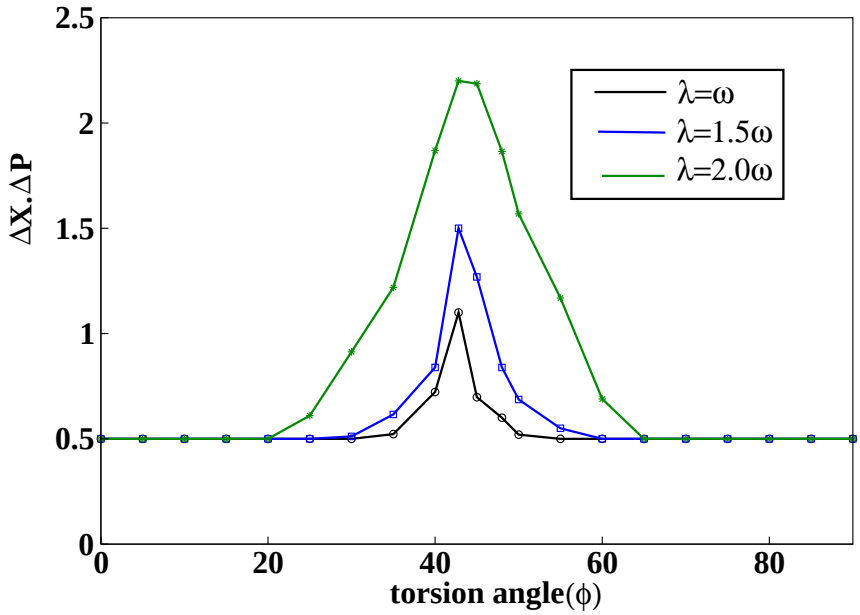

Figure 7.3: Plot of $\Delta X.\Delta P$ against ϕ for different parametric values of λ. $\Delta X.\Delta P$ maximizes for $\phi = 48.2$. Increase in the vibronic coupling, λ increases the overall electron-vibration entanglement (SE), which is also reflected in terms of the uncertainty product.

starts from $\phi \approx 40^o$ whereas for $\lambda = 2\omega$ it starts from $\phi \approx 20^o$. The deviation of the uncertainty product from the value 0.5 becomes maximum at the conical intersection point with its value being higher for higher value of the vibronic coupling, λ. This observation corresponds closely to the result from atom-phonon entanglement where it is established that the uncertainty product for the single particle measurement of a position coordinate and momentum of the particle is related to the entanglement parameter. Also, one can note that in the region apart from the CI, there is some residual entanglement through the parameter λ. This result is clearly in accordance to what we have obtained for Von-Neumann entropy S_{VN}.

Wigner distribution function

Here, we have considered the backaction of the electron transport characteristic to the vibrational mode of a molecule in a formal quantum transport setup in terms of Wigner function matrix[178] and the Wigner quasiprobability distribution function[166]. The Wigner function matrix $W_{ij}(\beta)$ is defined as[178]

$$W_{ij}(\beta) = Tr[\rho|j\rangle\langle i|\delta(\beta - a)], \tag{7.18}$$

where, β is the complex variable defined as $\beta = X + iP$ and $\delta(\beta - a)$ is the operator valued delta function[178] defined as Fourier transform of the displacement operator[166] $D(\xi) = \exp(\xi a^\dagger - \xi^* a)$ such that

$$\delta(\beta - a) = \frac{1}{\pi^2}\int d^2\xi D(\xi)\exp(\beta\xi^* - \beta^*\xi). \tag{7.19}$$

The off-diagonal elements $W_{ij}(\beta)[i \neq j]$ gives information of the electronic coherence and information regarding entanglement present in the system. In the fig.(7.4), we

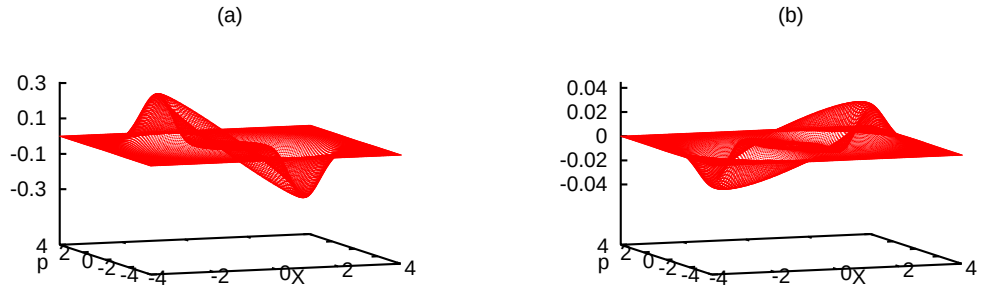

Figure 7.4: 3D plots of real and imaginary parts of W_{12} for $\phi = 48.2^o$ and $\lambda = 2\omega$. X denotes dimensionless normal coordinate of vibration and P denotes its conjugate momentum. Fig.(4.a) shows $Re(W_{12})$ and fig.(4.b) shows $Im(W_{12})$.

have shown the 3D plots for the real and imaginary parts of W_{12} for $\phi = 48.2^o$ and $\lambda = 2\omega$. From the fig.(7.4), it is clearly revealed that at the CI point, the electronic coherence assumes sufficient magnitude which physically signifies maximization of the entanglement(SE) that maximizes the entropy as well at the CI point. Since the molecular current is also related to the off-diagonal density matrix elements in the electronic basis, increase in the electronic coherence should magnify the electronic current which will be discussed subsequently. The negativity of the real and imaginary parts of W_{12} is clearly indication of the non-classicality of the state associated at $\phi = 48.2^o$, which is the point of conical intersection.

Next, we have calculated the Wigner quasiprobability distribution function[166, 56] defined as $W(X,P) = \sum_i W_{ii}(X,P)$ by taking trace over the Wigner function matrix element. Analytically the expression for Wigner distribution function is

$$W(X,P) = \frac{1}{\pi} \sum_{n,m=0} (-1)^n \rho_{n,m} \sqrt{\frac{n!}{m!}} (2\beta)^{m-n} e^{-2|\beta|^2} L_n^{m-n}(4|\beta|^2), \tag{7.20}$$

where, L_n^{m-n} is a Laguerre polynomial[108]. In the fig.(7.5), we have provided the 3D plots as well as the contours for Wigner distribution function for the molecule put in a formal quantum transport setup for $\lambda = 2\omega$. When the torsion angle $\phi = 0^o$, the Wigner function closely resembles a Gaussian[107][see fig.(7.5.a)], which corresponds to bosonic coherent state. This is also supported from 0.5 value of the uncertainty product. This state also refers to as having the entanglement, which is persistent(PE). As ϕ increases, the entanglement(SE) increases which is evidenced from enhancement in the value of $\Delta X \Delta P$. This causes the Wigner distribution function spread out in rings around the origin. Thus in the fig.(7.5.b), where $\phi =$

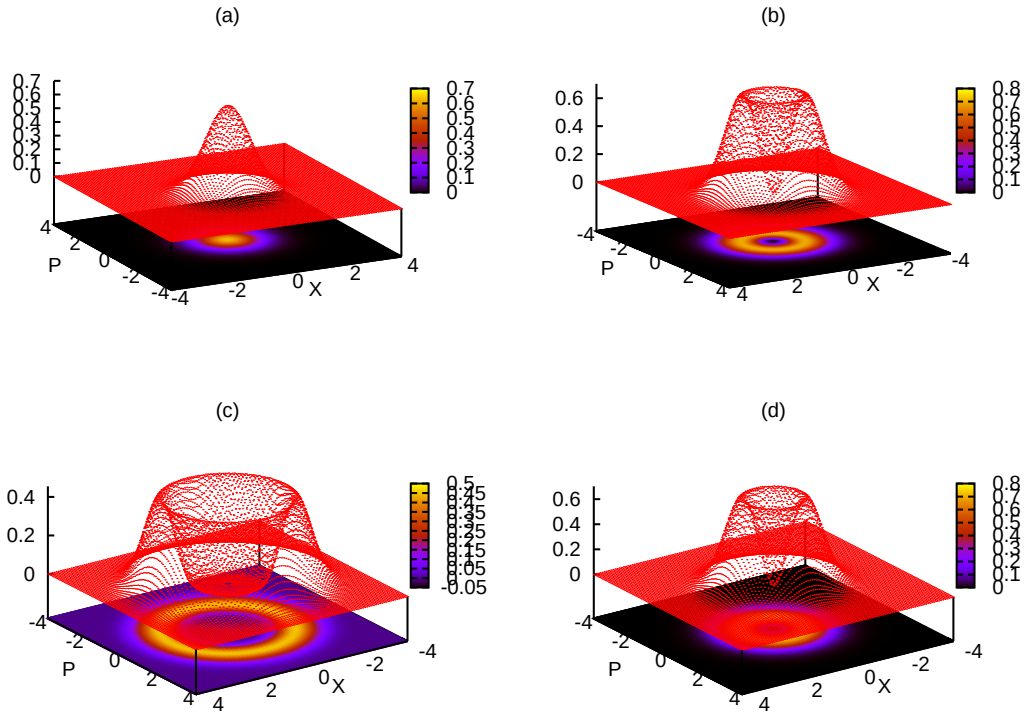

Figure 7.5: Plots of Wigner distribution function $W(X, P)$ and their contours for different parametric values of ϕ. The value of vibronic coupling parameter is fixed at $\lambda = 2\omega$. In fig.(7.5.a), $\phi = 0.0$, in fig.(7.5.b), $\phi = 38.0$, in fig.(7.5.c), $\phi = 48.2$(CI point) and in fig.(7.5.d), $\phi = 60.0$, The CI point shows maximum amount of splitting in the Wigner function.

38.0^o, we obtain a split Gaussian. The extent of splitting becomes maximum at the CI point where $\phi = 48.2^o$ characterizing maximum value of entanglement(SE and PE) and non-classicality of the states which is given in the fig.(7.5.c). On further changing the torsion angle the extent of splitting decreases which is given in the fig.(7.5.d) for $\phi = 60.0^o$. This result tallies very closely with that obtained earlier[107] where the Wigner distribution function spreads out in a ring at and near the resonance. The CI point in the molecule is that very point of resonance because of the closeness in energy of the two diabatic electronic energy states. The difference here, is that, the resonance occurs at CI through the vibrational mode with λ as the vibronic coupling parameter. In this context, one must note that the non-negative nature of the $W(X, P)$ near $\phi = 48.2^o$ hides the highly non-classical nature of the state may be due to the fact that the diagonal Wigner function matrix element cancels out each other at and near the CI point which is not shown here.

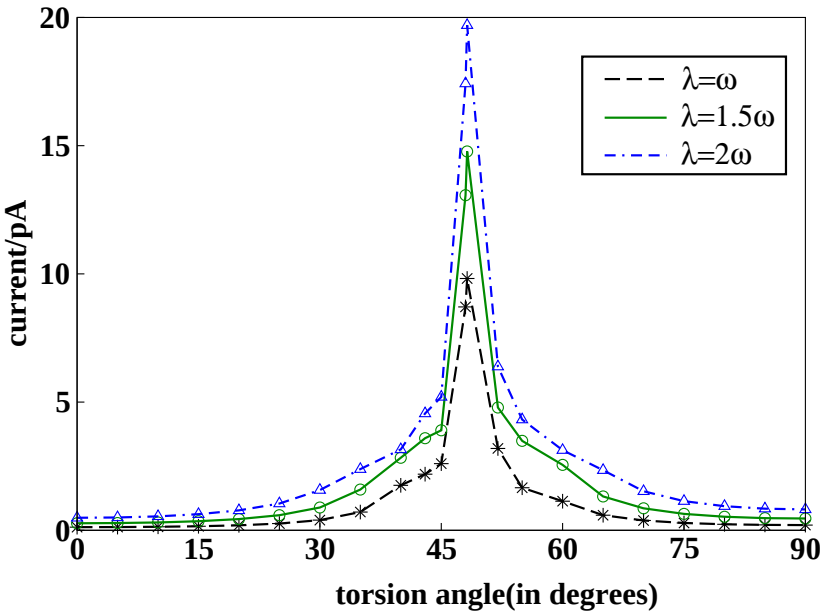

Figure 7.6: Variation of molecular current in pA as a function of the torsion angle ϕ, for different parametric values of the vibronic coupling λ. The value of ω is fixed at 0.17eV and the tunneling rate constants are kept fixed at $\Gamma_1 = \Gamma_2 = 0.13$meV. The current maximizes at the CI point which is given by $\phi = 48.2^o$. The extent of magnification increases with the increase in the phonon coupling parameter λ.

7.5 Current as an estimate of entanglement

Finally in this section, we have characterized the conical intersection and the electron-vibration entanglement through the molecular current. In the stationary state, the current is defined[100] as the rate at which electrons tunnel from the state $|1\rangle$ to $|2\rangle$. In terms of operator, it is formally expressed as[107]

$$\hat{I} = \frac{\partial}{\partial t}|1\rangle\langle 1| = i\lambda(|2\rangle\langle 1| - |1\rangle\langle 2|)(a + a^\dagger). \tag{7.21}$$

After performing trace operation, we find the expression for average current in terms of the electron-vibration entangled state density matrix elements as

$$\langle \hat{I} \rangle = i\lambda \sum_n [\sqrt{n+1}(\rho^{1,2}_{n+1,n} - \rho^{2,1}_{n+1,n}) + \sqrt{n}(\rho^{1,2}_{n-1,n} - \rho^{2,1}_{n-1,n})]. \tag{7.22}$$

In figure(7.6), we have shown the variation of the stationary current as a function of the torsion angle (ϕ). The results are presented under the condition of infinite external bias. The torsion angle practically plays the role of modulating the diabatic electronic energy states which is presented in literature commonly as internal bias[107, 108].

From the figure, it is clearly revealed that as the torsion angle increases from $\phi = 0^o$, the molecular current initially remains very close to few pA nearing zero.

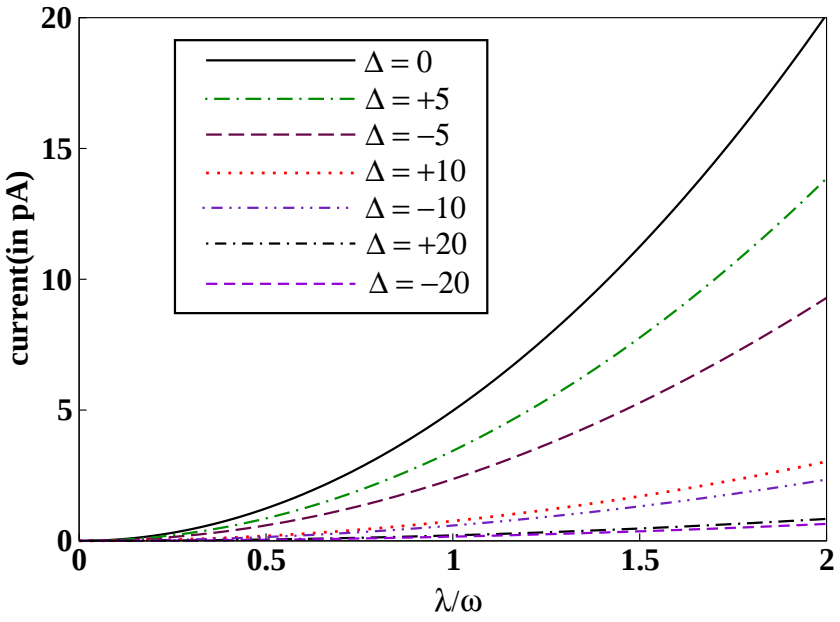

Figure 7.7: Variation of the avarage molecular current $\langle I \rangle$ against the vibronic coupling parameter, λ for different values of Δ, where $\phi = 48.2^0 + \Delta$. At the CI point($\Delta = 0$), the current almost increases quadratically with λ. For other values of ϕ, the current varies much insignificantly owing to only PE.

But as the angle approaches value of $\phi \approx 30^o$, the current rises slowly and we obtain a sharp peak right at the CI point having $\phi = 48.2^o$. At this point both kinds of entanglement becomes operative. Electron-vibration entanglement is enhanced due to coupling constant as well as the torsion angle ϕ. These two types of electron-vibration entanglement controls the magnitude of current in different ways. A systematic enhancement in current is obtained with increase in the coupling constant, λ whereas, the current is maximum for a particular value of λ at a critical value of the torsion angle, $\phi = 48.2$ which is the CI point.

This is in sharp contrast to the result obtained earlier[107, 108] and such differences would arise due to the inherent structure of the system Hamiltonian. Here, the role of the parameter λ becomes crucial since putting $\lambda = 0$ physically refers to switching off the electron-phonon coupling which makes the molecular current also zero. This is clearly revealed from Eq.(7.21). Thus current comes primarily from SE and very insignificantly from PE contribution in nature which gains its prominence at and near the CI point. As λ increases, there is a magnification in the current magnitude which is also supported from Eq.(7.22). and this feature is solely due to PE.

Next, in the fig.(7.7), we have shown a variation of the molecular current in pA against the vibronic coupling, λ. In fig.(7.7), it is clearly revealed that with the increase in λ, there is a significant increase in the molecular current at and very near to the CI point. A simple approximate expression of current can be

found analytically by only considering the ground vibrational state and a coherent distribution. Apart from this, to get the analytical result, one should employ the brute-force approximation of $\rho^{ij}_{nm} = \rho^{ij}\rho_{nm}$ which can result to a very crude outcome. Nevertheless, with these assumptions, the expression for the average current, $\langle I \rangle$ turns out as

$$\langle I \rangle = \frac{\lambda^2 \alpha^2 e^{-\alpha^2}(1 + \frac{\Gamma_2}{\Gamma_1})}{(\frac{\epsilon}{\hbar})^2 + \frac{\Gamma_2^2}{4} + \lambda^2 \alpha (1 + \frac{\Gamma_2}{\Gamma_1})}, \tag{7.23}$$

where, α is the coherent parameter considered. The variation in this domain appears to be almost quadratic which is counterintuitive if we consider Eq.(7.22), but can be understood in respect to the approximate expression of the current[see Eq.(7.23] for $\lambda \ll \epsilon$. But the variation happens to be almost linear at torsion angles apart from the CI point. Here, it has finally become clear that although we are not at the CI point, due to the presence of PE, there is some residual current flowing through the system which weakly varies with the vibronic coupling,λ. But at the CI, due to the dominance of the ϕ-dependent SE, the molecular current is amplified many fold giving rise to a high degree of non-classicality in the molecular system.

7.6 Conclusion

In a nutshell, in this chapter, we have studied the effect of conical intersection in a molecular system when it is coupled to two electronic reservoirs under infinite difference in the chemical potential. Conical intersection introduces non-classicality in vibrational coordinate and quantum entanglement due to electron-vibration coupling. We have taken a model example where two electronic states are coupled through a vibrational coordinate. These two electronic states correspond to a diabatic double-welled potential having bimodal electron density profile[153, 154]. For such an electron-vibration entangled state, one can principally encounter two distinct types of entanglement: one which arises purely from the degeneracy of the energy levels and is destroyed totally by slight energy asymmetry of the states which can be called *sensitive entanglement*(SE), while the other entanglement originates through strong coupling between the potential wells which is kind of *persistent* one. Persistent entanglement(PE) is developed due to strong vibronic coupling and does not depend appreciably on the energy asymmetry of the electronic states.

We have considered the torsional coordinate parametrically for understanding of the system in presence of a conical intersection of the adiabatic potential energy surfaces under electron transport setup. We have considered measure of entanglement in terms of the Wigner function matrices and the Wigner distribution function in the phase space of the vibrational mode which couples the two diabatic electronic states. The results are also compared in terms of the von-Neumann entanglement entropy and the uncertainty product. The principal result of this paper lies in the

fact that identification of the non-classicality of the states and hence the conical intersection point can be done also from the measurement of the electron current through the molecule when put in a formal quantum transport setup. As the torsion angle gradually reaches the value corresponding to the conical intersection(CI) point($\phi = 48.2^o$), the molecular electron current shows a sharp peak. We have thus provided a quantification of the PE and SE present in a quantum system under the electron transport setup. This result is in tune with that obtained on the basis on the variation of the uncertainty product $\Delta X.\Delta P$, the Von-Neumann entropy S_{VN} and the Wigner function $W(X, P)$.

Bibliography

[1] J. Bardeen, *Nobel lecture:Semiconductor research leading to the point contact transistor*, 11 December, 1956; W. H Brattain, entry of 16 December, 1947, laboratory notebook, case 38139-7, *Bell Laboratories archives*.

[2] J. Millman, C. Halkius and C. D. Parikh, *Millman's Integrated Electronics*(Tata McGraw Hill Ed. Pvt. Ltd., New Delhi, 2010).

[3] R. Landauer, *IBM J. Res. Develop.* **1**, 233 (1957).

[4] M. Buttiker, Y. Imry , R. Landauer and S. Pinhas, *Phys. Rev. B* **31**, 6207 (1985).

[5] Ya. M. Blanter and M. Buttiker, *Phys. Rep.* **336**, 1 (2000);Y. V. Nazarov and Y. M. Blanter, *Quantum Transport*(Cambridge University Press, 2009).

[6] S. Datta, *Quantum Transport-Atom to Transistor* (Cambridge, 2005).

[7] J. M. Tour, *Molecular Electronics: Commercial Insights, Chemistry, Devices, Architecture and Programming*(World Scientific, 2003).

[8] J. C. Cuevas and E. Scheer, *Molecular Electronics: An introduction to theory and Experiment*(World Scientific, 2010); M. C. Petty, *Molecular Electronics: From Principles to Practice*(John Wiley and Sons, 2007); G. Cuniberti, G. Fagas and K. Richter(eds.)*Introducing Molecular Electronics*(Springer, 2005).

[9] M. A. Ratner, *Nat. Nanotech.* **8**, 378 (2013).

[10] A. Nitzan and M. A. Ratner, *Science* **300**, 1384 (2003).

[11] C. A. Mirkin and M. A. Ratner, *Annu. Rev. Phys. Chem.* **43**, 719 (1992).

[12] A. Nitzan, *Chemical Dynamics in Condensed Phases: Relaxation, Transfer, and Reactions in Condensed Molecular Systems* (Oxford University Press, Oxford, 2006); V. May and O. Kuhn, *Charge and Energy Transfer Dynamics in Molecular Systems* (Wiley-VCH, Weinheim, 2004).

[13] A. Nitzan, *Annu. Rev. Phys. Chem.* **52**, 681 (2001).

[14] R. L. Carroll and C. B. Gorman, *Angew. Chem. Int. Edn* **41**, 4378 (2002).

[15] Y. Selzer and D. L. Allara, *Annu. Rev. Phys. Chem.* **57**, 593 (2006).

[16] M. Galperin, *Chem. Soc. Rev.* **46**, 4000 (2017).

[17] B. Mann and H. Kuhn, *J. Appl. Phys.* **42**, 4398 (1971).

[18] M. Tsutsui and M. Taniguchi, *Sensors* **12**, 7259 (2012).

[19] A. Aviram and M. A. Ratner, *Chem. Phys. Lett.* **29**, 277 (1974).

[20] H. Park, J. Park, A. K. L. Lim, E. H. Anderson, A. P. Alivisatos and P. L. McEuen, *Nature* **407**, 57 (2000).

[21] A. Z. Natalya and M. R. Pederson, *Phys. Rep.* **509**, 1 (2011).

[22] M. Galperin, M. A. Ratner, A. Nitzan and A. Troisi, *Science* **319**, 1056 (2008).

[23] B. Dong, H. L. Cui and X. L. Lei, *Phys. Rev. B* **69**, 205315 (2004); Erratum *Phys. Rev. B* **76**, 159901 (2007).

[24] N. Lambert, C. Flindt and F. Nori, *Europhys. Lett.* **103**, 17005 (2013).

[25] S. Walter, B. Trauzettel and Th. L. Schmidt, *Phys. Rev. B* **88**, 195425 (2013).

[26] C. Flindt, T. Novotny and A. P. Jauho, *Phys. Rev. B* **70**, 205334 (2004).

[27] L. D. C-Pulido and M. Bruderer, *J. Phys.: Cond. Matt.* **29**, 185301 (2017).

[28] G. Schaller, J. Cerrillo, G. Engelhardt and P. Strasberg, *Phys. Rev. B* **97**, 195104 (2018).

[29] C. Wang, J. Ren, B. W. Li, et al. *Eur. Phys. J. B* **85** (2012).

[30] J. Inarrea, G. Platero and A. H. MacDonald, *Phys. Rev. B* **76**, 085329 (2007).

[31] M. P. Blencowe, J. Imbers and A. D. Armour, *New J. Phys.* **7**, 236 (2005).

[32] D. A. Rodrigues, J. Imbers, T. J. Harvey and A. D. Armour, *New J. Phys.* **9**, 84 (2007).

[33] J. K. Sowa, J. A. Mol, G. A. D. Briggs, and E. M. Gauger, *Phys. Rev. B* **95**, 085423 (2017).

[34] S. Zippilli A. Bachtold and G. Morigi, *Phys. Rev. B* **81**, 205408 (2010).

[35] J. K. Sowa, J. A. Mol, G. A. D. Briggs, and E. M. Gauger, *Phys. Chem. Chem. Phys.* **19**, 29534 (2017).

[36] N. A. Zimbovskaya and A. Nitzan, *J. Chem. Phys.* **148**, 024303 (2018).

[37] P. Haughian, S. Walter, A. Nunnenkamp and Th. L. Schmidt, *Phys. Rev. B* **94**, 205412 (2016).

[38] P. Stadler, W. Belzig, and G. Rastelli, *Phys. Rev. B* **96**, 045429 (2017).

[39] W. Dou and J. E. Subotnik, *J. Chem. Phys.* **146**, 092304 (2017).

[40] W. Dou, G. Miao and J. E. Subotnik, *Phys. Rev. Lett.* **119**, 046001 (2017).

[41] W. Dou and J. E. Subotnik, *J. Chem. Phys.* **148**, 230901 (2018).

[42] B. K. Agarwalla, J-H. Jiang, and Dvira Segal, *Phys. Rev. B* **92**, 245418 (2015).

[43] C. Flindt, T. Novotny, A. Braggio and A-P Jauho, *Phys. Rev. B* **82**, 155407 (2010).

[44] Y-J Chang, T-K Yeh, C-H Wan, D. W. Utami, G. J. Milburn and H-S Goan, *Phys. Rev. B* **96**, 195440 (2017).

[45] J. D. V. Jaramillo and J. Fransson, *J. Phys. Chem. C* **121**, 27357 (2017).

[46] B. Dong, H. L. Cui, X. L. Lei, and N. J. M. Horing, *Phys. Rev. B* **71**, 045331 (2005).

[47] N. Lambert and F. Nori, *Phys. Rev. B* **78**, 214302 (2008).

[48] T. J. Harvey, D. A. Rodrigues, and A. D. Armour, *Phys. Rev. B* **78**, 024513 (2008).

[49] C. Schinabeck, R. Hartle, H. B. Weber and M. Thoss, *Phys. Rev. B* **90**, 075409 (2014).

[50] Secker. et. al, *Phys. Rev. Lett.* **106**, 136807 (2011).

[51] C. Timm, *Phys. Rev. B* **77**, 195416 (2008).

[52] Konig et. al., *Phys. Rev. Lett.* **76**, 1715 (1996); *Phys. Rev. B* **54**, 16820 (1996).

[53] R. P. Feynmann and F. L. Jr Vernon, *Ann. Phys.* **24**, 118 (1963).

[54] A. O. Caldeira and A. J. Leggett *Phys. Rev. Lett.* **46**, 211 (1981); *Ann. Phys.(NY)* **149**, 374 (1983); *Physica A* **121**, 587 (1983).

[55] H. J. Carmichael, *Statistical Methods in Quantum Optics 1* (Springer, New York, 1998).

[56] W. H. Louisell, *Quantum Statistical Properties of Radiation*(Wiley, New York, 1973); P. Meystre and M. Sargent, *Elements of Quantum Optics* (Springer-Verlag, New York, 1991).

[57] S. M. Barnett and P. M. Radmore, *Theoretical Quantum Optics*(Clarendon Press, Oxford, 1997).

[58] H. P. Breuer and F. Petruccione, *The Theory of Open Quantum Systems*(Oxford University Press, 2003).

[59] R. O' Connell, C. Savage and D. Walls, *Ann. N.Y. Acad. Sci.* **480**, 1697 (1993); G. Milburn and D. Walls, *Phys. Rev. A* **28**, 2646 (1983); C. Caves, K. Thorne, R. Drever, V. Sandberg and M. Zimmermann *Rev. Mod. Phys.* **52**, 341 (1980).

[60] A. Tameshtit and J. E. Sipe, *Phys. Rev. A* **47**, 1697 (1993); *Phys. Rev. A* **49**, 89 (1994); G. Gangopadhyay and S. H. Lin, *Pramana J. Phys.* **49**, 399 (1997).

[61] G. Gangopadhyay, M. S. Kumar and S. Dattagupta, *J. Phys. A* **34**, 5485 (2001).

[62] J. Shao, M. L. Ge and H. Chang, *Phys. Rev. E* **53**, 1243 (1996).

[63] N. V. Prokof'ev and P. C. E. Stamp, *Rep. Prog. Phys.* **63**, 669 (2000).

[64] A. S. Davydov, *Quantum Mechanics* **2nd ed.** (Oxford: Pergamon, 1976).

[65] A. O. Caldeira, A. H. Castro Neto and T. O. de Carvalho, *Phys. Rev. B* **48**, 13974 (1993).

[66] N. V. Prokof'ev and P. C. E. Stamp, *Phys. Rev. Lett.* **80**, 5794 (1998); *J. Low Temp. Phys.* **104**, 143 (1998).

[67] J. R. Anglin, J. P. Paz and W. H. Zurek, *Phys. Rev. A.* **55**, 4041 (1997).

[68] E. S. Harnandez and C. O. Dorso, *Phys. Rev. C* **29**, 1510 (1984); F. Guinea, V. Hakim and A. Muramatsu, *Phys. Rev. B* **32**, 4410 (1985).

[69] U. Weiss, *Quantum Dissipative Systems* (World Scientific, 2008); H. Grabert, P. Schramm and G. L. Ingold, *Phys. Rep.* **168** 115(1988); A. J. Leggett, S. Chakravarty, A. T. Dorsey, M. P. A. Fisher, A. Garg and W. Zwerger, *Rev. Mod. Phys.* **59**, (1987).

[70] T. Rom, Th. Best, D. van Oosten, U. Schneider, S. Folling, B. Peredes and I. Bloch, *Nature* **444**, 733 (2006).

[71] A. Malko, D. Y. Oberli, M. H. Baier, E. Pelucchi, F. Michelini, K. F. Karlsson, M. A. Dupertuis and E. Kapon, *Phys. Rev. B* **72**, 195332 (2005).

[72] R. P. Mirin, *Appl. Phys. Lett.* **84**, 1260 (2003).

[73] C. Santori, S. Gotzinger, Y. Yamamoto, S. Kako, K. Hoshino and Y. Arakawa, *Appl. Phys. Lett.* **87**, 051916 (2005).

[74] C. Gerry and P. L. Knight, *Am. J. Phys.* **65**, 964 (1997).

[75] C. Gerry and P. Knight, *Introductory Quantum Optics* (Cambridge University Press, 2005).

[76] B. R. Mollow *Phys. Rev.* **188**, 1969 (1969); B. R. Mollow *Phys. Rev. A* **5** 2217 (1972).

[77] X. Xu, B. Sun, R. P. Berman, G. S. Duncan, A. S. Bracker, D. Gammon and L. J. Sham, *Science* **317**, 929 (2007); D. Press, T. D. Ladd, B. Zhang and Y. Yamamoto, *Nature* **456**, 218 (2008).

[78] A. N. Vamivakas, Y. Zhao, C-Y. Lu and M. Atature *Nat. Phys.* **5**, 198 (2009).

[79] S. Ates, S. M. Ulrich, S. Reitzenstein, A. Lofer, A. Forchel and P. Michler, *Phys, Rev. Lett.* **103**, 167402 (2009).

[80] S. M. Ulrich, S. Ates, S. Reitzenstein, A. Lofer, A. Forchel, and P. Michler, *Phys, Rev. Lett.* **106**, 247402 (2011).

[81] H. W. Ch Postma, T. Teepen, Z. Yao, M. Grifoni and C. Dekker, *Science* **293**, 76 (2001).

[82] B. E. Kane, *Nature(London)* **393**, 133 (1998).

[83] L. Kouwenhoven, *Science* **275**, 1896 (1997).

[84] W. Liang, M. P. Shores, M. Bockrath, R. J. Long and H. Park, *Nature* **417**, 725 (2002).

[85] P. Michler, A. Kiraz, C. Becher, W. V. Schoenfeld, P. M. Petroff, L. Zhang, E. Hu and A. Imamoglu, *Science* **290**, 2282 (2000).

[86] H. R. Brown and R. Q. Twiss, *Nature* **177**, 27 (1956).

[87] S. Seidl, M. Kroner, P. A. Dalgarno, A. Hogele1, J. M. Smith, M. Ediger, B. D. Gerardot, J. M. Garcia, P. M. Petroff, M. K. Karrai and R. J. Warburton, *Phys. Rev B* **72**, 195339 (2005).

[88] J. R. Petta et. al., *Science* **309**, 2180 (2005).

[89] W. G. Wiel, S. D. Franceschi, J. M. Elzerman, T. Fujisawa, S. Tarucha and L. P. Kouwenhoven, *Rev. Mod. Phys.* **75**, 1 (2003).

[90] M. Galperin and A. Nitzan, *J. Chem. Phys* **124**, 234709 (2006).

[91] C. Wang , J. Ren, B. W. Li and Q. H. Chen, *Eur. Phys. J B* **85**, 110 (2012).

[92] R. Jorn and T. Seidemann, *Acc. Chem. Res* **43**, 1186 (2010).

[93] G. Feve *et. al.*, *Science* **316**, 1169 (2007).

[94] G. Q. Li and U. Kleinekathofer, *Eur J Phys B* **76**, 309 (2010).

[95] J. Y. Luo, X. Q. Li and Y. Yan, *Phys. Rev. B* **76**, 085325 (2007); X. Q. Li, J. Y. Luo, Y. G. Yang, P. Cui and Y. Yan, *Phys. Rev. B* **71**, 085325 (2005); H. B. Sun and G. J. Milburn, *Phys. Rev. B* **59**, 10748 (1999).

[96] M. Buttiker, *Phys. Rev. B* **46**, 12485 (1992).

[97] E. Bocquillon, *Phys. Rev. Lett* **108**, 196803 (2012).

[98] H. Schimd and H-W. Fink, *Appl. Phys. Lett.* **70**, 2679 (1997).

[99] G. Lachs, *Phys Rev* **138**, B 1012 (1965).

[100] A. Karmakar and G. Gangopadhyay, *Phys. Rev. E* **93**, 022141 (2016).

[101] L. Y. Gorelik, A. Isacsson, M. V. Voinova, B. Kasemo, R. I. Shekhter and M. Jonson, *Phys. Rev. Lett.* **80**, 4526 (1998).

[102] A. Erbe, R. H. Blick, A. Tilke, A. Kriele and J. P. Kotthaus, *Appl. Phys. Lett.* **73**, 3751 (1998); A. Erbe, C. Weiss, W. Zwerger, and R. H. Blick, *Phys. Rev. Lett.* **87**, 096106 (2001).

[103] D. V. Scheible, C. Weiss, J. P. Kotthaus and R. H. Blick, *Phys. Rev. Lett.* **93**, 186801 (2004).

[104] E. M. Weig, R. H. Blick, T. Brandes, J. Kirschbaum, W. Wegscheider, M. Bichler and J. P. Kotthaus, *Phys. Rev. Lett.* **92**, 046804 (2004).

[105] J. Koch and F. V Oppen, *Phys. Rev. Lett.* **94**, 206804 (2005).

[106] S. Sapmaz, P. Jarillo-Herrero, Ya. M. Blanter, C. Dekker, and H. S. J. van der Zant, *Phys. Rev. Lett.* **96**, 026801 (2006).

[107] T. Brandes, *Phys. Rep.* **408**, 315 (2005).

[108] T. Brandes and N. Lambert, *Phys. Rev. B* **67**, 125323 (2003).

[109] D. Segal and A. Nitzan, *Chem. Phys.* **281**, 235 (2002).

[110] M. Galperin, M. A. Ratner and A. Nitzan, *J. Phys.:Cond. Mat.* **19**, 103201 (2007).

[111] N. J. Tao, *Nature nanotech.* **1**, 173 (2006).

[112] H. Grabert (Ed.), M.H. Devoret, Single Charge Tunneling, *NATO ASI B*, **294**, (Plenum Press, New York, 1991).

[113] M. Born, R. Oppenheimer, *Ann. Phys.* **84**, 457 (1927).

[114] M. Born and K. Huang, *The Dynamical Theory of Crystal Lattices.* (Oxford, UK, 1954).

[115] M. Ben-Nun and T.J. Martinez, *J. Phys. Chem. A* **104**, 5161 (2000).

[116] W. Domcke, D.R. Yarkony, H. Kppel, Eds. *Conical Intersections: Electronic Structure, Dynamics and Spectroscopy* **15** (World Scientific, Singapore, 2004).

[117] M.J. Paterson, M.J. Bearpark, M.A. Robb, L. Blancafort, and G.A. Worth, *Phys. Chem. Chem. Phys.*, **7**, 2100 (2005).

[118] Xiaolei Zhu and D. R. Yarkony, *Mol. Phys.*, **114**, 1983 (2016).

[119] R. J. Glauber, *Phys. Rev* **131**, 2766 (1963); **130**, 2529 (1963); *Phys. Rev. Lett.* **10**, 84 (1963); E. C. G. Sudarshan, *Phys. Rev. Lett.* **10**, 277 (1963).

[120] F. Guinea, V. Hakim, and A. Muramatsu, *Phys. Rev. B* **32**, 4410 (1985).

[121] S. Chakravarty and J. Rudnick, *Phys. Rev. Lett.* **75**, 501 (1995).

[122] K. Volker, *Phys. Rev. B* **58**, 1862 (1998).

[123] A. Wurger, *Phys. Rev. Lett.* **78**, 1759 (1997).

[124] T. A. Costi and C. Kieffer, *Phys. Rev. Lett.* **76** 1683 (1996) ; T. A. Costi, *ibid.* **80**, 1038 (1998).

[125] J. T. Stockburger and C. H. Mak, *Phys. Rev. Lett.* **80**, 2657 (1998).

[126] R. Egger and C. H. Mak, *Phys. Rev. B* **50**, 15210 (1994); R. Egger, L. Muhlbacher and C. H. Mak, *Phys. Rev. E* **61**, 5961 (2000).

[127] M. Keil and H. Schoeller, *Phys. Rev. B* **63**, 180302 (2001).

[128] R. Silbey and R. A. Harris, *J. Chem. Phys.* **80**, 2615 (1984); R. A. Harris and R. Silbey, *ibid.* **83**, 1069 (1985).

[129] D. R. Reichman and R. J. Silbey, *J. Chem. Phys.* **104**, 1506 (1996).

[130] A. A. Golosov, R. A. Friesner and P. Pechukas, *J. Chem. Phys.* **112**, 2095 (2000).

[131] A. A. Golosov and D. R. Reichman, *J. Chem. Phys.* **115**, 1065 (2001).

[132] H. Wang, M. Thoss, and W. H. Miller, *J. Chem. Phys.* **115**, 2979 (2001); M. Thoss, H. Wang, and W. H. Miller, *ibid.* **115**, 2991 (2001).

[133] E. Joos, H. D. Zeh, C. Kiefer, D. Giulini, J. Kupsch, I. O. Stamatescu, *Decoherence and the Appearance of a Classical World in Quantum Theory* (Springer, 2003).

[134] W. H. Zurek, *Rev. Mod. Phys.* **75**, 715 (2003).

[135] M. A. Schlosshauer, *Decoherence and the quantum-to-classical transition* (Springer, 2007).

[136] S. Banerjee and R. Ghosh, *J. Phys. A: Math. Gen* **40**, 13735 (2007).

[137] S. Banerjee, J. Ghosh and R. Ghosh, *Phys. Rev. A.* **75**, 062106 (2007).

[138] S. Banerjee and R. Srikanth, *Phys. Rev. A.* **76** 062109 (2007).

[139] S. S. Sinha, D. Mondal, B. C. Bag and D. S. Ray, *Phys. Rev E* **82**, 051125 (2010).

[140] J. Shao and P. Hanggi, *Phys. Rev. Lett.* **81**, 5710 (1998).

[141] F. A. Villares and C. M. Smith, *Phys. Rev. B* **76**, 214303 (2007).

[142] F. A. Villares, A. O. Caldeira and C. M. Smith, *Phys. Rev. B* **74**, 184304 (2004).

[143] J. P. Gazeau, *Coherent States in Quantum Physics* (Wiley-VCH, 2009).

[144] W. Fuller and A. Lenard, *Commun. Math. Phys.* **67**, 69, (1979).

[145] J. M. Radcliffe, *J. Phys. A* **4**, 313, (1971).

[146] J. W. Negele and H. Orland, *Quantum Many Particle systems* (West View Press, 2009).

[147] K. E. Cahill and R. J. Glauber, *Phys. Rev. A* **59**, 1538 (1999).

[148] A. Dhar and B. S. Sastry, *Phys. Rev. B* **267**, 195405 (2003).

[149] W. Lai, Y. Cao and Z. Ma, *J. Phys: Cond. Mat* **24**, 175301 (2012).

[150] M. N. Mazziotta, *Nuclear Instruments and Methods in Physics Research A* **584**, 436 (2008).

[151] E. R. Bittner, S. Karabunarliev and L. M. Herz, *J. Chem. Phys.* **126**, 191102 (2007).

[152] K. Banerjee and G. Gangopadhyay, *J. Chem. Phys.* **130**, 084705 (2009).

[153] L. K. McKemmish, R. H. McKenzie, N. S. Hush and J. R. Reimers, *J. Chem. Phys.* **135**, 244110 (2011).

[154] L. K. McKemmish, R. H. McKenzie, N. S. Hush and J. R. Reimers, *Phys. Chem. Chem. Phys.* **17**, 24666 (2015).

[155] T. Dadosh, Y. Gordin, R. Krahne, I. Khivrich, D. Mahalu, V. Frydman, J. Sperling, A. Yacoby and I. B. Joseph, *Nature* **436**, 677 (2005).

[156] V. B. Kouteck and J. Michl, *J. Theor. Chim. Acta* **68**, 45 (1985).

[157] S. Takeuchi, S. Ruhman,T. Tsuneda, M. Chiba, T. Taketsugu and T. Tahara, *Science* **322**, 1073 (2008).

[158] A. L. Dobryakov, I. Ioffe, A. A. Granovsky, N. P. Ernsting and S. A. Kovalenko, *J. Chem. Phys.* **137**, 244505 (2012).

[159] A. Wand, I. Gdor, J. Zhu, M. Sheves, S. Ruhman, *Annu. Rev. Phys. Chem.* **64**, 437 (2013).

[160] J. P. Kraack, T. Buckup and M. Motzkus, *J. Phys. Chem. Lett.* **4**, 383 (2013).

[161] O. Bismuth, N. Friedman, M. Sheves and S. Ruhman, *Chem. Phys.* **341**, 267 (2007).

[162] W. Domcke and D. R. Yarkony, *Annu. Rev. Phys. Chem.* 2012, **63**, 325 (2012).

[163] C. Dugave and L. Demange, *Chem. Rev.* **103**, 2475 (2003).

[164] S. Hahn and G. Stock, *J. Phys. Chem. B* **104**, 1146 (2000).

[165] H. Rau, *In Photocromism, Molecules and Systems*, **1** 165, (Elsevier: Amsterdam, 1992).

[166] K.E. Cahill and R.J. Glauber, *Phys. Rev.* **177**, 1882 (1969).

[167] S. Stenholm and K. Suominen, *Quantum Approach to Informatics* (Wiley, New York, 2005).

[168] J. E. Baekhoj, C. Leveque and L. B. Madsen, *Phys. Rev. Lett.* **121**, 023203 (2018).

[169] J. S. Lim and S. K. Kim, *Nat. Chem.* **2** 627, (2010).

[170] J. A. Devine et al., *Science* **358**, 336 (2017).

[171] H. J. Worner et al., *Science* **334**, 208 (2011).

[172] A. Stolow, A. E. Bragg and D. M. Neumark, *Chem. Rev.* **104**, 1719 (2004).

[173] J. Brazard, L. A. Bizimana, T. Gellen, W. P. Carbery and D. B. Turner, *J. Phys. Chem. Lett.* **7**, 14 (2016).

[174] T. J. A. Wolf et al., *Nat. Commun.* **8**, 29 (2017).

[175] A. H. Zewail, *Angew. Chem. Int. Ed.* **39**, 2586 (2000).

[176] Jie Yang et al., *Science* **361**, 64 (2018).

[177] C. Monroe, D. M. Meekhof, B.E. King and D.J. Wineland, *Science* **272**, 1131 (1996); L. G. Lutterbach and L. Davidovich, *Phys. Rev. Lett.* **78**, 2547 (1997).

[178] S. Wallentowitz, Filho R. L. de Matos, W. Vogel, *Phys. Rev. A* **56**, 1205 (1997); S. Wallentowitz, Filho R. L. de Matos, S. C. Gou, W. Vogel, *Eur. Phys. J. D* **6**, 397 (1999).

[179] H. Goldstein, C. Poole and J. Safko, *Classical Mechanics*(Addison Wesley, 2000).

[180] R. K. Wangsness and F. Bloch, *Phys. Rev.* **89**, 728 (1953); F. Bloch, *Phys. Rev.* **105**, 1206 (1957).

[181] A. G. Redfield, *Adv. Magn. Reson.* **1**, 1 (1965).

[182] H. Schoeller and G. Schn, *Phys. Rev. B* **50**, 18436 (1994).

[183] J. Konig, H. Schoeller, and G. Schon, *Phys. Rev. Lett.* **76**, 1715 (1996); J. Konig, J. Schmid, H. Schoeller, and G. Schon, *Phys. Rev. B* **54**, 16820 (1996).

[184] J. Konig, H. Schoeller, and G. Schon, *Phys. Rev. Lett.* **78**, 4482 (1997); *Phys. Rev. B* **58**, 7882 (1998).

[185] A. Thielmann, M. H. Hettler, J. Knig, and G. Schon, *Phys. Rev. B* **68**, 115105 (2003).

[186] M. Tokuyama and H. Mori, *Prog. Theor. Phys.* **54**, 918 (1975); **55**, 411 (1976).

[187] Y. V. Nazarof, *Ann. Phys.* **8**, SI193 (1999); **16**, 72 (2007); Y. V. Nazrov and M. Kindermann, *Eur. Phys. J. B* **35**, 413 (2003).

[188] W. Belzig and Y. V. Nazarov, *Phys. Rev. Lett* **87**, 197006 (2001); 067006 (2001).

[189] M. Kindermann and S. Pilgram, *Phys. Rev. B* **69**, 155334 (2004).

[190] C. Jarzynski and D. K. Wojcik, *Phys. Rev. Lett.* **92**, 230602 (2004).

[191] M. Esposito and S. Mukamel, *Phys. Rev. E* **73**, 04612 (2006); M. Esposito U. Harbola and S. Mukamel, *Phys. Rev. B* **75**, 155316 (2007).

[192] E. P. Wigner, *Phys. Rev.*, **40**, 749 (1932).

[193] G. Lindblad, *Commun. Math. Phys.* **48**, 119 (1976).

[194] V. Gorini, A. Kossakowski and E. C. G. Sudarshan, *J. Math. Phys.* **17**, 821 (1976).

[195] Y. J. Yan, *Phys. Rev. A.* **58**, 2721 (1998).

[196] R. X. Xu and Y. J. Yan, *J. Chem. Phys* **116**, 9196 (2002); Y. J. Yan and R. X. Xu, *Annu. Rev. Phys. Chem.* **56**, 187 (2005).

[197] X. Xu, B. Sun, P. R. P. Berman, D. G. Steel, A. S. Bracker, D. Gammon and L. J. Sham, *Science* **317** 929 (2007).

[198] R. Kubo *J. Math. Phys.* **4**, 174 (1963).

[199] A. Karmakar and G. Gangopadhyay, *Phys. Scr* **85**, 045008 (2012).

[200] G. W. Ford, M. Kac and P. Mazur *J. Math. Phys.* **6**, 504 (1965); P. Ullorsma *Physica* **32**, 27 (1966); **32**, 74 (1966); **32**, 90 (1966); R. Zwanzig, *J. Stat. Phys.* **9**, 215 (1973).

[201] K. Lindenberg and B. J. West, *The Non-equilibrium Statistical Mechanics of Open and Closed systems* (VCH, New York, 1990); N. G. Van Kampen, *Stochastic processes in physics and chemistry* (Elsevier, Amsterdam, 1992).

[202] V. I. Balykin, V. G. Minogin and V. S. Letokhov, *Rep. Prog. Phys.* **63**, 1429 (2000); S. Aubin *et.al J. Low. Temp. Phys.* **140**, 377 (2005).

[203] H. T. C. Stoof, M. Houbiers, C. A. Sackett and R. G. Hulet, *Phys. Rev. Lett.* **76**, 10 (1966); M. J. Holland, B. DeMarco and D. S. Jin, *Phys. Rev. A* **61**, 053610 (2000).

[204] G. Modugno, G. Ferrari, G. Roati, R. J. Brecha, A. Simoni and M. Inguscio, *Science* **294**, 1320 (2001); S. Aubin, S. Myrskog, M. H. T . Extravour, L. J. Lablanc, D. Mckay, A. Strammer and J. H. Thywissen, *Nat. Phys.* **2**, 384 (2006).

[205] F. A. Berezin, *The Method of Second Quantization* (New York: Academic Press, 1966); S. Weinberg, *The Quantum Theory of Fields: Volume I: Foundations*, (Cambridge: Cambridge University Press, 1995),

[206] J. Schwinger, *Phys. Rev.* **92**, 1283 (1953).

[207] L. Brown, *Quantum Field Theory* (Cambridge University Press, Cambridge, England, 1992); A. Das, *Field Theory: A Path Integral Approach* (World Scientific, New Delhi, 2002).

[208] E. Schrodinger, *Naturwiss.* **14**, 664 (1926).

[209] W. P. Schleich *Quantum Optics in Phase Space* (Wiley-VCH, Germany, 2001).

[210] T. J. Dunn, I. A. Walmsley and S. Mukamel, *Phys. Rev. Lett.* **74**, 884 (1995).

[211] U. Leonhardt, *Phys. Rev. A* **55**, 3164 (1997).

[212] C. Monroe, D. M. Meekhof, B. E. King and D. J. Wineland, *Science* **272**, 1131 (1996).

[213] C. Kurtsiefer, R. Pfau and J. Mlvnek, *Nature* **386**, 150 (1997).

[214] E. Schrodinger, *Naturwissenschaften* **23**, 807 (1935).

[215] G. Gangopadhyay *J. Phys. A*, **32**, L433 (1999); **31**, L771, (1998).

[216] R. J. Glauber *Physics of Quantum Electronics, Conference Proceedings*, edited by P. L. Kelley, B. Lax and P. E. Tannenwald, McGraw-Hill Book Co., New York, (1966).

[217] H. M. Srivastava and G. Gangopadhyay *Russ. J. Math. Phys.*, **11**, 359, (2004); S. Banerjee and G. Gangopadhyay *J. Chem. Phys.* **126**, 034102, (2007).

[218] I. S. Gradshteyn and I. M. Rhyzhik *Table of Integrals, Series and Products*, (1980).

[219] P. Filipowicz *J. Phys. A*, **19**, 3785, (1986).

[220] Th. Martin, in: D.C. Glattli, M. Sanquer, J. Tran Thanh Van (Eds.), *Coulomb and Interference Effects in Small Electronic Structures, Editions Frontieres*, (Gif-sur-Yvette, 1994).

[221] N. Zhao, J-L. Zhu, R-B. Liu and C. P. Sun, *New J. Phys* **13**, 013005 (2011); M. Esposito, H. Upendra and S. Mukamel, *Rev. Mod. Phys* **81**, 1665 (2009); S. Walter, T. Bjorn and T. L. Schmidt, *Phys. Rev. B* **88**, 195425 (2013).

[222] G. S. Agarwal, S. Chaturvedi, K. Tara, and V. Srinivasan, *Phys.Rev. A.* **45**, 4904 (1992).

[223] L. Susskind and J. Glogower, *Physics* **1**, 49 (1964).

[224] F. A. Villares and C. M. Smith, *Phys. Rev. B* **76**, 214303 (2007);H. H. Jorch, K. G. Lynn, and I. K. MacKenzie, *Phys. Rev. Lett.* **47**, 36 (1981).

[225] A. Berthelot, I. Favero, G. Cassabois, C. Voisin, C. Delalande, Ph. Roussignol, R. Ferreira and J. M. Gerard, *Nat. Phys.* **2** 759 (2006).

[226] W. D. Oliver, J. Kim, R. C. Liu and Y. Yamanto, *Science* **284**, 299 (1999).

[227] H. Kiesel, A. Renz and F. Hasselbach *Nature* **418**, 392 (2002).

[228] S. Liang, H. L. Zhu and W. Wang, *J. Chem. Phys.* **131**, 154704 (2009); K. H. Schmidt, G. M. Ribeiro, U. Kunze, G. Abssreiter, M. Han and P. M. Petroff, *J. Appl. Phys.* **84**, 4268 (1998).

[229] A. Karmakar and G. Gangopadhyay, *Phys. Scr.* **85**, 045008 (2012).

[230] L-J. Wei, N. Kalechofsky and D. Candela *Phys. Rev. Lett* **71**, 879 (1993); S. Perisanu and G. Vermeulen *Phys. Rev. B* **73**, 214519 (2006).

[231] P. L. Knight and P. W. Milloni, *Phys. Rep.* **66**, 21 (1980).

[232] G. Gangopadhyay, S. Ghoshal and Y. Tanimura, *Chem. Phys.* **242**, 367 (1999); G. Gangopadhyay and S. Ghoshal, *Chem. Phys. Lett* **289**, 287 (1998).

[233] A. Ghosh, S. S. Sinha and D. S. Ray, *Phys. Rev. E* **83**, 061154 (2011).

[234] F. Braakman, P. Barthelemy, C.Reichl, W. Wegscheider and L. Vandersypen *Nat. Nanotechnology* **8**, 432 (2013)

[235] G. Haack, M. Moskalets and M. Buttiker *Phys. Rev. B* **87**, 201302(R) (2013)

[236] S. Sivakumar *Eur. Phys. J. D* **66**, 277 (2012).

[237] H. J. W. Haug and A. P. Jauho *Quantum Kinetics in Transport and Optics* (Springer, Berlin, 2007)

[238] D. F. Walls and G. J. Milburn *Quantum Optics* (Springer, Berlin, 1994); M. Orszag *Quantum Optics* (Springer, 2008).

[239] I. G. Lang and Y. A. Firsov *Sov. Phys. JETP* **16**, 1301 (1962).

[240] A. Nazir *Phys. Rev. Lett* **103**, 146404 (2009).

[241] D. P. S. McCutcheon and A. Nazir *J. Chem. Phys.* **135**, 114501 (2011).

[242] C. K. Lee, J. Moix and J. Chao *J. Chem. Phys.* **136**, 204120 (2012).

[243] O. Adak, R. Korytar, A. Y. Joe, F. Evers and L. Venkataraman *Nano lett.* **15**, 3716 (2015).

[244] S. Ballmann, W. Hieringer, R. Hartle, P. B. Coto, M. R. Brycl, A. Gorling. M. Thoss and H. B. Weber *Phys. Status Solidi B* **11**, 2452 (2013).

[245] Y. Ie, T. Hirose, H. Nakamura, M. Kiguchi, N. Takagi, M. Kawai and Y. Aso *J. Am. Chem. Soc* **133**, 3014 (2011).

[246] E. S. Tam, J. J. Parks, W. W. Shum, Yu-Wu Zhong, M. E. B. Santiago-Berros, X. Zheng, W. Yang, G. K. L. Chan, H. D. Abruna, and D. C. Ralph *ACS Nano* **5**, 5115 (2011).

[247] J. M. Warman, M. P. de Haas, M. N. Paddon-Row, E. Cotsaris, N. S. Hush, H. Oevering and J. W. Verhoeven *Nature* **320**, 615 (1986).

[248] T. Krause, T. Brandes, M. Esposito and G. Schaller *J. Chem. Phys.* **142**, 134106 (2015).

[249] K. Banerjee and G. Gangopadhyay *J. Math. Chem.* **53**, 1733 (2015).

[250] L. Seidner and W. Domcke, *Chem. Phys.* **186**, 27 (1994); W. Domcke and G. Stock, in *Advances in Chemical Physics*, **100**, 1 (1997).

[251] J.P. Dahl, H. Mack, A. Wolf and W.P. Schleich, *Phys. Rev. A* **74**, 042323 (2006); S. Parker, S. Bose and M.B. Plenio, *Phys. Rev. A* **61**, 032305 (2000).

List of Publications

1. **Decoherence without dissipation due to fermionic bath** ,
   A. Karmakar and G. Gangopadhyay,
   Phys. Scr., **85**, 0450058 (2012).

2. **A fermionic bath induced antibunching and coherence in Mollow spectra** ,
   A. Karmakar and G. Gangopadhyay,
   Phys. Scr., **89**, 045001 (2014).

3. **Fermionic thermocoherent state: Efficiency of electron transport** ,
   A. Karmakar and G. Gangopadhyay,
   Phys. Rev. E, **93**, 022141 (2016).

4. **Electron-vibration entanglement of resonating dimeric structures in electron transport: Suppression of current noise** ,
   A. Karmakar and G. Gangopadhyay (**Communicated**).

5. **Conical-intersection in a molecule in electron transport setup**
   A. Karmakar and G. Gangopadhyay (**Communicated**).

6. *__Energy funneling in light harvesting complex through Excitonic Quantum Transport__ ,
   A. Karmakar and G. Gangopadhyay (**Communicated**).

   * not included in the thesis